ROLE OF KCC3 IN THE HEREDITARY SENSORY MOTOR NEUROPATHY: HMSN/ACC

By

JINLONG DING

Dissertation

Submitted to the Faculty of the

Graduate School of Vanderbilt University

in partial fulfillment of the requirements

for the degree of

DOCTOR OF PHILOSOPHY

in

Molecular Physiology & Biophysics

December, 2014

Nashville, Tennessee

Approved:

Professor Danny Winder

Professor Bruce Carter

Professor Anne Kenworthy

Professor David Jacobson

Professor Eric Delpire

ACKNOWLEDGEMENTS

This dissertation would not have been finished without the help of so many people in so many ways. First of all, I would like to thank my mentor, Dr. Eric Delpire, who is wonderful to work with, an efficient, kind and inspiring mentor. In the summer of 2005, Eric opened his laboratory to me, despite difficulties I was facing in the IGP program. I can never thank him enough for believing in me and offering his support and encouragements all along. The door of his office has always been opened, whenever I needed help or advice. I also appreciate his understanding and support when I investigated other non-academic career paths, particularly in regard to my internship in NextGxDx and the Vanderbilt Center for Technology Transfer. I would like to also thank my thesis committee chair, Danny Winder, who also provided invaluable guidance during the progress of my study, and Dr. Tiffany Wills from his laboratory for helping me in collecting brain slices for some experiments. I also want to thank my other committee members Drs. Bruce Carter, Anne Kenworthy and David Jacobson. They provided many insightful suggestions for my project and ensured I remained on track to reach and maintain the standards of a Vanderbilt Ph.D. graduate.

I also want to thank members of the Delpire laboratory for daily support and help. My animal experiments would have been unsuccessful without the expertise and care of Mr. Ghali Abdelmessih. I also want to give special Thanks to Dr. Jose Ponce-Coria for helping me with the studies described in Chapter 2.

The departments of MP&B department and Anesthesiology have also helped me on many occasions. Dr. Alyssa Hasty, our Director of Graduate Studies, enhanced my graduate

school experience through her openness, support, and insightful suggestions. I also thank Angie Pernell, Kelen Taylor, Kristie Lee, and Karen Gieg for helping me organize my life as a graduate student.

I would also like to thank my teachers who inspired my initial interest in biomedical science research. Mr. Tian Xi'an is my high school biology teacher who introduced me to the fantastic world of biology. Dr Xue Ding, my undergraduate advisor in Tsinghua University, gave me personal attention during my first days of experimentation in biomedical research.

There are also many friends I would like to thank for their contributions to my experience in this graduate school. Huapeng Yu, Dewei Tang and Jing Jin entered the IGP program at the same time and stood alongside during our initial days, when I was feeling lonely in a new country. I am also lucky to have friends like Qi Sun, Yujian Su, Yike Li and Dayi Bian. They were always around when I needed support, especially during those tough days that are part of the life of a graduate student.

As a member of the Vanderbilt Table Tennis Club, I was able to make a lot of friends from different background, but similar interests. I want to thank the Vanderbilt Recreation Center for their support to the Table Tennis Club, for including me in the varsity team and allowing me to participate to the National Collegiate Table Tennis Association tournament in Atlanta, GA. The Vanderbilt BRET career development office and the Vanderbilt International Students and Scholars Service office also provided help whenever needed.

At last, I would like to thank my parents in China, my mother and my father. They understood that graduate school in the US is not easy but they never tried to pressure me

to stay in China. I thank them for telling me that the most important thing to them was that I am healthy and happy. Without their love and support, I would never have been able to finish this degree.

TABLE of CONTENTS

Page

LIST OF TABLES

LIST OF FIGURES

I. Introduction

1. The family of cation-chloride cotransporters

Cation-chloride cotransporters are integral membrane proteins encoded by the SLC12A genes. They transport cations such as Na^+ and/or K^+ together with Cl^- across the plasma membrane. There are nine members in this family: one sodium-chloride cotransporter (NCC), two sodium-potassium-chloride cotransporters (NKCC1-2), four potassium-chloride cotransporters (KCC1-4), and two orphan members: CCC8 and CCC9 with no known functions (Table 1). The transport of these ions does not directly consume energy or change the electrical charge across the plasma membrane, therefore these transporters are called "secondary active electroneutral" cotransporters. The cation-chloride cotransporters take their energy from the Na^+ or K^+ gradient generated by the Na^+/K^+-ATPase (Figure 1) (Price et al., 2009). In this family of proteins, members have different expression patterns in mammals, thereby they show a very wide range of physiological functions. Due to the ion gradient across the cell membrane, in most cases, NKCC and NCC cotransporters move Na^+, K^+ and Cl^- into the cell, whereas KCCs transport these ions out of the cells (Gagnon and Delpire, 2013). The major functions of these transporters are regulation of intracellular chloride concentration ($[Cl^-]_i$), trans-epithelial movement of ions, and cell volume regulation following osmotic challenges.

A few human genetic diseases have been linked with mutations of genes in this family. For examples, mutations in NCC and NKCC2 lead to two syndromes called Gitleman's syndrome (NCC, (Simon and Lifton, 1996)) and Bartter's (NKCC2, (Simon et al., 1996)) syndromes. In Bartter syndrome, the deficit is located in the ascending thick limb of the

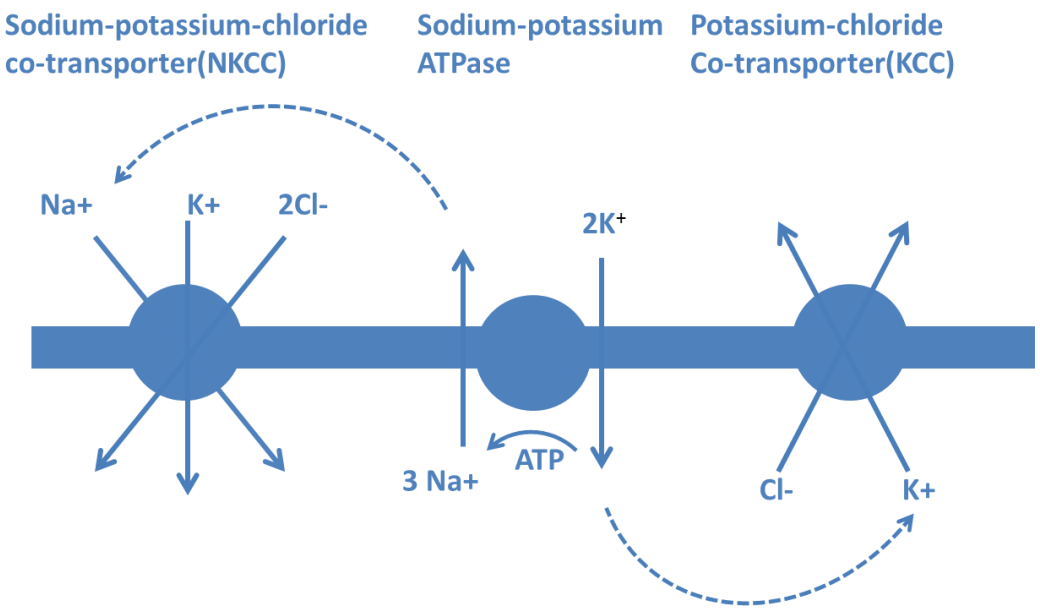

Figure 1. Cation-chloride cotransporters.

NKCC transports Cl^- into the cell, whereas KCC transports Cl^- out of the cell. Both processes are electroneutral and take advantage of concentration gradients generated by the Na^+/K^+-ATPase (dotted arrows).

loop of Henle, whereas in Gitelman syndrome, the deficit happens in the distal convoluted tubule (Ng et al., 2006). The phenotypes of these two renal diseases include imbalance of ions resulting in hypokalemic metabolic alkalosis, hypomagnesaemia, and hypercalciuria (Roser et al., 2009). In both syndromes, the impairment of NaCl reabsorption causes mild volume depletion, which leads to increases in renin and aldosterone release, resulting in K^+ and H^+ losses. Mouse models have been created with disruption of the genes encoding NCC and NKCC2 (Kemter et al., 2010; Schultheis et al., 1998; Takahashi et al., 2000). These mice recapitulate the major symptoms of Gitleman and Bartter patients such as ion imbalance, metabolic acidosis and hypokalemia. Even though no human diseases resulting from NKCC1 mutations have been discovered, mouse models where NKCC1 is deleted have been established by several groups. The NKCC1 knockout mice have hearing loss, reproduction deficit, and impairment of salivation among other phenotypes (Delpire et al., 1999; Dixon et al., 1999; Flagella et al., 1999). NKCC1 is expressed in certain epithelial cells of the mouse inner ear, and when it is deleted, we observe significant structural changes due to disrupted endolymph and endocochlear potential. NKCC1 is also expressed in spermatogonia (testis), sensory neurons (DRG), and many Cl^- secreting epithelia, explaining the multitude of phenotypes observed in the knockout mouse.

For the four potassium chloride cotransporters, KCC2 is a neuron-specific member, found only in central neurons, i.e. brain and spinal cord. Currently, there are no human diseases related to KCC2 mutations, however, KCC2 has been shown to play a very important role during the development of mammalian neurons. KCC2 knockout mice

have been made but they die shortly after birth because of respiratory failure (Hubner et al., 2001).

In the mammalian nervous system, KCC2 and NKCC1 is a pair of transporters which are important in modulating the activity of GABAergic (γ-amino butyric acid) neurons. In immature neurons (young animals), NKCC1 expression is high, leading to strong inward transport of chloride and high $[Cl^-]_i$. When GABA activates its receptor, the high $[Cl^-]_i$ in the neuron facilitates the generation of a depolarizing current, which increases the chance of triggering an action potential. Upon neuronal maturation, the expression of NKCC1 gradually decreases while KCC2 expression increases, strengthening or favoring the transport of Cl^- out of cell. Eventually the $[Cl^-]_i$ is reduced to values that are lower than the electrochemical equilibrium potential of Cl^-. In this situation, when GABA binds to its receptor, the current becomes hyperpolarizing and inhibitory, which is the normal condition for adult neurons (Ben-Ari et al., 2012; Lu et al., 1999; Plotkin et al., 1997) (Figure 2).

In contrast, this "developmental switch" between NKCC1 and KCC2 does not occur in peripheral/dorsal root ganglion (DRG) neurons, where GABA-mediated current remains constantly depolarizing, due to sustained NKCC1 expression and absence of KCC2 expression. The high NKCC1expression and activity leads to $[Cl^-]i$ accumulation, leading to partial depolarization of the terminals of primary afferent neurons. This partial depolarization filters sensory noise and reduces the number of available Ca^{2+} channels upon activation, thus imposing an inhibitory effect (Rathmayer and Djokaj, 2000). This inhibitory input in primary afferents leads to a very important concept in neuroscience: presynaptic inhibition (Rudomin and Schmidt, 1999)(Figure 3). In a NKCC1 knockout

mouse model, severe locomotor deficit and nociception deficits were observed, revealing a key role for NKCC1in sensory perception.

2. The K-Cl cotransporter-3, KCC3

2.1. Discovery and Structure

K-Cl cotransporters were first discovered from swelling- and *N*-ethylmaleimide (NEM)-activated K^+ efflux studies in sheep red blood cells (Dunham and Ellory, 1981; Lauf and Theg, 1980). Since then, four K-Cl cotransporters have been identified in a variety of tissues and cells: neurons, vascular smooth muscle, endothelium, heart (Adragna et al., 2000; Amlal et al., 1994; Greger and Schlatter, 1983; Perry and O'Neill, 1993; Rivera et al., 1999; Weil-Maslansky et al., 1994; Yan et al., 1996). KCC1 and KCC2 were first identified in 1996 (Gillen et al., 1996; Payne et al., 1996), followed three years later with the identification of KCC3 and KCC4 (Hiki et al., 1999; Mount et al., 1999; Race et al., 1999).

The structure of four KCC proteins is very similar with 12 transmembrane domains (TM) and a large extracellular loop located between TM5 and TM6 (Figure 4) (Gamba, 2005). KCC3 has a variety of potential phosphorylation sites, which make it a natural target of kinases for regulation (Gagnon and Delpire, 2012). Human KCC2 and KCC3, for instance possess the Arg-Phe-Xaa-Val (RFXV) amino acid sequences, which are binding sites for STE20/SPS1-related proline/alanine-rich kinase (SPAK) and oxidative stress responsive kinase 1 (OSR1) kinases.

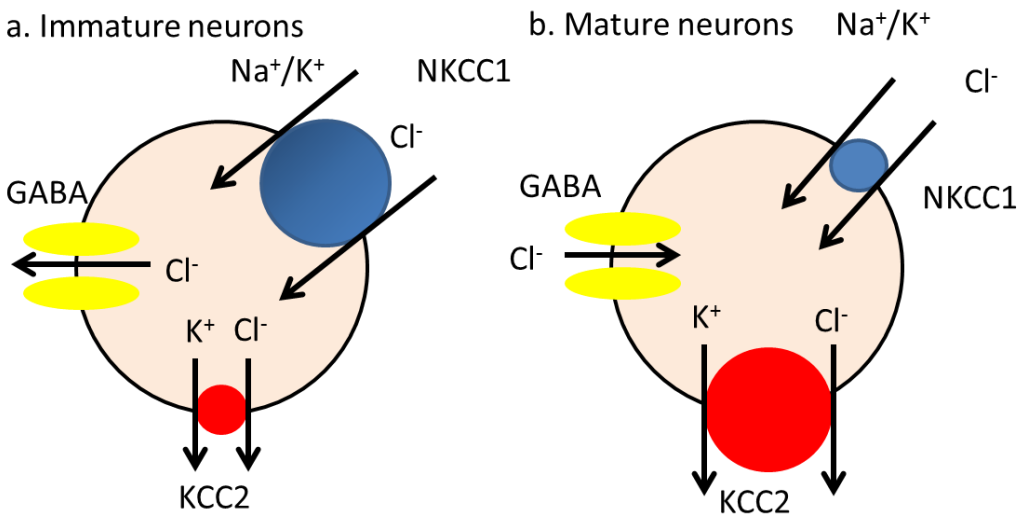

Figure 2. Diagram showing NKCC1, KCC2 and the switch of the Cl^- movement in neuron development.

A, In immature neurons, NKCC1 expression is high and GABAergic current is depolarizing and excitatory. B, In mature neurons, KCC2 expression is high and GABAergic current is hyperpolarizing and inhibitory.

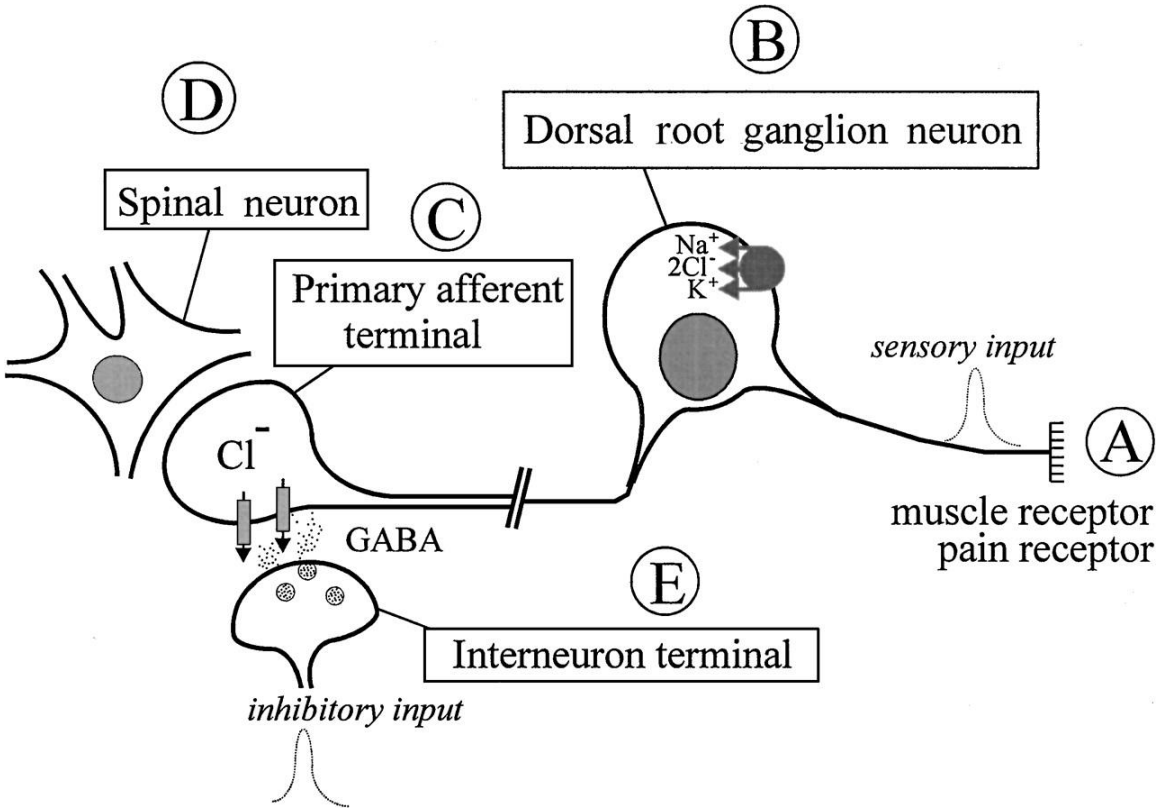

Figure 3. NKCC1 cotransporter in dorsal root ganglion neurons. (Figure from Delpire lab).

(*A*) Sensory inputs from peripheral receptors are sent to the spinal cord through primary afferent fibers. (*B*) Sensory information is processed through dorsal root ganglion neurons where NKCC1 is expressed abundantly. (*C*) Due to the high activity of NKCC1, intracellular chloride concentration is high and induces depolarizing GABAergic currents. (*D*) Sensory information is transmitted to neurons in the spinal cord for further processing. (*E*) Interneurons send inhibitory input into primary afferent terminals, releasing GABA neurotransmitters and causing presynaptic inhibition.

Our laboratory showed that SPAK and OSR1 are two kinases directly regulating KCC activity (Piechotta et al., 2002). There are several reports showing that WNK kinases and SPAK and OSR1 kinases in heterologous systems inhibit K-Cl cotransport, whereas another study failed to observe an inhibitory effect of SPAK on KCC through overexpressing the kinase(de Los Heros et al., 2006; Garzon-Muvdi et al., 2007; Kahle et al., 2005; Kahle et al., 2006). These discrepancies reveal the complexity of the phosphorylation studies for this family of transporters.

2.2 Spatial KCC3 Expression

Through detailed studies, the expression of KCC3 transcript has been confirmed in a wide variety of organs and tissues: muscle, brain, spinal cord, kidney, and placenta (Hiki et al., 1999; Mount et al., 1999). Because of the presence of two alternative promoters, there are two KCC3 transcripts. The longer transcript expressing exon1a is called KCC3a and the shorter transcript is KCC3b (exon1b) (Pearson et al., 2001). Exon 2, which is a cassette exon, produces isoforms that contain or miss a 15 amino acid peptide (Mercado et al., 2005). KCC3a has a stronger presence in the brain whereas KCC3b is more abundant in the kidney. KCC3a is found in many regions of the nervous systems such as hypothalamus, cerebellum, brain stem, cerebral cortex and choroid plexus. While neurons mostly express KCC3a, there are a few non-neuronal cells such as radial glial-like cells that also express KCC3a (Shekarabi et al., 2011). A human disease called Andermann syndrome has been linked to mutations in KCC3 and this will be discussed later.

2.3. KCC3 function and activity

Since its discovery in 1999, KCC3 has been studied in a variety of tissues, and the cotransporter mediates different functions, depending on its location. One of the best characterized roles of KCC cotransport is cell volume regulation, the process by which a cell is able to restore its normal volume following an osmotic challenge (Waldegger et al., 1998). In a KCC3 knockout mouse model created by a German Group, renal cells and hippocampal neurons displayed deficit on cell volume regulation (Boettger et al., 2003). By taking advantage of this KCC3–/– mouse model, Rust and coworkers created a double knockout mouse in which both KCC1 and KCC3 were deleted (Rust et al., 2007). While the $KCC1^{-/-}$ mouse did not show any transport deficit in red blood cells and $KCC3^{-/-}$ mice exhibited decreased K-Cl cotransport activity, in the double knockout mouse, the K-Cl cotransport activity was almost completely abolished, suggesting a bigger role of KCC3 in these cells (Rust et al., 2007).This KCC3 knockout mouse displayed progressive hearing loss, which was also observed in KCC4 knockout mice as well. Detailed analysis showed that KCC3 was expressed in several key cell populations of the inner ear, including supporting cells of the hair cells and the organ of Corti epithelial cells. Loss of KCC3 leads to disrupted K^+ transport and ion balance in the cochlea, which would eventually cause degeneration of sensory hair cells and ultimately deafness.

Another phenotype exhibited by $KCC3^{-/-}$ mice is an increased arterial blood pressure. Since chloride concentrations affects contraction activity of smooth muscle cells and thereby influence arterial blood pressure, it was tempting to assume that KCC3 might play a key role in vascular muscle tone activity. However, further analysis showed that this hypertension phenotype was actually due to increased activity of the sympathetic

Table 1. The SLC12 family of cation-coupled Cl^- cotransporters

Member	Co-transport ions	Tissue distribution	Disease
SLC12A1 (NKCC2)	Na^+-K^+-2Cl^-	Kidney-specific (TAL)	Bartter's syndrome type I
SLC12A2 (NKCC1)	Na^+-K^+-2Cl^-	Ubiquitous	None
SLC12A3 (NCC)	Na^+-Cl^-	Kidney-specific (DCT); bone?	Gitelman's syndrome
SLC12A4 (KCC1)	K^+-Cl^-	Ubiquitous	None
SLC12A5 (KCC2)	K^+-Cl^-	Neuron-specific	None
SLC12A6 (KCC3)	K^+-Cl^-	Widespread	Anderman's syndrome
SLC12A7 (KCC4)	K^+-Cl^-	Widespread	None
SLC12A8 (CCC9)	Unknown	Widespread	Psoriasis
SLC12A9 (CIP)	Unknown	Widespread	None

The SLC12 family consists of nine members. The transported ions, tissue distribution in mammals, and corresponding disease due to genetic mutations in humans are shown.

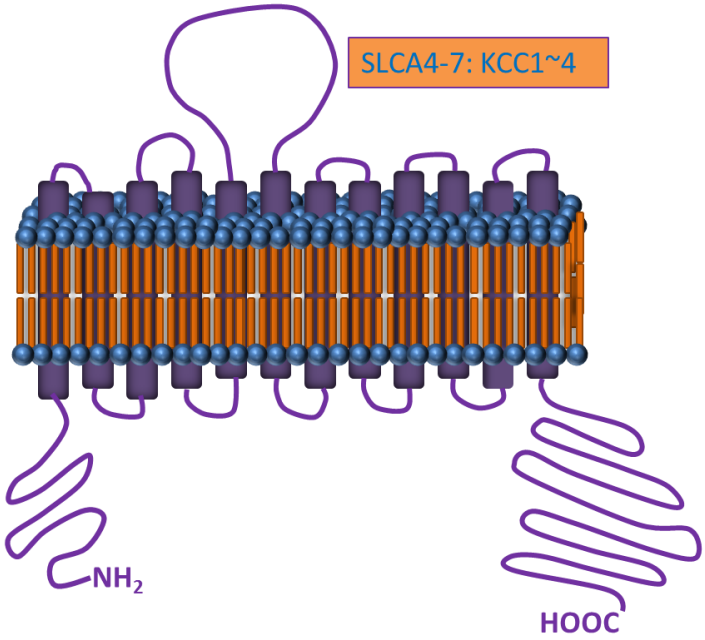

Figure 4. Structural topology for KCC cotransporters.

For KCC proteins, there are 12 transmembrane domains, a large extracellular loop between the fifth and sixth transmembrane domain and a long carboxyl end.

nervous system (Rust et al., 2006). More importantly, mice lacking the KCC3 cotransporter also display severe locomotor deficit and progressive sensorimotor neuropathy in both peripheral and central nervous systems, which is addressed in the next section (Boettger et al., 2003; Byun and Delpire, 2007; Howard et al., 2002).

3. Peripheral Neuropathy Disorders

Peripheral neuropathy is the occurrence of a neuropathy in the peripheral nerves, which include motor, sensory, and autonomic nerves transmitting information between the central nervous system and peripheral organs (Hughes, 2002). It is a very common symptom with a fairly high prevalence rate. Indeed, it is estimated to affect about 2.4% of the US population, and this incidence rate increases to 8% for people older than 55 years. A recent study estimated the patient population suffering from peripheral neuropathy in the US to be around 20 million.

Because of the wide range of peripheral nerves, the clinical symptoms of peripheral neuropathy vary widely (England and Asbury, 2004). Generally there are three major types of symptoms: sensory symptoms, weakness symptoms (motor) and autonomic symptoms. The diagnosis of this disorder requires detailed research on the patient's history, clinical examination, electromyogram (EEM) studies, blood testing, glucose levels, nerve conduction studies, and lumbar puncture (Huan, 2010). Based on the number and distribution of nerves affected, or the process affecting the nerves, peripheral neuropathy can be further classified into different subtypes for treatment. The most common neuropathy is the diabetic sensorimotor polyneuropathy, which appears in more

than half of the total diabetic population. Since the diabetes prevalence has been increasing all the time, it is estimated that diabetic neuropathy may affect 1% of the total US population currently (Van Acker et al., 2009). Another common neuropathy is idiopathic neuropathy, meaning that the cause of this neuropathy is unknown (Hughes, 1995). In other parts of the world such as Southeast Asia, India, Africa, the highly prevalent leprous neuritis disease is still the leading cause of neuropathy (Martyn and Hughes, 1997). Beside these causes mentioned above, other factors such as infectious agents, vasculitis and toxins can also induce peripheral neuropathy. The treatment of neuropathy depends on accurate diagnosis of specific peripheral nerves affected. Glycemic control is very important for diabetic neuropathy, while a few immune-based modulating methods are available for idiopathic neuropathy. Right now there are no effective and potent strategy to completely cure this disorder, most of the current treatment methods focus on improvement of patient conditions (Torpy et al., 2010).

4. HMSN/ACC

4.1. Disease overview

Peripheral neuropathy associated with agenesis of the corpus callosum (ACCPN, OMIM#: 218000), also known as hereditary motor and sensory neuropathy associated with agenesis of the corpus callosum (HMSN/ACC), or Andermann syndrome, is a hereditary autosomal recessive human disease (Dupre et al., 2003). This disease was first described in 1966 by Leblanc and colleagues and then subsequently characterized by Andermann and colleagues in 1970s (Andermann et al., 1975; Andermann et al., 1972). One of the

hallmarks of this disorder is the agenesis of the corpus callosum, which is a thick band of nerve fibers connecting the left and right hemisphere. Corpus callosum is very important for communication between the two cerebral hemispheres and the agenesis and degeneration lead to multiple neurological symptoms for both motor and sensory functions. It was found that not all ACCPN patients have this symptom in postmortem examination, and the degree of agenesis also varied among patients. Other common symptoms include abnormal or absent reflexes, intellectual disability, weak muscle tone, and dysmorphism of different organs. Most patients can live until adulthood, but usually they will die by their third decade, although the care of patients is improving and extending life (Dupre et al., 2003).

This is a very rare hereditary human disease with only a few sporadic reports available from most parts of the world. However, ACCPN has a very high prevalence in two regions of Quebec, Canada: the Saguenay-Lac-St-Jean region and in Charlevoix County. In the local French Canadian population, the overall incidence rate of ACCPN is 1 in 2,117 live births and the carrier rate is 1 in 23. The genetic mutations of ACCPN in this area was traced back to a set of 22 French individuals from Poitou, Perche, and other regions who migrated to Canada in the 17^{th} century (De Braekeleer et al., 1993). Therefore, this founder effect is the major reason for such a high disease prevalence in this region of Canada.

Since its first description, extensive studies have been performed to uncover the cause of the disease. In 1996, a genome wide analysis in Quebec French Canadian population was performed using microsatellite DNA markers (Casaubon et al., 1996). The authors were

able to map the ACCPN gene to a region on the long arm of chromosome 15, thus making a significant step towards the identification of the ACCPN gene. It was the cloning of KCC3 at Vanderbilt University (Mount et al., 1999), the mapping of the gene to the same region of chromosome 15, the foresight of the possible connection, and the collaborative work of the Vanderbilt and McGill groups that led to the identification of the KCC3 gene as the gene involved in HMSN/ACC (Howard et al., 2002) .

Ten different KCC3 mutations have been found in ACCPN patients around the world. Among them the most common one is the mutation found in the French Canadian population in Quebec, Canada. It is a guanine deletion in exon 18 of the SLC12A6 gene (c.2436delG, Thr813fsX813), resulting in a frame shift mutation and truncated KCC3 protein (Howard et al., 2002). Another frame shift mutation was found in exon 15 (c.2023C-T, Arg675X) in an Italy case, resulting a truncated KCC3 protein as well. In fact most of the known ACCPN mutations lead to a truncated KCC3 protein where the C-terminus is absent, suggesting a possible role of the C-terminus of KCC3 in the development of ACCPN.

4.2. Animal models

In 2001-2002, our laboratory generated the first animal model for ACCPN by deleting exon 3 from the mouse Slc12a6 gene by homologous recombination (Howard et al., 2002). Exon 3 (95 bp) encodes a small portion (31 amino acids) of the N-terminal of the cotransporter and its deletion not only eliminates this sequence, but places the remainder of the protein out-of-frame, so that no functional protein can be expressed. Initial

observations failed to show an overt phenotype, except a low posture. However, closer observations revealed the presence of a significant locomotor deficit in these knockout mice. Three tests were used to assess the locomotor deficit: a rotorod test, a wire-hang test and a beam-task test. Compared with the control or heterozygotes, the homozygote knock outs failed all three tests, suggesting a severe impairment of the normal locomotor function (Figure 5). The pathology of the knockout mice was also examined. In the knockout, anatomical analysis showed severe neuron degeneration in the sciatic nerves, including myelin debris and thin myelin layers. Further analysis of the sciatic nerves of the mutant mice showed axonal and periaxonal swelling and axon and myelin degeneration (Byun and Delpire, 2007). These results explained the locomotor deficit phenotype and recapitulated the pathology seen in peripheral nerves of patients with ACCPN (Dupre et al., 2003).

In 2003, a group in Germany created a separate mouse model of ACCPN by deleting the whole region after exon 1 of KCC3 (Boettger et al., 2003). In this independent study, the authors also observed severe motor function deficit and progressive neurodegeneration as seen in the previous mouse model. In addition, this new $KCC3^{-/-}$ mice revealed some additional important phenotypes. Even though no seizure activity was observed in these mice, the seizure threshold in the knockout mice was reduced. The electrocorticograms of the mutant mice had a very similar pattern to those obtained from patients with Andermann syndrome. As mentioned above, arterial blood pressure of the mutant mice was significantly higher than that of control mice, likely due to an elevated sympathetic tone. The mutant mice also lost their hearing ability slowly, revealing a new role of

KCC3 in inner ear. By revealing additional roles of KCC3, this study provided an invaluable mouse model for ACCPN disease.

In order to further define the role of KCC3 in the pathogenic mechanisms leading to ACCPN, Guy Rouleau and colleagues recently created a neuron-specific KCC3-null mouse line (Shekarabi et al., 2012). The neuron-specific KCC3-null mice showed similar locomotor deficit as the straight KCC3-null mice, however, the auditory defects observed in ubiquitous KCC3-null mice were missing in the neuron-specific ones, consistent with intact function of KCC3 in non-neuronal cells in the cochlea. This novel model confirmed a key role of KCC3 in the nervous system and provided important insights about the origins of this disease.

5. Creation of genetically-modified mouse models

In current biomedical research, model organisms have become critical tools in helping scientists understand specific biological processes. The principle of biological universality, which infers that "rigorous and analytic study of the biology of any organism is likely to lead to findings of importance in the understanding of other organisms" , has been widely accepted among scientists (Horvitz, 2003). Model organisms include the bacterium *Escherichia coli*, bakers' yeast *Saccharomyces cerevisia*e, the nematode worm *Caenorhabditis elegans*, the fruit fly *Drosophila melanogaster*, and the mouse *Mus musculus* (Fields and Johnston, 2005). Every model

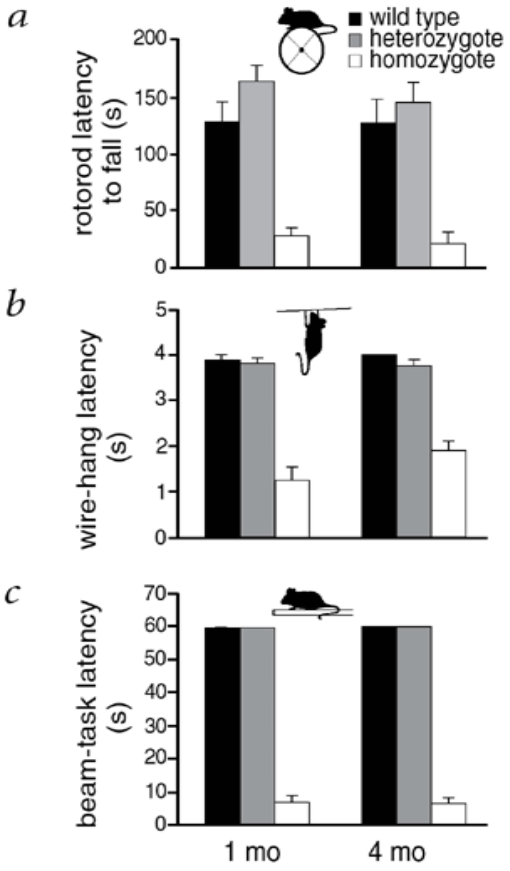

Figure 5. Slc12a6-mutated mice showed significant motor deficit. (Figure from Delpire lab).

In three different motor function tests (a−c), significant deficits were observed in homozygous but not heterozygous mutant mice as compared to wildtype mice.

organism has a unique set of advantages and disadvantages which make it useful for a particular set of scientific problems. In the study of a complex human disease such as ACCPN, the mouse *Mus musculus* has emerged as a premier candidate for understanding the human disorder. The mouse shares 99% of its genes with human, and it has been used to study many important human disorders, such as hypertension, diabetes, cancer, heart disease and neurological illnesses. Compared to larger mammals such as dogs or primates, the mouse is advantageous due to its small size, relatively shorter gestation period, and cost of maintenance (Peters et al., 2007). In 2007, a trio of scientists (Drs. Mario R. Capecchi, Martin J. Evans, and Oliver Smithies) was awarded the Nobel Prize in Physiology/Medicine for their innovative work in producing genetically modified mice with the embryonic stem (ES) cells and homologous recombination technology.

With the gene targeting technology, scientists are able to introduce foreign genes into the mouse genome to create transgenic mice, or modify existing genes by homologous recombination in embryonic stem cells, thus generating knockout or knock-in mice (Figure 6). A knockout mouse is genetically engineered to inactivate a gene or "knock out" its product. This can be achieved by either introducing a piece of DNA or removing an exon with the goal of disrupting the transcript (Anagnostopoulos et al., 2001). The deletion of the gene will mostly induce relevant phenotypes associated with the normal function of the corresponding gene, including behavior and other physical and biochemical features. In contrast, a mouse “knock-in” takes advantage of the native promoter to either drive expression of the protein which has been changed with the addition of an epitope tag or with a mutation. The knock-in strategy can also be used to

drive the expression of another protein. A knock-in mouse can result in a phenotype similar to that of a knockout if the mutation also leads to a non-functional protein.

Knockout mice with a specifically targeted gene are often used as animal models of hereditary human diseases (Friedel et al., 2011). However, in many cases the gene deleted is very essential therefore the knockout mouse is embryonic lethal. An alternative strategy to go around the lethality is to deactivate the gene in certain and specific conditions by taking advantage of the Cre-loxP system where a Cre mouse line and a loxP mouse line are both required (Garcia-Otin and Guillou, 2006). For the loxP mouse line, a targeted gene is modified by inserting two loxP sites flanking the exon, therefore allowing the exon to be targeted and excised by Cre-mediated recombination. This is achieved by mating the mice containing the modified loxP gene with mice carrying the Cre recombinase under a specific promoter. This strategy will lead to gene knockout in a specific spatial or temporal manner. Indeed, there are two main subtypes of conditional knockouts: tissue specific knockouts where protein is deleted in a specific tissue or cell type, and an inducible knockout where protein disruption can be induced through diet manipulation or chemical reagents. In order to obtain expression of an altered protein, a knock-in mutation can be introduced into the mouse genome, using the same technology for knock-outs (Roebroek et al., 2011). For instance, rather than deleting an exon, the wild-type exon can be replaced with a mutated exon with altered protein product. The exon may also need to be flanked by loxP sites to allow for homologous recombination.

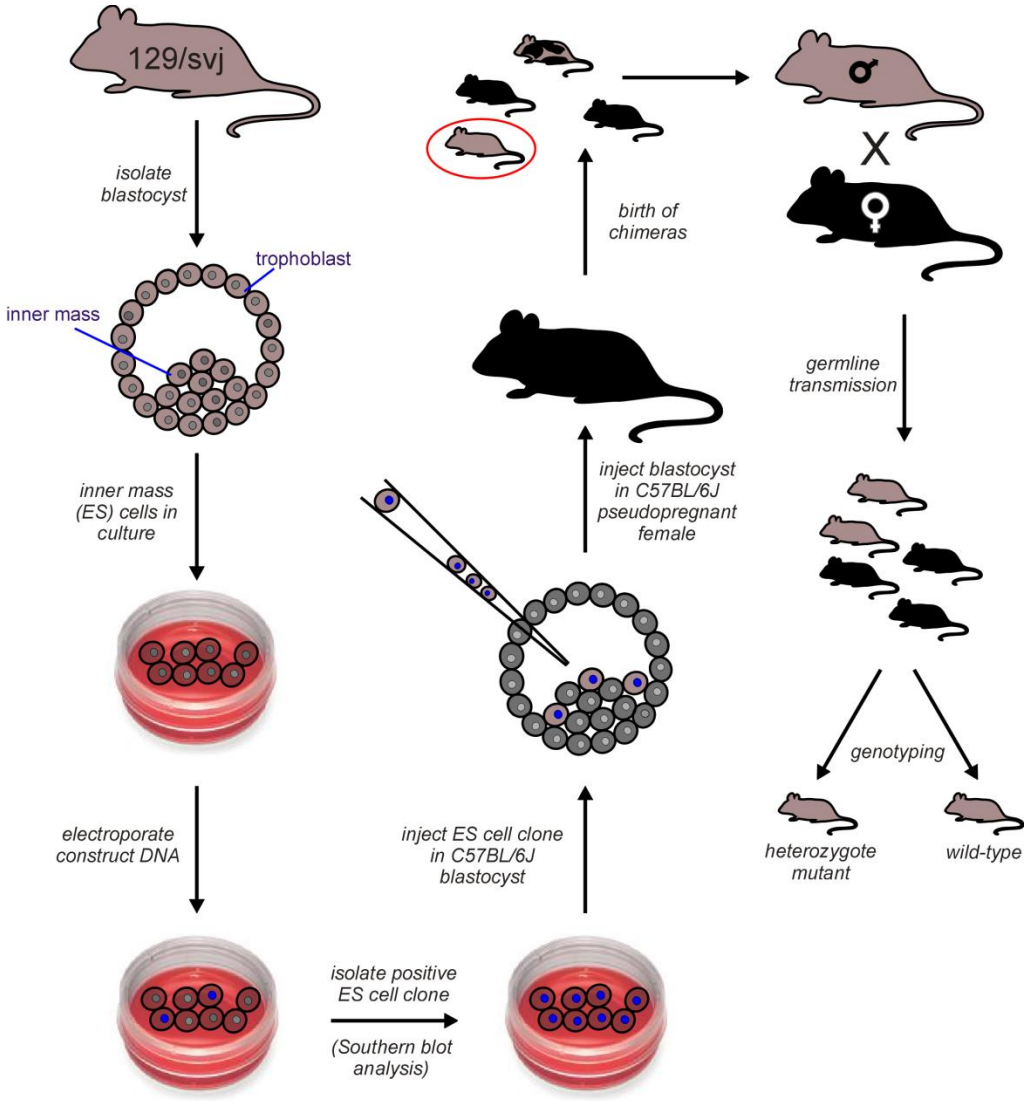

Figure 6. General procedures for creating transgenic mice.

Embryonic stem (ES) cells or inner mass cells were isolated from a mouse blastocyst and DNA construct is inserted into the cell through electroporation. After homologous recombination, positive ES cell clones are injected into C57BL/6J blastocysts which are implanted into pseudopregnant females. The newborn mice are chimeric animals created from both donor (blastocyst) and recipient (mutated ES) cells. If these chimeric animals transfer the mutation to the next generation, the progeny will carry the mutated gene.

Hypothesis and Specific Aims

Hypothesis I:

While it is clear that KCC3 is responsible for HSN/ACC (ACCPN), the precise mechanism by which the cotransporter causes the disorder is unknown. The first symptoms of ACCPN are observed in early childhood and worsen with age. The first posture and locomotion deficits are also observed early in the KCC3 knockout mouse, and also worsen with age. Whether the disorder has developmental and/or degenerative components is still unknown. In fact, it is not even known if absence of the K-Cl cotransport function of KCC3 is required to produce the disorder. Indeed, since all (but one) ACCPN-causing mutations in KCC3 result in either absence of protein or in truncated proteins, and the knockout models also generate absence of KCC3, it is possible that absence of the protein or a specific protein domain, rather than the absence of the K-Cl cotransport function of KCC3, is responsible for the disorder.

During the cloning of the mouse KCC3 by RT-PCR, the laboratory created a cDNA which when transcribed failed to demonstrate K^+ transport in *Xenopus laevis* oocytes. The cDNA was re-sequenced and an adenine to guanine substitution at nucleotide position 866, leading to mutation of glutamic acid residue 289 into a glycine (E289G), was identified. As this mutation is located in an extracellular loop between two transmembrane domains, the mutation is unlikely to affect the structure of the cotransporter. **Therefore, I hypothesize that an E289G knock-in mutation resulting in absence of K-Cl cotransport function in the mouse will tell us if the absence of K-Cl cotransport function is required for the development of the neuropathy.**

Specific Aim I: To characterize the absence of KCC3-E289G function *in vitro*. This will be achieved by studying KCC3-E289G in *Xenopus laevis* oocytes and in HEK293 cells. Expression and trafficking of the KCC3-E289G protein will be examined in both heterologous expression systems.

Specific Aim II: To create and characterize the phenotype of a KCC3-E289G knock-in mouse. This will be achieved by knocking-in mutated exon 7 by homologous recombination, obtaining viable homozygous animals and studying its locomotor phenotype.

Hypothesis II:

In humans, morphological abnormalities are found in both grey and white matter, suggesting that the ACCPN disorder affects both neurons and supporting cells. In the mouse of KCC3 *null* mice, although the agenesis of the corpus callosum (white matter tracts dividing the two brain hemispheres) is not observed, vacuoles are observed in brain, spinal cord, and nerves, suggesting pathology of supporting cells. Nerves in particular present deficits that seem to affect both neurons and Schwann cells. Thus, understanding the precise cellular origin of the disorder might help us design strategies to understand the role that the cotransporter plays in the disease. **Thus, I hypothesize that a very specific population of neurons is responsible for the development of ACCPN.**

Specific Aim I: To create a novel KCC3flox mouse and several tissue-specific KCC3 knockout to identify the cellular origin of the neuropathy. This will be achieved by targeting the KCC3 locus by homologous recombination and obtaining a viable KCC3

floxed line and crossing this line with several transgenic CRE lines, thus targeting neurons in general, proprioceptive neurons, nociceptive neurons, and Schwann cells.

Specific Aim II: Characterize the locomotor phenotype of these tissue-specific KCC3 knockout mice. This will be achieved by creating cohort of each tissue-specific knockout mouse and appropriate controls and assess locomotor activity through the use of accelerated rotorad test and distance traveled in open field. When appropriate, combine these studies with immunohistochemistry studies to further characterize these mice.

II. Characterization of KCC3 E289G mutant *in vitro*

1. Introduction

In mammals, electroneutral and Na^+-independent K–Cl cotransport is mediated by 4 distinct genes: SLC12A4-A7 (Gagnon and Delpire, 2013). The products of these genes (KCC1-KCC4) fulfill a variety of physiological roles which include cell volume maintenance and regulation (Hoffmann et al., 2009) , Cl^- homeostasis (Blaesse et al., 2009; Delpire, 2000; Kahle et al., 2008; Lauf et al., 2006), epithelial transport (Lauf et al., 2006), control of migration, proliferation, and invasiveness (Chen et al., 2010). K–Cl cotransporters are regulated by phosphatases (Jennings and Schulz, 1991) and the WNK-SPAK/OSR1 phosphorylation cascade (Gagnon and Delpire, 2012; Kahle et al., 2010) .

Mutations in SLC12A6, the gene which encodes for the K–Cl cotransporter-3 (KCC3), results in a rare autosomal recessive neurological disorder known as Hereditary Motor and Sensory Neuropathy/Agenesis of the Corpus Callosum (HSMN/ACC) (OMIM 218000; (Boettger et al., 2003; Howard et al., 2002)). The pathological hallmarks of this syndrome, with high prevalence in the French-Canadian population of Quebec, are a peripheral neuropathy which is often associated with variable agenesis of the corpus callosum, areflexia, mental retardation, and psychosis (Filteau et al., 1991; Larbrisseau et al., 1984). KCC3-deficient mice exhibit not only the early onset and severe locomotor deficits similar to the crippling human peripheral neuropathy disorder (Howard et al., 2002), but also high blood pressure, age-related deafness, and renal dysfunction (Boettger et al., 2003). At the ultrastructural level, KCC3-deficient mice exhibit axonal and peri-axonal swelling indicating both neuronal and Schwann cell defects (Byun and Delpire,

2007). A recent study that used a synapsin 1-CRE mouse to drive deletion of neuronal KCC3 expression reproduced the neuropathy phenotype observed in the KCC3 knockout mouse (Shekarabi et al., 2012).

Injection of KCC3-T813X, the prevalent mutation observed in the French-Canadian population, in *Xenopus laevis* oocytes demonstrated expression of a glycosylated protein of a smaller molecular size at or near the oocyte plasma membrane similar to wild-type KCC3. In contrast, a novel and more distal HMSN/ACC truncating mutant (KCC3-R1134X) failed to traffic properly to the plasma membrane (Salin-Cantegrel et al., 2011).

Several studies have reported expression of more than one K–Cl cotransporter isoform in cells and tissues, including red blood cells (Crable et al., 2005); glial cells (Gagnon et al., 2007); vascular smooth muscle cells (Di Fulvio et al., 2001); and suprachiasmatic neurons (Belenky et al., 2010). In fact, most large CNS neurons such as cortical or hippocampal pyramidal cells express both KCC2 and KCC3 (Pearson et al., 2001), and disruption of either cotransporter elicits shifts in the GABA reversal potential (Boettger et al., 2003). The fact that cells express multiple KCC isoforms suggests the intriguing possibility that these cotransporters interact with one another, a view supported by an early evidence of isoform hetero-dimerization (Casula et al., 2001).

In this study, we take advantage of a full-length KCC3-E289G mutant that maintains the entire open reading frame, but renders the cotransporter functionally inactive to assess interaction, trafficking, and function of co-expressed K-Cl cotransporters. While this mutation is not found in nature, it still provides important information on a specific residue of the K–Cl cotransporter and constitutes a very useful tool to study its trafficking

and hetero-oligomerization. We provide evidence that K–Cl cotransporter isoforms interact in *Xenopus laevis* oocytes and affect each other's function. We demonstrate that the mutant KCC3-E289G protein resides in the endoplasmic reticulum (ER), is not properly glycosylated, and does not traffic to the plasma membrane. Furthermore, we show that the E289G mutant also prevents wild-type KCC3 as well as another K–Cl cotransporter isoform to traffic to the plasma membrane.

2. Methods

Cloning of mouse KCC3 cDNA. The entire open reading frame of the mouse KCC3a was constructed by ligating into Bluescript (pBSK+) several PCR fragments obtained from David B. Mount (Vanderbilt University). The clone was sequenced and moved into the oocyte expression vector pBF. As the cDNA failed to demonstrate K^+ transport, the cDNA was re-sequenced and an adenine to guanine substitution at nucleotide position 866, leading to mutation of glutamic acid residue 289 into a glycine was identified. After the mutation was corrected using QuikChange mutagenesis, the clone was re-sequenced and re-tested for functionality.

Isolation of *Xenopus laevis* oocytes. All procedures performed with frogs were approved by the Vanderbilt University Institutional Animal Care and Use Committee. Stages V and VI *Xenopus laevis* oocytes were isolated from 16 different frogs as previously described (Delpire et al., 2011) and were maintained at 16°C in modified L15 medium (Leibovitz's L15 solution diluted with water to a final osmolarity of 195-200 mOsM, supplemented with 10 mM HEPES and 44 μg of gentamicin sulfate). The next day, oocytes were

injected with 50 nl of water containing 2-15 ng of cotransporter cRNA (concentrations are indicated in specific experiments) and oocytes are incubated for 3 days prior to use.

K^+ uptakes in *Xenopus laevis* oocytes. Groups of 20-25 oocytes were washed once with 3 ml isosmotic saline (96 mM NaCl, 4 mM KCl, 2 mM $CaCl_2$ 1 mM $MgCl_2$, 5 mM HEPES buffered to pH 7.4, 200 mOsM) and pre-incubated for 15 min in 1 ml Na^+ free isosmotic or hyposmotic saline containing 1 mM ouabain. The solution was then aspirated and replaced with 1 ml Na^+ free isosmotic or hyposmotic flux solution containing 5 µCi ^{86}Rb. Two 5 µl aliquots of flux solution were sampled at the beginning f each ^{86}Rb uptake period and used as standards. After 1 h uptake at room temperature, the radioactive solution was aspirated and the oocytes were washed 4 times with 3 ml ice-cold Na^+ free isosmotic or hyposmotic solution. Single oocytes were transferred into glass vials, lysed for 1 h with 200 µl 0.25N NaOH, neutralized with 100 µl glacial acetic acid, and ^{86}Rb tracer activity was measured by β-scintillation counting. KCC flux is expressed in nmoles K^+/oocyte/h.

Immunoprecipitation. Stage V-VI *Xenopus laevis* oocytes were microinjected with 15 ng each mKCC3 and/or rKCC2 cRNAs and incubated for 3 days at 16^{o}C. Oocytes were then homogenized by passing them through a pipet tip (50 µl / oocyte) in 50 mM HEPES supplemented with Complete™ Protease Inhibitor Cocktail Tablet, EDTA-free (Roche). Homogenates were then centrifuged at 15,000 x g for 1 min and supernatants were saved for protein assay (Bradford, BioRad). An equal amount of protein was added to the HEPES buffer to a final volume of 1 ml. Immunoprecipitation was achieved by adding 10 µl of anti-GFP (IgG negative control), anti-KCC3, or anti-KCC2 antibody to the homogenate sample under gentle rotation overnight at 4°C. Then, 30 µl of pre-washed

Protein A sepharose (Santa Cruz Biotechnology, Santa Cruz, CA) was added to each homogenate and incubated for 2 h at 4 ℃. The sepharose beads or expected immunoprecipitates were washed three times with 1 ml of lysis buffer (centrifugation at 4 °C, 2000 rpm, 2 min). The immunoprecipitates were re-suspended in 75 µl of loading buffer that contained 8% β-mercaptoethanol, heated at 75 ℃ for 15 min, and subjected to SDS-PAGE.

Western Blot Analysis. Protein samples were denatured in SDS-PAGE loading buffer at 75 ℃ for 15 min and separated on a 6%, 7.5% or 9% SDS-polyacrylamide gels. The separated proteins were electroblotted onto polyvinylidine fluoride membranes through a semi-dry process, and membranes were incubated for 2 h at room temperature in blocking solution (5% nonfat milk in Tris-buffered saline with 0.5% Tween 20). Incubation of primary antibody was performed overnight at 4 °C. The dilutions used for the antibodies were: KCC3 1:250, KCC2 1:250, PDI-ER marker 1:1000, GAPDH-cytosol marker 1:1000. Membranes were washed in TBST for 3 h, incubated with their corresponding horseradish peroxidase-conjugated secondary antibody in blocking solution (1:5000) for 1 hour at RT, and washed again for 2 h in TBST. Protein bands were visualized by chemiluminescence (ECL Plus, Amersham Biosciences).

Cell surface expression in *Xenopus laevis* oocytes. Isolation of plasma membrane bound proteins was done following (Leduc-Nadeau et al., 2007). Briefly, 3 days after microinjection of cRNA, 40-60 oocytes were rinsed three times in modified MBSS (80 mM NaCl, 20 mM MOPS pH 6.0) and incubated for 10 min at room temperature with modified MBSS supplemented with 0.005% subtilisin A (Sigma, St. Louis, MO) under

gentle agitation to promote vitelline membrane digestion. Membrane polymerization was performed at 4^{o}C under mild agitation by first incubating the oocytes with modified MBSS with 1% ludox colloidal silica (Sigma), and then with modified MBSS with 0.1% polyacrylic acid (Sigma). Between each incubation period, oocytes were rinsed three times in modified MBSS. The oocytes were then homogenized with 0.5 ml of cold HbA (5 mM $MgCl_2$, 5 mM NaH_2PO_4, 1 mM EDTA, 80 mM sucrose, and 20 mM Tris pH 7.4). This homogenization was carried out manually by passing the oocytes through a 200 ul pipette tip. The homogenates were washed with 1.5 ml with HbA and centrifuged at 16 g for 30 sec at 4 ℃. The pellets were resuspended and subjected to a series of centrifugations: 16 g, 25 g and 35 g for 30 sec and max speed for 20 min. The pellets of purified plasma membranes were resuspended in 45 µl of HbA and frozen until use.

Cell culture and Transfection. HEK 293FT (Invitrogen, Carlsbad, CA) cells were maintained and routinely passaged in DMEM-F12 supplemented with 10% fetal bovine serum and 1% Penicillin/Streptomycin (Invitrogen) at 37 ℃ under 95% air, 5% CO_2. For transfection, cells were trypsinized and plated at 30% density the day prior to transfection. The cDNAs were then transfected into the cells using FuGENE 6 (Roche Applied Science) at a 3:1 ratio (DNA:transfection reagent). Transfected cells were incubated at 37 ℃ under 95% air, 5% CO_2 for 48 h prior to use.

HEK 293FT sub-cellular fractionation. The method was adapted from (Holden and Horton, 2009). HEK 293FT cells grown in 10-cm dishes were transfected with 16 ug of KCC3-pIRES _puro2 or KCC2-pIRES_puro2 and 48 h later, the culture medium was removed and cells were detached with 500 µL of Trypsin-EDTA (0.05%, Invitrogen).

Cells were resuspended in 10 ml of complete culture medium, centrifuged at 100 x g at 4^{o}C for 2 min. Next, the supernantant was aspirated and the cells were washed by gentle pipetting in 10 ml of Hank's Balanced Salt Solution. Cell suspension was centrifuged again at 100 x g at RT to pellet the cells. Supernatant was removed and the cell pellet was resuspended by gently adding 1 ml of ice cold buffer 1 (25 µg/ml digitonin, 150 mM NaCl, 40 mM HEPES pH 7.4) containing protease inhibitors (1 tablet of complete protease inhibitor cocktail per 10 ml). Cell suspension was gently rotated at 4^{o}C for 5 min. The sample was then centrifuged at 2000 x g. Supernatant which constitutes the cytosol - membrane enriched fraction was recovered and saved. The pellet was resuspended by vortexing in 1 ml of ice-cold buffer 2 (1% NP40, 150 mM NaCl, 40 mM HEPES pH 7.4). Samples were incubated on ice for 30 min and then centrifuged at 7000 x g to pellet nuclei and cell debris. The supernatant which comprises membrane bound organelles such as the ER, Golgi, mitochondria and some nuclear lumenal proteins was recovered and saved. Finally, the pellet was resuspended by vortexing in 1 ml of ice cold buffer 3 (0.5% Na-deoxycholate, 0.1% SDS, 1U/ml benzonase, 150 mM NaCl, 40 mM HEPES pH7.4). Samples were rotated gently overnight at 4^{o}C to allow complete solubilization of nuclei and digestion of genomic DNA. The supernatant which comprises nuclear membranes and nuclear proteins was finally recovered.

Immunofluorescence. HEK 293FT cells grown on glass coverslips and transfected with wild-type or mutant KCC3 were washed in PBS twice at room temperature and fixed with 2% paraformaldehyde in PBS for 30 minutes. The cells were then permeabilized by incubating them twice for 5 min with PBS containing 0.075 % saponin (Sigma, St Louis, MO). After blocking with PBS containing 0.075 % saponin and 0.2 % BSA for 30

minutes, the cells were incubated for 1 hour at RT with 150 µl primary antibodies: rabbit polyclonal anti-KCC3 antibody (1:250, (Byun and Delpire, 2007)) and mouse monoclonal anti-PDI antibody (Abcam, Ab27043 1:200), followed by 3 x 5 min washes with PBS/saponin/BSA and then incubated for 1 hour at RT with 150 µl secondary antibodies: Cy3 conjugated anti-rabbit antibody (1:1000, Jackson Immunochemicals) and Alexa Fluor anti-mouse IgG (H+L) (1:400, Invitrogen). After final 3 x 5 min washes in PBS/saponin/BSA solution, coverslips were mounted on slides using VectaShield (Vector Laboratories, Burlingame, CA) and sealed with nail polish. Fluorescence signal was visualized using a Carl Zeiss LMS 510 META confocal microscope.

3. Results

During the process of cloning the mouse KCC3 cDNA, we came across a mutation resulting in the substitution of glutamic acid residue E289 into a glycine (E289G). This negatively charge residue, located at the end of trans-membrane domain 3 (TM3) or beginning of extracellular loop 2 (ECL2) is highly conserved in all mammalian cation-chloride cotransporters (Figure 7A). Although the KCC3-E289G mutant was non-functional when expressed in *Xenopus laevis* oocytes, function was restored when the residue was mutated back into a glutamic acid (Figure 7B).

To demonstrate hetero-dimerization of K-Cl cotransporters, we chose to study the interaction between KCC3 and KCC2, a cotransporter that demonstrates activity under isosmotic conditions. In Figure 8, we co-expressed, wild-type KCC3, and KCC3-E289G in *Xenopus laevis* oocytes and used co-immunoprecipitation to show specific protein-

protein interactions. First, we immunoprecipitated KCC3 proteins and immunoblotted for KCC2 (Figure 8, panel A: lanes 4 & 5) or inversely immunoprecipitated KCC2 and immunoblotted for KCC3 (Figure 8, panel B: lanes 2 & 3). No immunoprecipitation was observed with unrelated IgG, and neither antibody cross-reacted with the other K-Cl cotransporter (Figure 8, panel A: lane 6, panel B: lane 1). Lanes 1-3 of panel A constitute internal controls. Note the smaller molecular size of the KCC3-E289G band, indicating possible impairment in glycosylation.

Next, we measured K-Cl transport activity through K^+ influx measurements in *Xenopus laevis* oocytes (Figure 9A). Under isotonic conditions, KCC2-injected oocytes showed significant K^+ influx compared to water-injected oocytes. Under isotonic conditions, KCC3-injected oocytes showed no activity, but the activity could be observed upon hyposmotic treatment. When co-injected with wild-type or E289G mutated KCC3, KCC2 activity was significantly reduced compared to KCC2 alone under isotonic conditions. Because KCC3 is inactive under isosmotic conditions, we also examined the effect of KCC3 wild-type and KCC3-E289G on KCC2 under hypotonic conditions. Based on the activity of each cotransporter under hypotonic conditions, we anticipated an additive effect (showed by the arrowed vertical line). However, we again observed a flux that was smaller than KCC2 alone. To demonstrate that this was not due to cRNA saturation, we injected 6 ng KCC2 RNA and observed a significant increase in flux, compared to a 2 ng KCC2 injection. Importantly, we demonstrated that the inhibitory effect of KCC3-E289G on KCC2 function was specific to K-Cl cotransporters, by co-injecting mRNA encoding KCC3-E289G and NKCC1, and observing no inhibitory effect on NKCC1-mediated K^+ uptake (Figure 9B). This control experiment was important as it demonstrated that

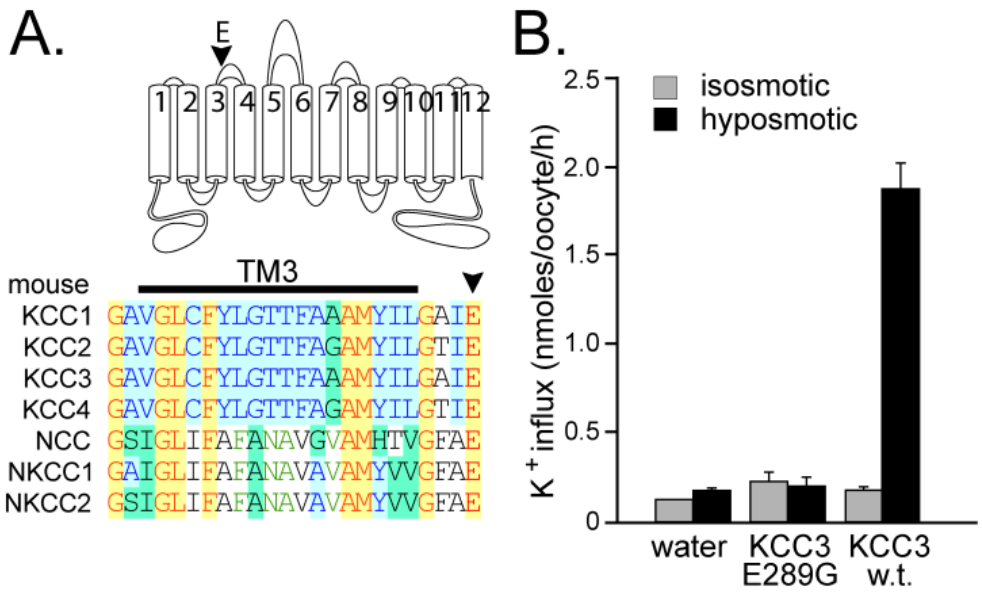

Figure 7. Absence of function of the KCC3-E289G mutant protein.

A) Conservation of glutamic acid residue (E289 in mouse KCC3) within mouse SLC12A cotransporters. The residue, highlighted by an arrowhead in cartoon and sequence alignment, is localized at the end or right downstream of transmembrane domain 3 (TM3). B) K^+ influx was measured through unidirectional ^{86}Rb tracer uptake under isosmotic and hyposmotic conditions, in oocytes injected with water, KCC3-E289G mutant cRNA, and wild-type KCC3 cRNA. Bars represent mean ± SEM (n = 25 oocytes).

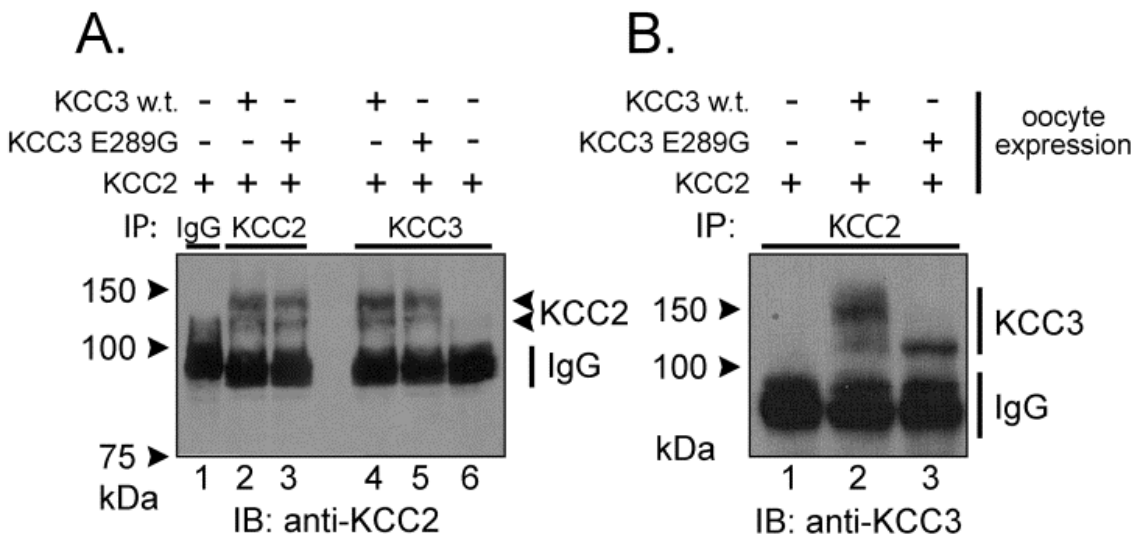

Figure 8. Co-immunoprecipitation reveals interaction between KCC3 and KCC2.

Xenopus laevis oocytes were injected with KCC2 cRNA in the presence or absence of wild-type KCC3 or KCC3-E289G cRNAs. KCC2 or KCC3 were then immunoprecipitated and the complex was analyzed by Western blot analysis using rabbit polyclonal anti-KCC2 or anti-KCC3 antibodies. Immunodetection of KCC2, KCC3 and IgG are indicated on the right of the panels. Note that both KCC2 (panel A) and KCC3 (panel B) when immunoprecipitated are observed as 2 bands: unglycosylated and glycosylated forms. Experiment was repeated once and yielded similar data.

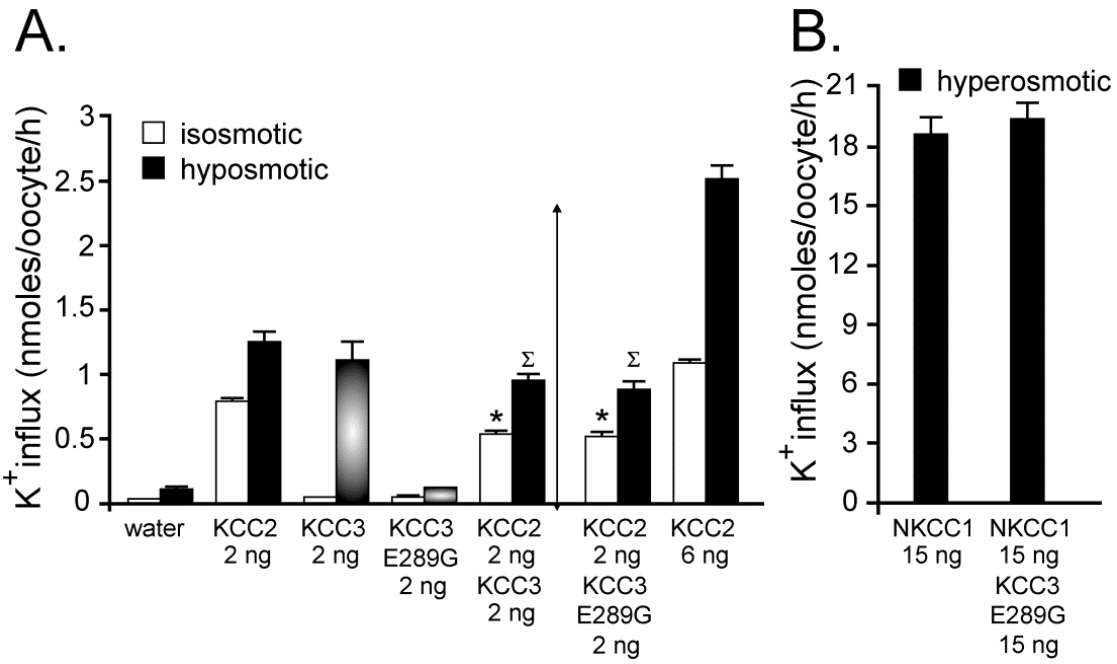

Figure 9. Evidence for dominant-negative effect of KCC3 on KCC2 function.

A) *Xenopus laevis* oocytes were injected with KCC2 cRNA in the presence or absence of wild-type KCC3 or KCC3-E289G cRNAs. Three days following injection, K^+ influx was measured under isosmotic conditions where only KCC2 function is active, or under hyposmotic conditions where both KCC2 and KCC3 function are stimulated. Bars represent mean ± S.E.M. (n = 20–25 oocytes). Flux is expressed in nmoles K^+/oocyte/h. $^{(*)}$ $P < 0.01$ (ANOVA) compared with KCC2 alone under isosmotic condition, $^{(\Sigma)}$ $P < 0.01$ (ANOVA) compared with KCC2 alone under hyposmotic solution. Arrow indicates the anticipated flux mediated by the combined activity of KCC2 and KCC3. This is a representative experiment. Each condition (bar) was reproduced multiple times. B) K^+ influx was measured under hyperosmotic conditions in oocytes injected with NKCC1 cRNA in the presence or absence of KCC3-E289G cRNA. Bars represent mean ± S.E.M. (n = 20–25 oocytes). Flux is also expressed in nmoles K^+/oocyte/h.

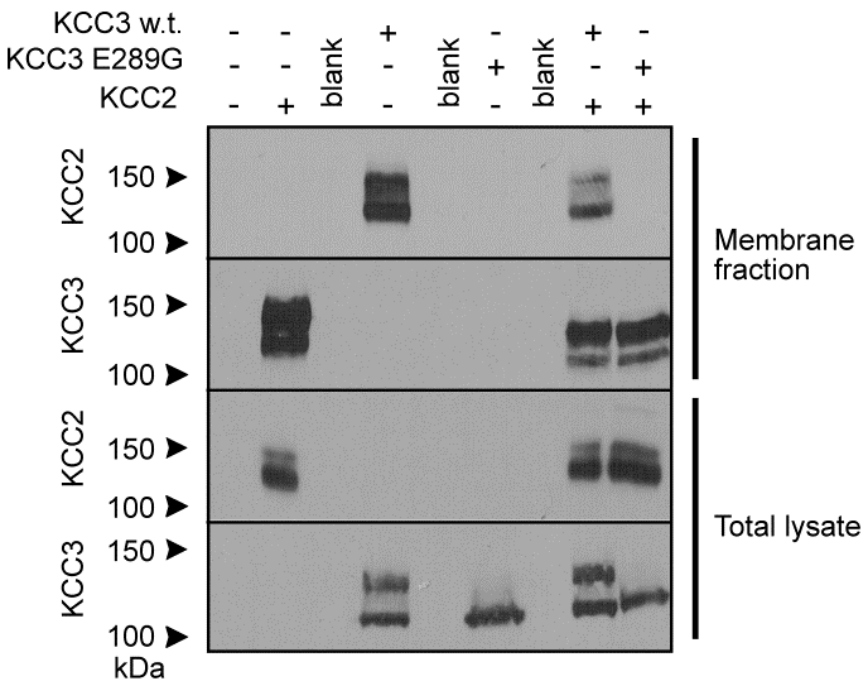

Figure 10. Evidence for dominant-negative effect of KCC3 on KCC2 trafficking.

Xenopus laevis oocytes were injected with KCC2 in the presence or absence of wild-type KCC3 or KCC3-E289G cRNAs and membrane fractions were isolated using a silica cross-linking method. Membrane proteins and whole oocyte lysates were subjected to Western blot analysis using rabbit polyclonal anti-KCC2 or anti-KCC3 antibodies. Experiment was reproduced 3 times.

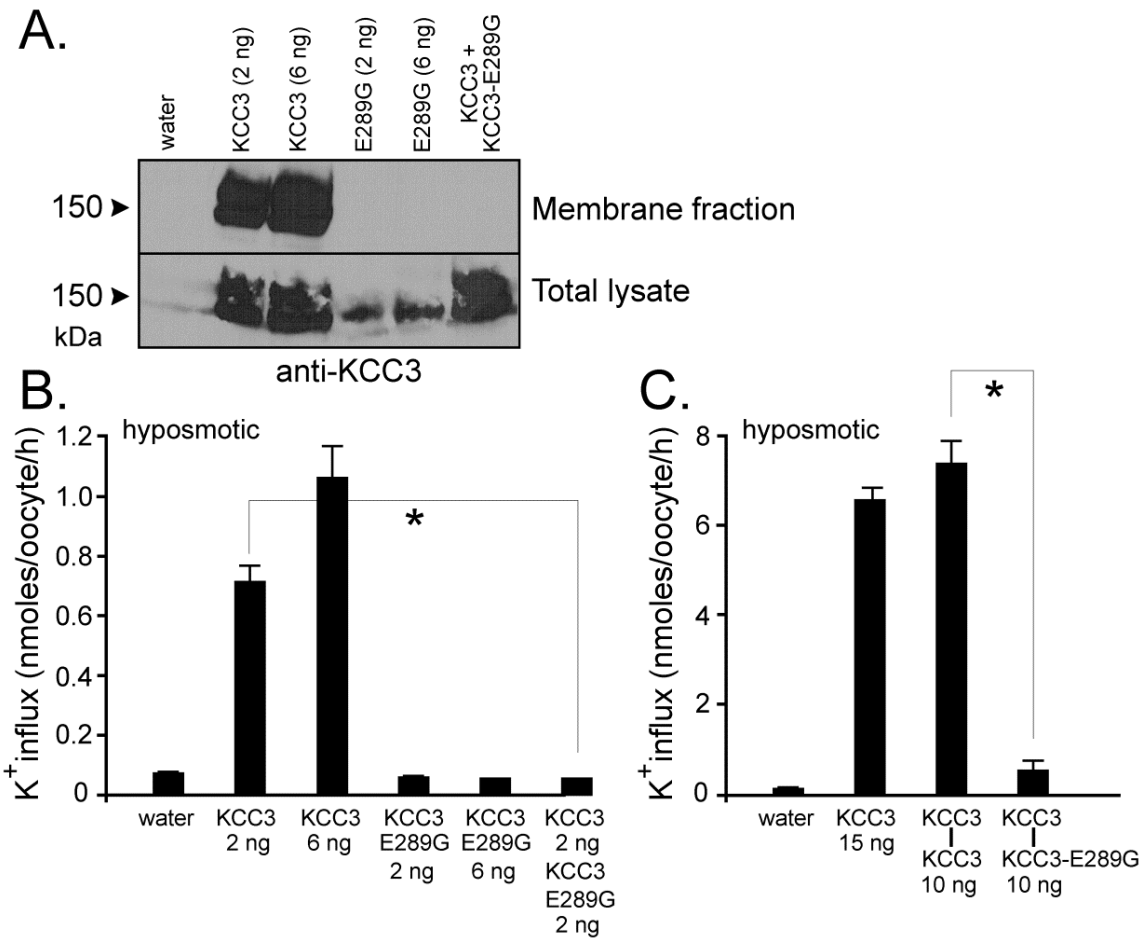

Figure 11. Evidence for dominant-negative effect of KCC3 on KCC2 trafficking and function.

Xenopus laevis oocytes were injected with KCC3, KCC3-E289G, or both. A) Membrane fraction was isolated using a silica based cross-linking method and membrane proteins and whole oocyte lysates were subjected to Western blot analysis using rabbit polyclonal anti-KCC2 or anti-KCC3 antibodies. B) K^+ influx was measured under hyposmotic conditions. C) K^+ influx generated by KCC3-KCC3 and KCC3-KCC3-E289G concatamers. Bars represent mean ± S.E.M. (n = 20–25 oocytes). Flux is expressed in nmoles K^+/oocyte/h. *P<0.001 (ANOVA) compared with KCC3 controls. Experiment was performed 6 times with similar data.

the KCC3-E289G mutation did not poison the endoplasmic reticulum.

KCC3-E289G mutant prevented wild-type KCC3 to reach the plasma membrane (Figure 10A) which resulted in dominant-negative effect on KCC3 function (Figure 10B). As K-Cl cotransporter likely functions as homodimers, we forced dimerization through the use of concatamers or mRNA molecules encoding two KCC3 cotransporters, linked head to tail and separated by a 9-glutamine linker. As seen in Figure 11C, concatamers made of wild-type KCC3 molecules were functional, whereas addition of mutant KCC3-E289G monomer downstream of a wild-type monomer eliminated the function of the dimer.

The lower molecular size of the KCC3-E289G band observed in Figure 10 indicates a defect in glycosylation. To further substantiate this defect, we transfected HEK 293FT cells with wild-type and mutant KCC3 and observed absence of larger molecular weight products in the KCC3-E289G mutant (Figure 12A). As KCC3 is natively expressed in Chinese hamster ovary (CHO) cells, we took advantage of mutant CHO cell lines (Figure 12) to evaluate the extent of the KCC3-E289G glycosylation deficit. As shown in Figure 13A, the signal from the KCC3-E289G mutant is similar to the signal shown in the CHO Lec8 and Lec1 samples, indicating early glycosylation deficit. Treatment with tunicamycin, which blocks the synthesis of all N-linked glycoproteins (Figure 13A), and PNGase, an enzyme that cleaves asparagine-linked mannose rich oligosaccharides (Figure 13B), slightly reduced the molecular size of the KCC3-E289G band, indicating the presence of a core glycosylation. These data are consistent with the protein being partially modified in the endoplasmic reticulum. Staining of HEK 293FT cells transfected with wild-type KCC3 (Figure 14A-F)

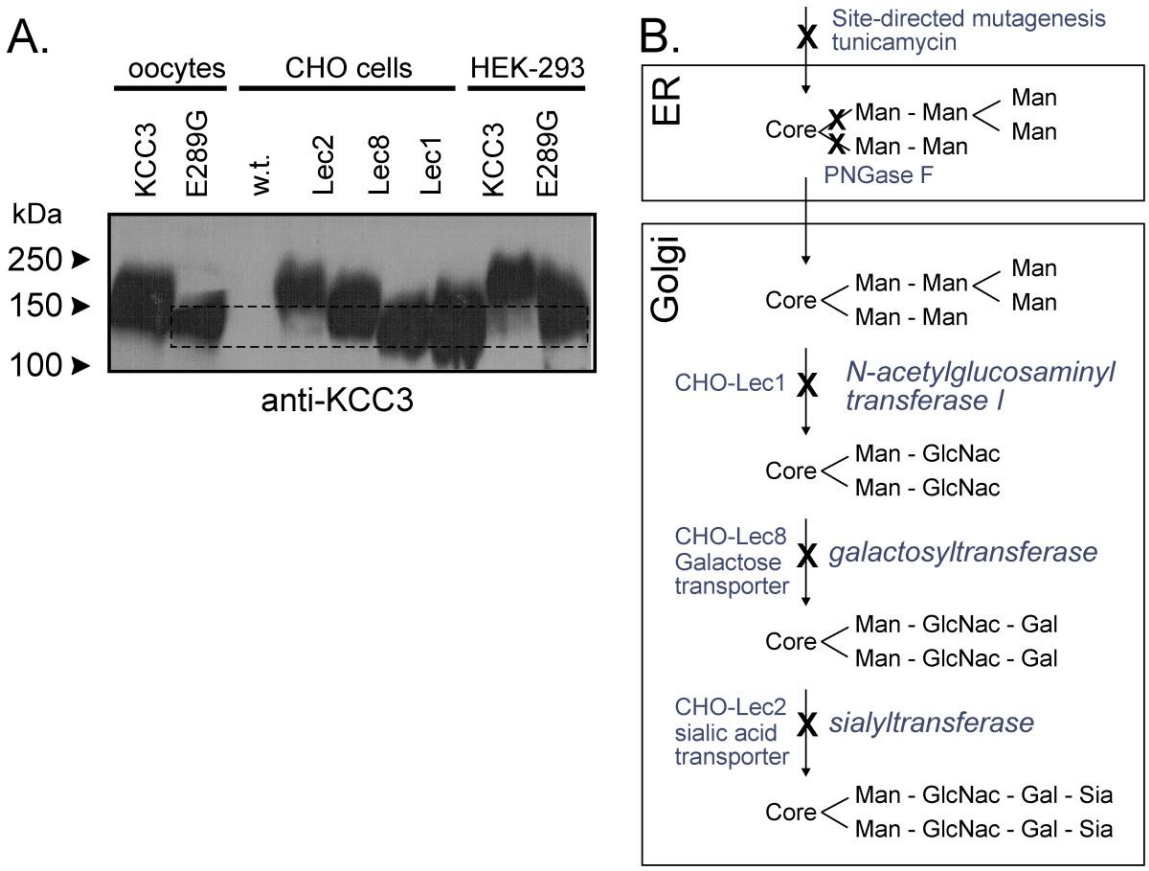

Figure 12. N-Glycolsylation deficiency of the KCC3-E289G mutant.

A) Western blot analyses of KCC3-E289G mutant in HEK 293FT cells and *Xenopus laevis* oocytes compared to wild-type KCC3 in HEK 293FT cells, wild-type and mutant CHO cells, and *Xenopus laevis* oocytes, using rabbit polyclonal anti-KCC3 antibody. CHO-Lec1 cells have mutation in N-acetylglucosaminyl transferase, whereas CHO-Lec8 and CHO-Lec2 have deficient galactose and sialic acid transporters, respectively. Two independent experiments are shown. Experiment was performed 4 times. B) Scheme represents the main steps in N-linked oligosaccharide biosynthetic pathway. First, core Glc-Nac-Glc-Nac-Man with branched mannose residues are added to the Asparagines in the ER. In the Golgi, mannose molecules are replaced by acethylglucosamyl groups, followed by the addition of galactose and sialic acid groups. These steps require the availability of galactose and sialic acid in the cells, which is prevented in the mutant CHO cells by elimination of specific transporters.

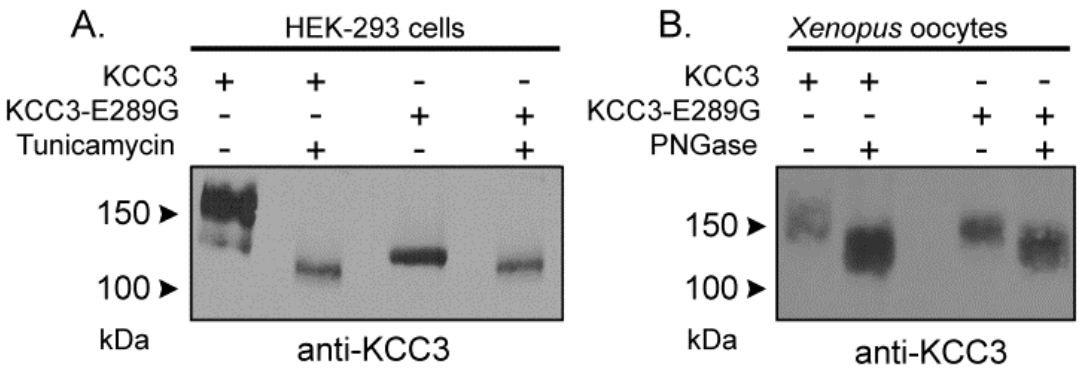

Figure 13. N-Glycolsylation deficiency of the KCC3-E289G mutant.

A) Western blot analysis of wild-type KCC3 and KCC3-E289G mutant in HEK 293FT cells treated with tunicamycin (exposed to 10 µg/ml for 18 hours). B) Western blot analysis of wild-type KCC3 and KCC3-E289G mutant proteins isolated from *Xenopus laevis* oocytes and treated with PNGase (0.25U, 12 h at 37 ℃). The membranes were exposed to a rabbit polyclonal anti-KCC3 antibody. The experiment was repeated once with identical data.

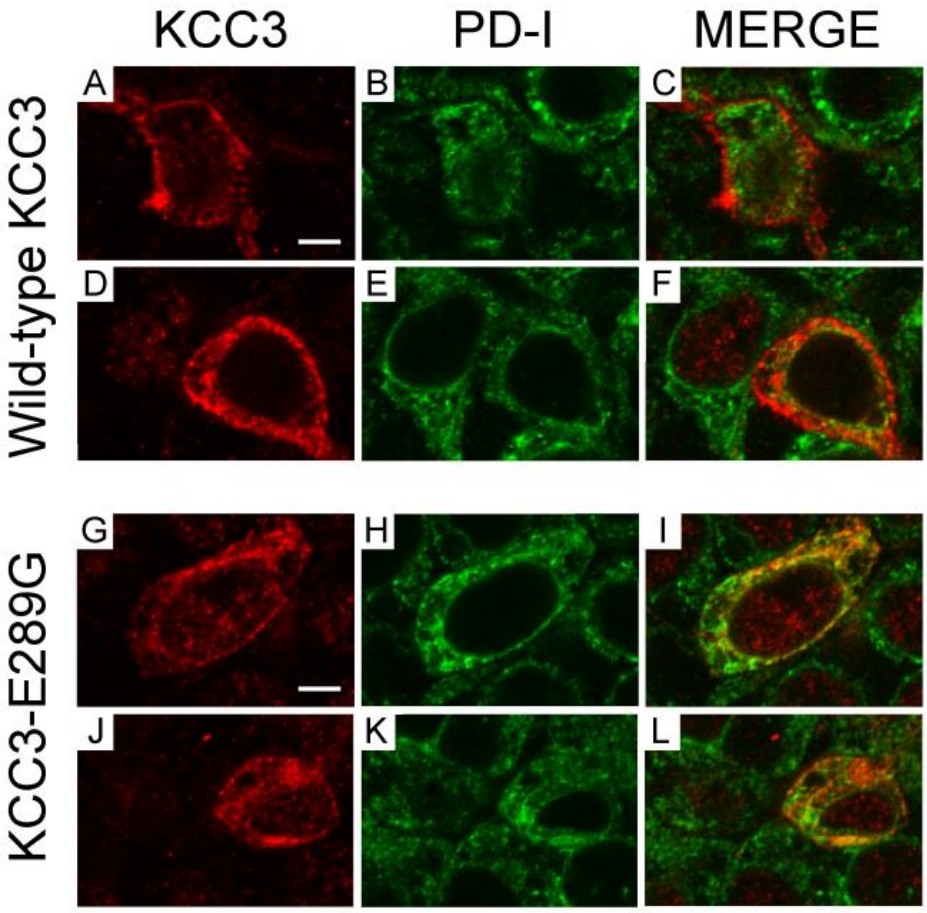

Figure 14. Evidence for KCC3-E289G localizing in the endoplasmic reticulum.

HEK 293FT cells were transfected with wild-type KCC3 (A–F) or KCC3-E289G mutant (G–L). Two days post- transfection, the cells were fixed with paraformaldehyde, treated with saponin, and exposed to rabbit polyclonal anti-KCC3 and mouse monoclonal anti-PDI antibodies followed by cy3-conjugated anti-rabbit and Alexa Fluor–conjugated goat anti-mouse antibodies. Focal plane images of KCC3 signal (A, D, J, G), ER marker signal (B, E, H, K), and combined signals (C, F, I, L). Bar = 5 μm.

demonstrates cotransporter localization in the plasma membrane and intracellular compartments but with minimal co-localization with the ER marker (PDI). However, the KCC3-E289G (Figure 14G-L) mutant revealed strong co-localization with PDI (Figure 14G-L). Using a subcellular fractionation protocol, we were able to confirm in HEK 293FT cells that the KCC3-E289G mutant does not make it to the plasma membrane, but is exclusively located in intracellular organelles, whereas wild-type KCC3 signal is observed both in membrane and intracellular organelles (Figure 15). No KCC3 signal is observed in water-injected oocytes (over 5 experiments). Note the presence of a sizable fraction of wild-type KCC3 and KCC3-E289G associated in the nuclear fraction, this signal might partially originate from nuclei-associated endoplasmic reticulum, as PDI signal was also observed in the nuclear fraction.

Because the glutamic acid residue is highly conserved within cation-chloride cotransporters, we examined the effect of mutating the corresponding residues in KCC2 and NKCC1. As seen in Figure 17, mutation of KCC2 glutamic acid residue 201 into glycine completely abrogated KCC2 function under both isosmotic and hyposmotic conditions. Interestingly, the glutamic acid residue could not be substituted with a negatively charged aspartic acid residue. In contrast, there was minimal effect of mutating the corresponding glutamic acid residue in NKCC1, as cotransporter function was similar for mutants NKCC1-E383G or E383D when compared to wild-type NKCC1 under isosmotic conditions. To demonstrate that NKCC1 was expressed in the plasma membrane to similar levels, we utilized a constitutively-active form of SPAK to activate the cotransporter (Gagnon and Delpire, 2012; Gagnon et al., 2011). Under SPAK activation, the levels of cotransporter activity were similar between wild-type and mutant

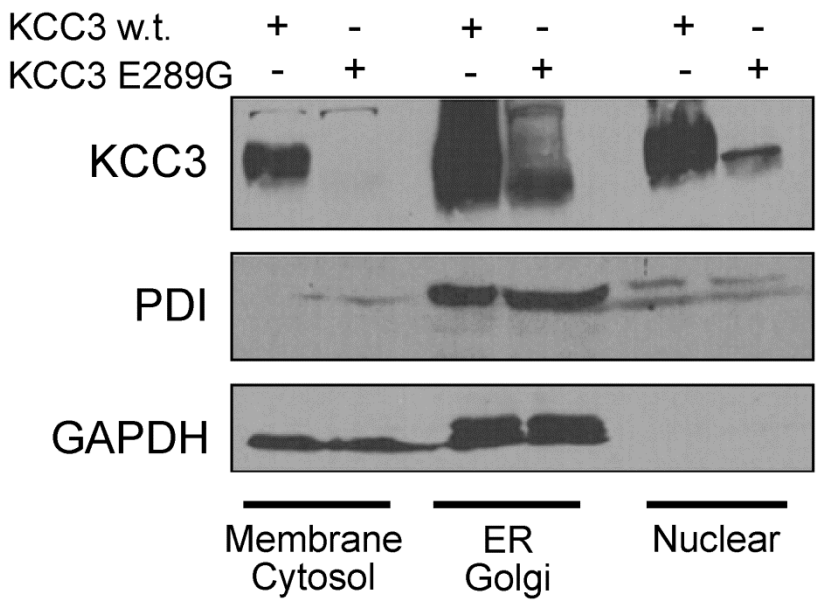

Figure 15. Sub-cellular localization of KCC3 and KCC3-E289G in HEK 293FT cells.

HEK 293FT cells were transfected with wild-type KCC3 or KCC3-E289G mutant. Two days post-transfection, the cells were treated with digitonin to extract proteins from cholesterol-rich (plasma) membranes (membrane/cytosol fraction), followed by NP40 treatment to isolate proteins from ER/Golgi fraction, followed by deoxycholate + SDS detergents to isolate proteins from nuclear fraction. Western blots were probed with rabbit polyclonal anti-KCC3 and mouse monoclonal anti-PDI and anti-GAPDH antibodies. Experiment was reproduced at least 5 times with similar data.

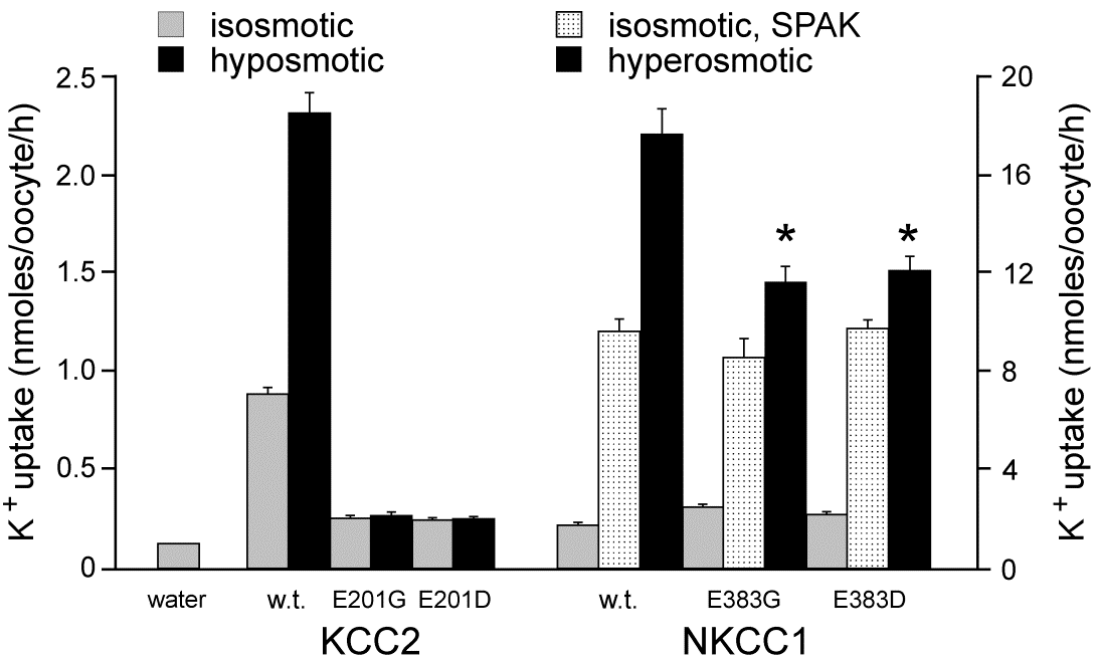

Figure 16. Effect of E289G-like mutations in KCC2 and NKCC1.

K^+ influx was measured through unidirectional ^{86}Rb tracer uptake in oocytes injected with water, wild-type KCC2 or KCC2-E201G or KCC2-E201D mutant cRNAs, and wild-type or NKCC1-E383G or NKCC1-E383D mutant cRNAs. Uptakes were measured under isosmotic (200 mOsM) and hypotonic (100 mOsM) solutions for KCC2 and under isotonic and hypertonic (265 mOsM) solutions for NKCC1. Bars represent mean ± SEM (n = 20–25 oocytes). Fluxes are expressed in nmoles K^+/oocyte/h. (*) Denotes statistical significance with $P < 0.001$ (ANOVA followed by Tukey-Kramer Multiple Comparisons Test). Experiment was done once.

NKCC1cotransporters. However, there was a significant reduction in cotransporter activation in the mutants versus wild-type NKCC1 under hyperosmotic conditions.

4. Discussion

K-Cl cotransporters are encoded by four distinct genes each of which generates many variants due to the use of alternative promoters and alternative splicing (For reviews, see (Hebert et al., 2004; Payne, 2009)). Published Western blot data indicate the presence of dimers or oligomers and functional studies have demonstrated that K-Cl cotransporters form homo-dimers. An intriguing consensus emerging in the field of cation-chloride cotransporter is that cells often co-express multiple isoforms of the K-Cl cotransporter. While this might not necessarily be too surprising for an bipolar epithelial cell that might express one form of the cotransporter on the apical membrane and another on the basolateral membrane, or even for a neuron which might express one form in dendritic spines and another at the cell body, this observation still raises the intriguing possibility that one isoform might affect the expression and/or function of another. To address this possibility, we made use of a functional cotransporter (KCC3), a non-functional cotransporter mutant (KCC3-E289G), and a second functional cotransporter (KCC2) to examine the possibility of hetero-dimerization and co-regulation. The present studies were performed with the specific aim to examine whether a non-functional but full-length cotransporter affects the function of an active cotransporter. We started our studies with a KCC3 mutant that fails to demonstrate hypotonic-stimulation of K^+ influx when expressed in *Xenopus laevis* oocytes. As the residue is located in an extracellular loop, it

is unlikely that the deficit is due to regulation by intracellular signaling/regulatory proteins, such as kinases or phosphatases.

Co-immunoprecipitation experiments revealed that both wild-type and KCC3-E289G mutant interact with KCC2 when co-injected in oocytes. These data indicate that not only KCC2 and KCC3 can be co-expressed in neurons (Le Rouzic et al., 2006; Pearson et al., 2001; Shekarabi et al., 2011), but that they are able to form oligomers. Functional data argue that expression of KCC3 affects KCC2 function or vice-versa, irrespective of the nature of the KCC3 clone co-expressed (wild-type versus mutant). Indeed, it was striking that K^+ influx measurements were never additive when both cotransporters were expressed in the oocytes. As our experiments were controlled for the level of cRNA injected, it was clear that these effects were true dominant-negative effects and not related to RNA saturation in the oocytes. To explain these data, we examined expression of the cotransporters at the cell surface. Instead of biotinylation, we utilized a method that was developed specifically for *Xenopus laevis* oocytes and which was shown to be of high sensitivity (Leduc-Nadeau et al., 2007). Protein expressed at the plasma membrane were cross-linked to silica and simply isolated by centrifugation. Indeed, after washing excess silica, lysing the oocytes, pelleting and washing the silica, wild-type KCC2 and KCC3 protein were readily observed by Western blot analysis. In contrast, no signal was observed from oocytes expressing KCC3-E289G, indicating that the mutant cotransporter does not reach the plasma membrane, or if some of it reaches the membrane, it is below the level of detection of the silica method. Co-expression of KCC3-E289G with KCC2 resulted in absence of KCC2 expression in the oocyte membrane, whereas co-expression of wild-type KCC3 with KCC2 resulted in decreased expression of KCC2 in the

membrane. These data indicate that the mutant KCC3 protein prevents proper trafficking of KCC2 to the cell surface. The fact that expression of wild-type KCC3 also affects expression of KCC2 is puzzling. This indicates that when the two cotransporters interact, trafficking of this hetero-dimer to the plasma membrane is impaired. However, this interaction would only take place when mRNA molecules are translated simultaneously and the dimer forms in the endoplasmic reticulum. Thus, to prevent this specific mechanism of regulation, cells might have ways to separate translation spatially and/or temporally in order to express full complements of each transporter to the plasma membrane.

Our data indicate that mutation of extracellular glutamic acid residue 289 into a glycine impairs trafficking of KCC3 to the plasma membrane. If trafficking of KCC3-E289G to the cell surface is fully prevented, this by itself explains the absence of function. We attempted to 'force' the transporter to the cell surface by using a molecular chaperone utilized to rescue trafficking of the CFTR-Δ508 mutation (Rubenstein et al., 1997; Zeitlin et al., 2002). Incubation of the oocytes with 2.5 mM 4-phenylbutyrate for 3 days during translation, had no effect on trafficking and function of the mutant KCC3 cotransporter (1002 ± 62 pmoles/oocyte/h (n = 26) for wild-type KCC3 alone versus 1129 ± 42 (n = 26) for wild-type KCC3 in oocytes treated with 4-PBA and 86 ± 12 pmoles/oocyte/h (n = 26) for mutant KCC3 alone versus 90 ± 10 (n = 24) for mutant KCC3 in oocytes treated with 4-PBA). Because the silica method likely has a detection threshold below which there is no cell surface detection, there is a possibility that some of the mutant cotransporter does reach the plasma membrane. If it is the case, this would indicate that the transporters that have reached the membrane are also functionally silent. The precise mechanism by which

a single substitution of a glutamic acid residue to a glycine at the end of transmembrane 3 affects trafficking is unknown. It is tempting to speculate that the negatively charged residue at the end of the transmembrane domain affects the threading of the domain across the reticular membrane and that in turn affects the overall topology and folding of the protein. It is, however, important to note that the glutamic acid cannot be substituted by an aspartic acid, which also carries a negative charge (see Figure 16). We did not test additional amino acid substitutions in this study. It will be of interest to expand the analysis to other residues such as glutamine which has a side chain similar to glutamic acid and alanine which has a size similar to glycine. An independent confirmation which supports our observation that the transporter is not properly trafficked to the plasma membrane comes from the migration pattern of the mutant KCC3 protein in an acrylamide gel. Western blot analysis data show absence of a broad band typical of a glycosylated membrane protein for the KCC3-E289G mutant. Treatment of protein lysates isolated from oocytes expressing KCC3-E289 with PNGase demonstrated a small shift in molecular size, indicating that the core glycosylation (or addition of mannose sugars) had taken place in the KCC3-E289G cotransporter mutant. Comparison of the glycosylation pattern of KCC3-E289G in HEK 293FT cells or in *Xenopus laevis* oocytes with the pattern of native KCC3 in CHO cells with mutation in glycosylation genes revealed deficits in the early glycosylation steps that typically occur in the Golgi. This would indicate that trafficking of the mutant transporter might be arrested in the endoplasmic reticulum or early Golgi. This conclusion was further supported by immunofluorescence data and cell fractionation data that demonstrate co-localization of the KCC3-E289G mutant with the ER marker, PDI. Thus, we have uncovered a glutamic

acid residue in KCC3 which when substituted into a glycine affects glycosylation and trafficking of the cotransporter to the plasma membrane. As the mutant cotransporter is full-length it can interact in the ER with wild-type cotransporters (KCC3 or KCC2) and prevent their trafficking as well. Control experiments with co-injection of KCC3-E289G with NKCC1 revealed that trafficking is impaired due to interaction of KCC monomers instead of ER poisoning. As the interaction of K-Cl cotransporters occurs at the C-terminal tail (Simard et al., 2007), we also tested whether trafficking of KCC2 would be affected by a transporter lacking part of the C-terminal tail. Indeed, co-expression of KCC2 in oocytes with twice the amount of RNA encoding KCC3-T813X, the Quebec HSMN/ACC mutant, had no effect on the function of wild-type KCC2 (2777 ± 162 (n = 25) for KCC2 + KCC3-T813X versus 2997 ± 180 (n = 23) for KCC2 alone), indicating that the absence of a C-terminal tail prevents the KCC3-T813X mutant to interact with wild-type and affects its trafficking.

As the KCC3 glutamic acid residue 289 is conserved within cation-chloride cotransporters, we wondered if mutation of the corresponding residue in other K-Cl cotransporters or even one of the Na-K-2Cl cotransporter would also affect their function. Interestingly, KCC2 function was completely eliminated in the KCC2-E201G mutant, whereas function of NKCC1 was only partially affected in the NKCC1-E383G mutant. These data indicate that the residue is far more essential to K-Cl cotransport than Na-K-2Cl cotransporter function. Because the levels of isosmotic transport (under control conditions and SPAK-activated conditions) are identical in the two NKCC1 mutants versus wild-type, it is likely that trafficking of NKCC1 is not affected by the mutations. In contrast, the function of NKCC1 is significantly reduced under hyperosmotic

conditions. These data are in agreement with a previous study showing that the second extracellular loop is involved in the sensitivity of NKCC1 and NKCC2 to hyperosmolarity (Gagnon and Delpire, 2010).

In conclusion, our results show that E289 in KCC3 and E201 in KCC2 are essential residues for proper trafficking of the cotransporters, respectively. Experiments performed in *Xenopus laevis* oocytes and mammalian HEK 293FT cells revealed that the KCC3-E289G mutant cotransporter is stuck in the endoplasmic reticulum and likely receives only the core mannose glycosylation. Our results also demonstrate that hetero-dimerization of KCC2 and KCC3 is possible and that co-expression of one cotransporter affects expression of the other. These data also indicate that expression of a full-length mutant cotransporter, even if non-functional, might have dominant-negative effects on other related cotransporters, suggesting the possibility that single residue mutations that do not lead to protein truncation might lead to different phenotypes than knockout of the protein.

III. Characterization of KCC3-E289G mutant *in vivo*

1. Introduction

Peripheral neuropathy with or without agenesis of the corpus callosum (Andermann syndrome or ACCPN) is an autosomal recessive disorder characterized by a progressive sensorimotor neuropathy, general learning disability, as well as bone deformities (facial abnormalities and fused fingers) (Dupre et al., 2003) . This autosomal recessive hereditary disease is caused by genetic mutations in the SLC12A6 gene, which encode the potassium-chloride co-transporter 3(KCC3). During the study for similar genetic diseases caused by mutations of this family, such as the Gitelman syndrome caused by mutations in the SLC12A3/NCC gene (OMIM 2638000) and Bartter syndrome which is caused by mutations in the SLC12A1/NKCC2 gene (OMIM 601678), many pathogenic mechanisms have been established, such as biosynthesis, trafficking, conductance, mutant protein degradation; however, even though several KCC3 knock out mouse models have been established to study the development of ACCPN disease, the specific pathogenic mechanism remains to be understood.

Currently there are 8 KCC3 mutations found in ACCPN patients, including seven truncating nonsense mutations, and one missense mutation (Figure 17). The majority are truncating mutations which lead to premature termination of the protein, resulting in various length truncations of the carboxyl terminal fragment of the protein. The C-terminal of KCC3 has been shown to interact with creatine kinase B, an important kinase for ATP generation and KCC3 activation. Absence of the C-terminal domain leads to systematical disruption of KCC3 activation and proper trafficking to the plasma

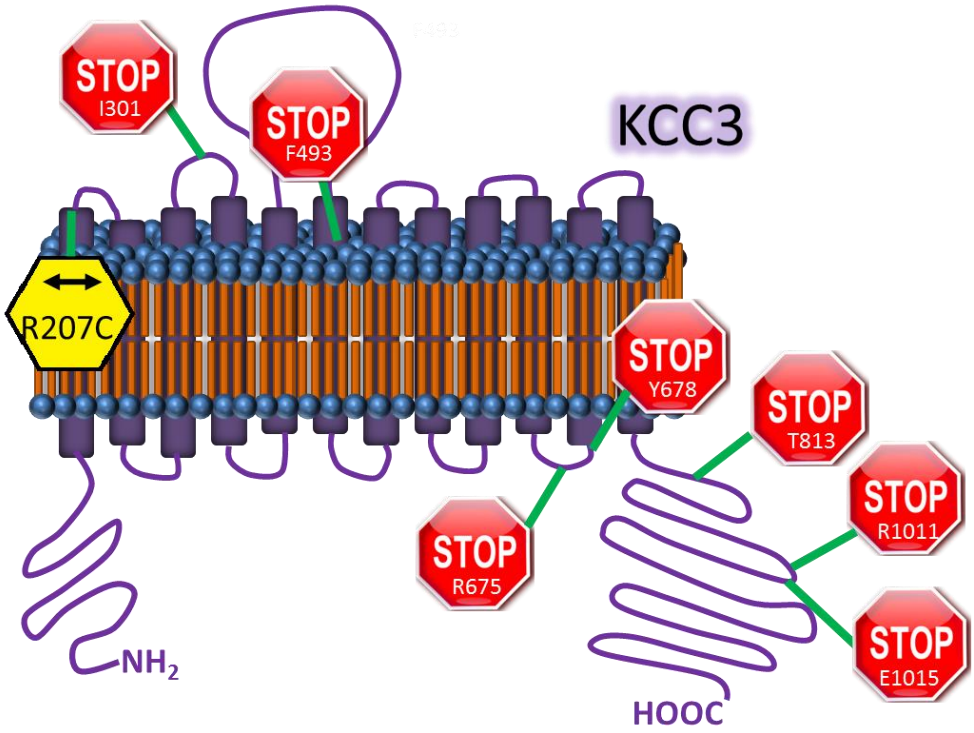

Figure 17. Location of KCC3 mutations associated with ACCPN.

Most ACCPN mutations results in truncation of the protein. The distal c-terminal portion contains a creatine kinase B domain (CK-B). Interaction with CK-B in the C-terminus is required for normal KCC3 function.

membrane as well (Inoue et al., 2006; Salin-Cantegrel et al., 2008). Among the two missense mutations, the R207C mutation showed an enhanced dimerization presence in mammalian cells and prevented the normal trafficking to the plasma membrane, while the missense G539D mutation was found in a compound heterozygous mutation: a maternal missense mutation c.1616G > A (p.G539D) and a paternal splice mutation c.1118 + 1G > A, which eventually leads to a truncated protein as well. Therefore, there is not a known natural KCC3 mutation which still produces a full length that causes HSN/ACC.

As discussed in the previous chapter, during the process of cloning the mouse KCC3 cDNA, we came across a mutation resulting in the substitution of glutamic acid residue E289 into a glycine (E289G). This negatively charge residue, located at the end of trans-membrane domain 3 (TM3) or beginning of extracellular loop 2 (ECL2) is highly conserved in all mammalian cation-chloride cotransporters. Although the KCC3-E289G mutant was non-functional when expressed in *Xenopus laevis* oocytes, function was restored when the residue was mutated back into a glutamic acid. The KCC3-E289G protein is expressed as a full-length protein in *Xenopus laevis* oocytes and mammalian cells (Ding et al., 2013).

When we obtained the KCC3-E289G mutant, we realized that this particular KCC3 mutation may help us understand the detailed pathogenic properties of KCC3 leading to HSN/ACC. In this study, we created two transgenic lines of KCC3-E289G knockin mice where the wild-type KCC3 was replaced with the E289G mutation. We found that one of the line generated showed a significant locomotor deficit in the rotarod test, whereas the second line failed to demonstrate this phenotype. Immunostaining studies on isolated

dorsal root ganglion neurons slices, demonstrated that the KCC3-E289G mutant protein did not reach properly the plasma membrane.

2. Methods

Generation of the floxed SLC12A6 and knock-in mouse. We replaced the mouse wild-type *Slc12a6* gene by inserting loxP sites around exon 7 (131 bp), followed by a neomycin resistance gene cassette flanked by Frt sites. The targeting vector was constructed using recombineering techniques to drop the short 5' end and long 3' end arms of recombination from BAC clone bMQ-302F12 (Geneservice Ltd, Cambridge, UK) into a vector containing 3 loxP sites, 2 Frt sites, and a PGK-driven neomycin resistance gene cassette. Briefly, a 2526 bp fragment (short arm) was dropped from the BAC clone between unique sites located upstream of the first *lox*P site. A small PCR fragment consisting of exon 7 surrounded by short intronic sequences was then ligated downstream of the first *lox*P site. Finally, a larger 7.5 kb fragment (large arm) was dropped from the BAC clone downstream of the last *lox*P site. The construct, verified by map digest and sequencing, was linearized using *Not*I. TL-1 ES cells were then electroporated with the linearized construct and grown on fibroblast feeder cells in Dulbecco's Modified Eagle Medium (D-MEM) medium supplemented with 15% fetal bovine serum, 50 mg/ml gentamicin, 1000U/ml LIF, 90 mM β-mercaptoethanol, and 0.2 mg/ml G418. Three hundred and fifty independent neomycin-resistant colonies were picked and grown in 96-well plates on feeder layer, expanded them and analyzed for the presence of the mutant gene by performing Southern blot analysis using genomic DNA digested with *Spe*I and hybridized with a ^{32}P-labeled probe consisting of 406 bp downstream of the right arm of

recombination. Seven positive clones were identified and one clone (5H6) was injected into C57BL/6J blastocysts. Two chimeric males (> 90% brown fur) were mated with C57BL/6J females and germline transmission was obtained. Since these mice carried one allele containing the neomycin-resistance gene cassette (3 *lox*P), they were mated with FLPeR mice (obtained from Susan Dymicki, Harvard and backcrossed in our laboratory for >10 generations in C57BL/6J background) to eliminate the neomycin-resistance gene cassette.

Accelerated Rotarod. The accelerated rotarod test was performed as previously described (Geng et al., 20010). Briefly, neuromotor coordination task was performed using an accelerating rotating cylinder (model 47600: Ugo Basile, S.R. Biological Research Apparatus, Comerio, Italy). The cylinder was 3 cm in diameter and was covered with scored plastic. Mice were confined to a 4 cm long section of the cylinder by gray Plexiglas dividers. Three to five mice were placed on the cylinder at once. The rotation rate of the cylinder increased over a 5 min period from 4 to 40 rpm. The latency of each mouse to fall off the rotating cylinder was automatically recorded by the device. Mice that remained on the rotarod during the 300 s trial period were removed and given a score of 300 s. The test was performed for three trials a day for 3 consecutive days.

Open field. This test was also executed as described earlier (Geng et al., 2010). Exploratory and locomotor activities were tested using an open-field activity chamber surrounded by a Plexglas enclosure within sound-attenuating cubicles (ENV-022MD-027; Med Associates, Inc., St. Albans, VT). The mice were placed in the center of the open field and their activity was monitored for 60 min. The test was performed at ambient room temperature (25 ◦C), moderate light (60 lx), and background noise (80 dB).

Distance traveled and time spend in the periphery (thigmotaxis) of the chamber were quantified by the number of beam crossings.

DRG neuron isolation. Wild-type and homozygote mice were killed by cervical dislocation. DRGs were dissected from the lower thoracic to mid-lumbar regions of the vertebral column and placed in 0.1M PBS. The connective tissue sheath around the ganglia was removed, and DRGs were minced two to three times with iridectomy scissors. The minced DRGs were then placed in a flask containing 5 ml of 4% (w/v) solution of PFA (Sigma Aldrich) in 0.1 M PBS (4 ℃, pH 7.4) over night.

Dorsal root ganglia fixation and staining. Dorsal root ganglia were dissected from the lower thoracic to mid-lumbar regions of the vertebral column and were placed in a 4% (w/v) solution of PFA (Sigma Aldrich) in 0.1 M PBS (4 ℃, pH 7.4) overnight . Following fixation, DRG neurons were transferred to a 30% (w/v) sucrose solution in 0.1 M PBS for 24 hours~48 hours before embedding into OCT(OCT®) blocks. The OCT blocks were stored at −20°C before being transferred for cryostat sectioning. Sections were cut 10 μm thick in the cryostat microtome at −20°C and were immediately transferred to a room temperature microscope slide by touching the slide to the tissue. The slides were stored at −20°C for further histology study. Routine H&E staining was performed for general histology. For immunostaining, the slides were defrost in room temperature for 10 min then permeabilized with 0.1% Triton X-100 for 5 min. After washing in PBS for 2x5 min, slides were then blocked for 30 min with 1% BSA in PBS with 1% goat serum. Then primary antibodies (anti-PDI antibody (Abcam, Ab27043 1:200), anti-KCC3 antibody (Delpire lab, 1:250), anti-T4 NKCC1 antibody

(Developmental Studies Hybridoma Bank (University of Iowa, Iowa City, IA), 1:200)) were applied in 1%BSA with PBS at 4℃ overnight. On the second day, the slides were washed twice separately by high salt PBS and regular PBS, and then blocked with 1% BSA in PBS with 4% goat serum for 30 min. Then secondary antibodies (100 ul, Cy3 conjugated anti-rabbit antibody (1:1000, Jackson Immunochemicals) and Alexa Fluor anti-mouse IgG (H+L) (1:400, Invitrogen) were applied and incubated for 60 min at room temperature. Cells were then incubated with the DNA dye TO-PRO-3 (Invitrogen) at a dilution of 1:300 in PBS for 15 min. Slides were then washed 3 times for 10 min each in PBS, mounted in Vectashield mounting medium (Vector Laboratories, Burlingame, CA), and examined using fluorescence microscopy. Fluorescence signal was visualized using a Carl Zeiss LMS 510 META confocal microscope.

3. Results

3.1. Lethality of the first KCC3-E289G homozygote mouse line

In order to create a KCC3-E289G knock in mouse, we generated a targeting vector that included the E289G mutation within exon 7 of the Slc12a6 gene. Exon 7 was also flanked by *lox*P sites, which we will see later was a very useful addition (Figure 18A). Several ES cell clones carrying the mutation were identified and one clone (5H6) was injected into C57BL/6J blastocysts. Two chimeric males were obtained and mated to C57BL/6J female mice. After germline transmission, elimination of the neomycin-resistance gene cassette by crossing mutant mice with FlpE mice, a 3 kb fragment was PCR amplified to demonstrate recombination in the proper locus. Sequencing of the fragment revealed correct 5' sequence and presence of the mutated exon and of the two *lox*P sites at the 3'

end of the fragment (Figure 18B), demonstrating recombination in the proper KCC3 locus. Breeding of one heterozygous male with one heterozygous female resulted in 9 pups with 6 heterozygotes and 3 wild-types, no homozygotes (Figure 18C). Sequencing of the PCR product from 1 heterozygote animal revealed the presence of the E289G mutation as well as the wild-type allele (Figure 18D). Altogether breeding of 11 heterozygous males and females resulted in no mice that were homozygous for the mutation. Out of 86 pups, there were 64 heterozygous and 22 control mice (Table 2). Note that while we genotyped the mice at age P21, we observed the pups daily from birth to P21 and genotyped any pup that died during this postnatal period.

This result infers embryonic lethality. In order to understand what caused the embryonic lethality phenotype seen in the homozygous mutant mice, we dissected the mouse embryos in different stages and genotyped these embryos. Surprisingly, no homozygous mutant embryos were detected as early as E3.5 (embryonic day 3.5), which still corresponds to the blastocyst stage (Table 2).

Because the embryonic lethality prevented us from studying the KCC3-E289G mutant protein *in vivo*, we devised alternative ways to proceed without obtaining the homozygous mutants. We crossed the heterozygous KCC3-E289G mouse with our KCC3 *null* mice which are described in Howard et al. (Howard et al., 2002). These mice have exon 3 permanently removed from the Slc12a6 gene. In a first breeding scheme, we obtained 6 offsprings, among which we identified two pups carrying one copy of the E289G allele and one copy of the *null* allele ($KCC3^{-/E289G}$). Because the *null* allele does

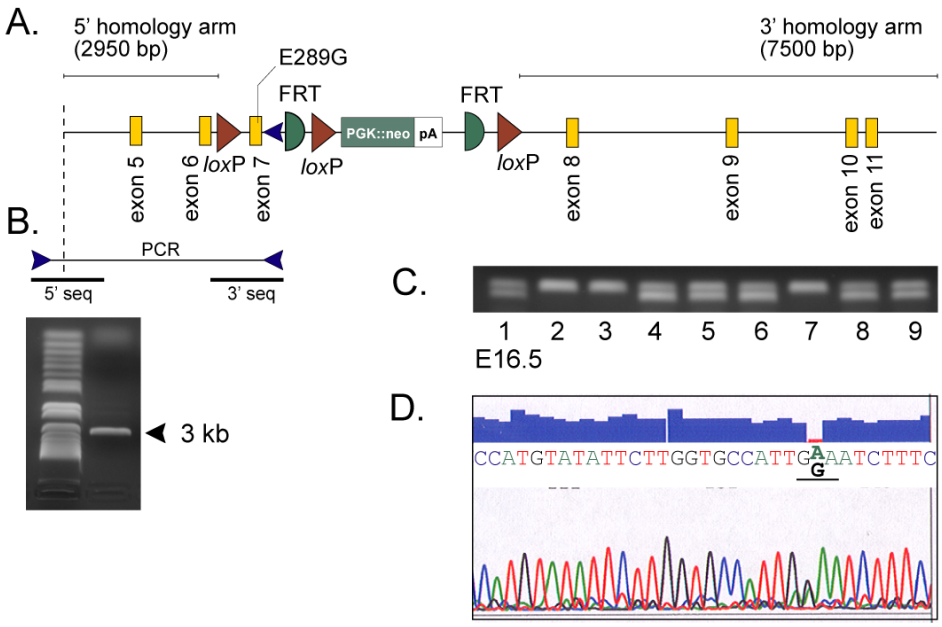

Figure 18. Targeting construct of KCC3 E289G knock in.

A. Schematic representation of the *Slc12a6* (KCC3) gene around exon 5-11. Highlighted are two S*ph*I restriction sites separated by 8 kb genomic sequence. **B**. Construct containing a 2950 bp genomic DNA sequence representing the 5' arm of recombination *lox*P sites flanking exon 7, followed by a PGK-driven neomycin resistance gene cassette flanked by FRT sites, and a 7500 bp 3' arm of recombination . **C**. Genotyping of 2 litters of pups from heterozygous breeding showing PCR fragments from wild-type and mutant alleles. **D**. DNA Sequencing showing the A to G mutation resulting in the substitution of glutamic acid residue E289 into a glycine (E289G).

Table 2. Breeding revealed absence of E289G homozygous mice.

Genotyping	# of females	Pups per female	Total pups	Heterozygous	Control	Homogyous
P21	11	7.8	86	64	22	0
E16.5	1	9	9	6	3	0
E12.5	2	7	14	7	7	0
E8.5	2	7.5	15	*	*	*
E3.5	5	12.4	48	36	12	0

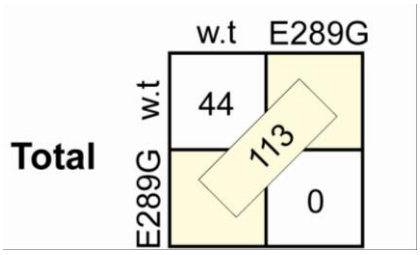

Breeding of 11 heterozygous males and females resulted in no mice that were homozygous for the E289G mutation. Analysis of embryos from 12.5 -16.5 days also revealed absence of homozygotes. Finally, isolation of blastocysts at E3.5 days demonstrated early lethality. Lower right corner: distribution of genotypes for all embryonic and postnatal ages. * All embryos were genotyped as heterozygous, suggesting that embryo tissues might be contaminated with tissues from the mother.

not produce any KCC3 protein, these animals only expressed KCC3-E289G. As these two animals were viable, we crossed additional animals and obtained a small cohort of mice to assess their locomotion phenotype using the rotarod (Figure 19). Interestingly, no locomotor phenotype characteristic of KCC3 knockout mice was observed.

To determine if the lethality is caused by the mutated (E289G) exon, or to other unforeseen events related to the recombination in embryonic stem cells, we made use of the *lox*P sites flanking the mutated exon 7. To eliminate the exon, we crossed the KCC3-E289G mice with E2a-CRE transgenic mice, which express the recombinase in the one cell zygote. Without the mutated exon, homozygous mice should be viable and exhibit the ACCPN phenotype, as they are KCC3 *null* mice.

Heterozygous 1 loxP mice were identified by genotyping and bred together to generate homozygous mice. However, again no homozygous mice were found among the first 16 pups generated (11 wild-types and 5 heterozygotes), indicating that deletion of exon 7 did not rescue the lethality phenotype. We concluded that the embryonic lethality was not caused by the mutated exon but by some other events that occurred during targeting.

We therefore went back to the frozen embryonic stem cell clones and injected an independent clone (5G8) into C57BL/6J blastocysts. After germline transmission and crossing again with FlpE mice to eliminate the neomycin resistance gene cassette, we obtained a new line of KCC3-E289G heterozygous mice. The exon was PCR amplified and sequenced to verify the presence of the mutation. Breeding of heterozygous males and females generated viable mutant homozygous ($KCC3^{E289G/E289G}$) mice. Initial observation did not show any posture or locomotor phenotype. However, when placed on

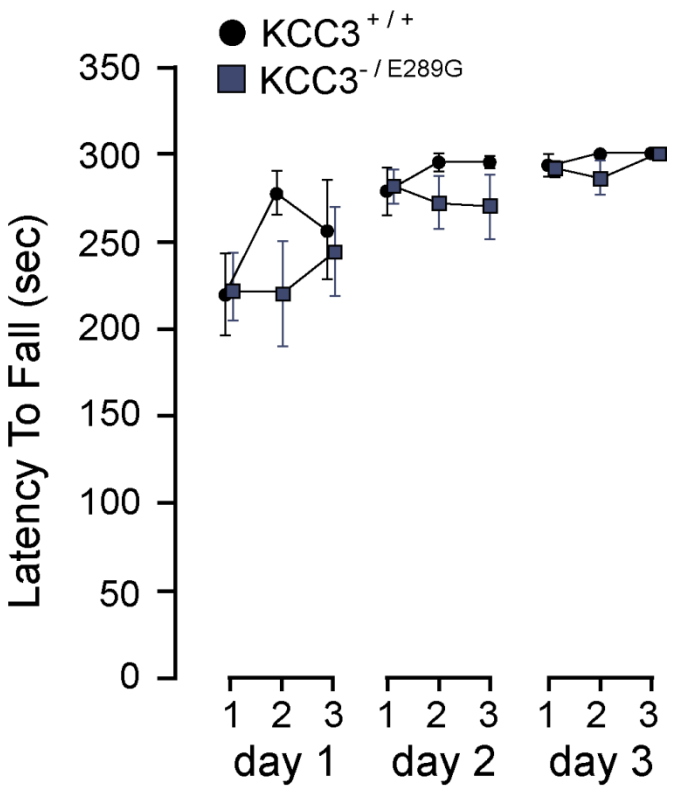

Figure 19. Absence of locomotor phenotype in KCC3$^{-/E289G}$ double mutant mice.

Accelerated rotorod test (4 to 40 rpm, 5 min) performed in control (KCC3$^{f/f}$) and KCC3$^{-/E289G}$ double mutant mice. Test was given three times a day for 3 consecutive days. The latency to fall from the rotating rod to the platform was measured in seconds. N = 6 mice per group.

the accelerated rotarod, the animals demonstrated a significant locomotor deficit (Figure 20A). No significant phenotype was observed with the open field activity test (Figure 20B).

Most of other KCC3 mutations affect the plasma membrane localization of the mutant transporter, preventing the normal trafficking to the membrane with significant retention of the protein in the endoplasmic reticulum (ER). In order to understand whether this is also the case for E289G mutation, we isolated DRG neurons from the $KCC3^{E289G/E289G}$ mice and performed immunostaining with the plasma membrane marker NKCC1 antibody, the KCC3 antibody and the nucleus marker TO-PRO®-3. As shown in Figure 21, KCC3 in controls tissues were localized outside the ER marker (PDI = protein disulphide isomerase), while in many cells from the knock in mice, the KCC3 was retained in the ER and co-localized with the PDI marker. This result demonstrated that the mutant KCC3E289G protein showed the same trafficking deficit, as we observed *in vitro* (see Chapter 3).

4. Discussion

KCC3 is expressed in many different tissues and organs in both mice and humans. By functioning as an electroneutral transporter of potassium and chloride ions, KCC3 plays important roles in epithelial chloride transport, cell volume regulation, and intracellular Cl^- homeostasis, thereby potentially affecting neuronal excitability. All the known KCC3 mutations in ACCPN patients led to either truncated proteins or proteins which are not properly folded and failed to express, therefore we do not know whether the neuropathy

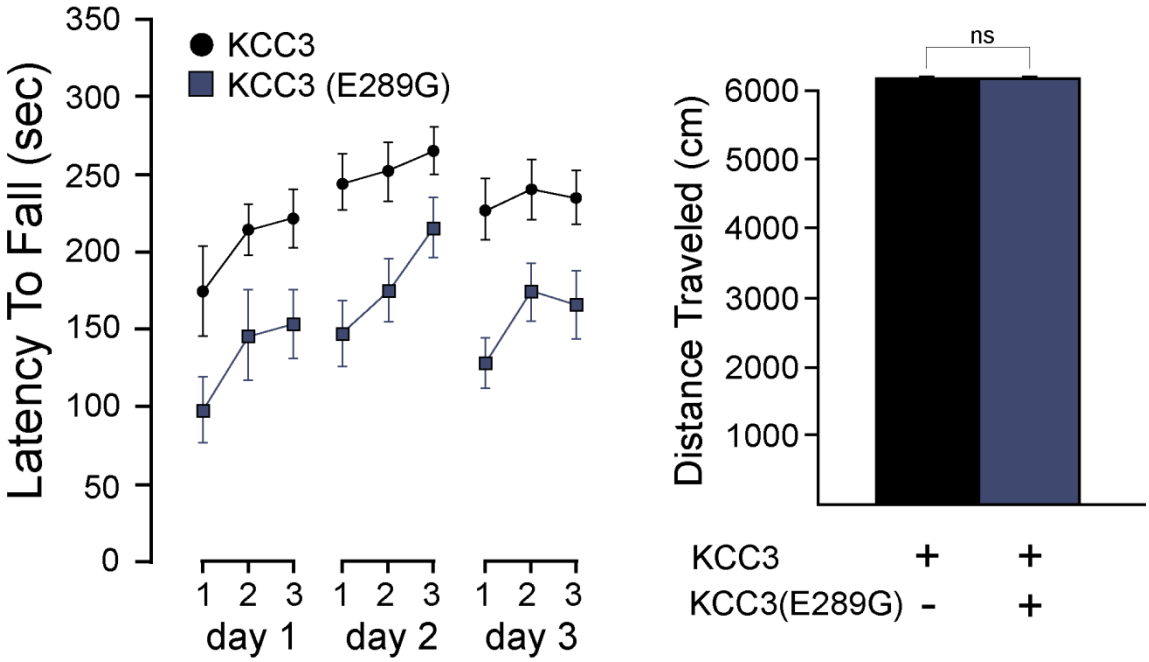

Figure 20. KCC3E289G knock in mice exhibit strong locomotor deficit.

A, Data were analyzed using paired t-test. The difference between the two groups was highly significant ($P < 0.001$, $t = 9.986$, $df = 17$). B, Mice were placed in open field chambers for 60 min. Total distance traveled was examined. Two tailed t-test demonstrated a *P* value of 0.2966 ($t = 0.9270$, $df = 17$, non-significant). N = 10 mice per group.

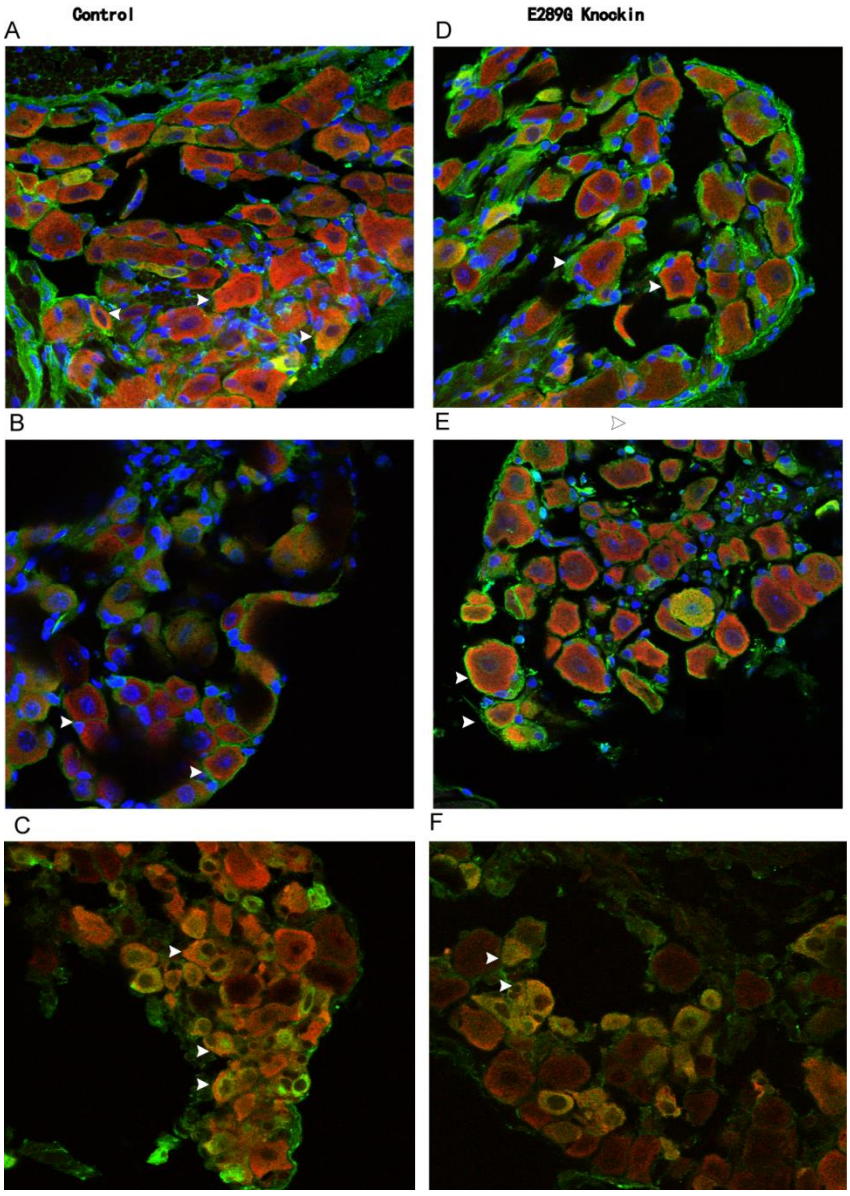

Figure 21. KCC3-E289G mutant protein did not reach the plasma membrane.

A-C. Longitudinal sections of DRG neurons from wild-type (n=3) mice were analyzed using immunofluorescence antibody against NKCC1 T4 (green, A&B), ER marker PDI (green, C) KCC3 (red, A-C) and nucleus marker TO-PRO®-3(blue, A&B). **D-F**. Longitudinal sections of DRG neurons from $KCC3^{E289G/E289G}$ mice (n=3) and were analyzed using the same immunofluorescence antibody (D&E: green-NKCC1 T4, red-KCC3, blue-TO-PRO-3; F: green-PDI, red-KCC3).

phenotype is due to the loss of K-Cl transport function of the protein, or due to the absence of the KCC3 protein *per se*. Indeed, it is possible that the cotransporter scaffolds a specific protein that is more directly involved with the neuropathy. Here, we introduce a novel mutation (E289G), which we showed in Chapter 2, disrupts the K-Cl transport function but expresses a full-length protein in heterologous expression systems. Using the transgenic knock-in technology, we created two separate lines of $KCC3^{E289G/E289G}$ mice: the first one being embryonic lethal, while the second one produced viable homozygous mutants.

For the first line, we demonstrated recombination within the proper locus by using long range PCR and sequencing. As the KCC3 *null* mouse is viable, it was unexpected to obtain embryonic lethality from a single amino acid substitution. Our first idea was that the mutation was causing the lethality possibly by affecting other cotransporters through direct interaction and dominant negative effects. This view was supported by the dominant-negative effects of KCC3-E289G that we observed on KCC2 function in *Xenopus laevis* oocytes (see Chapter 2). This hypothesis was, however, later dismissed when we eliminated the mutant exon and did not rescue the lethality phenotype. At this point, we do not understand the origin of the lethality. The construct used to introduce the mutation from the beginning (5') of the short arm of recombination to the end (3') of the long arm only covers a small portion of the Slc12a6 gene. Therefore, the deleterious event that occurred during recombination has to have occurred within the Slc12a6 gene, and any event leading to absence of protein expression should produce a viable mouse. If an additional event had occurred outside the Slc12a6 locus, it is likely that we would have been able to breed it out during our multiple crossings. Therefore, it is possible that

specific regions of the Slc12a6 gene have functions that are unrelated to the KCC3 protein. For example, there could be some regulatory elements within introns that control other genes, e.g. microRNA, and these could have been altered during recombination.

Of interest, we showed that substituting one of the two E289G alleles with a knockout allele (no exon 3) rescued the phenotype. Indeed, as with heterozygous mice that have a wild-type allele alongside the E289G mutant allele, mice carrying a knockout allele alongside the E289G mutant allele were also fully viable. In contrast to the heterozygotes, no KCC3 protein is produced from the knockout allele and therefore, only the KCC3-E289G mutant is expressed in these mice. Experiments preformed in Chapter 2 demonstrated that the mutant cotransporter does not make it to the plasma membrane and therefore does not promote transport of K^+ (or Cl^-). It was therefore unexpected to observe no locomotor deficit in these mice (Figure 19). These data need to be reconciled with the data obtained with our second line of KCC3-E289G knock-in mice. In this case, a separate embryonic stem cell clone was used to generate the mice and viable homozygous knock-in mice were produced. These mice demonstrated a locomotor phenotype. While a statistically significant difference was observed between the mutant and control mice, the deficit was far less severe than the one observed in KCC3 knockout mice. These $KCC3^{E289G/E2899G}$ knock-in mice are not very different from the double mutant $KCC3^{E289G/-}$ mice, in that they also only express the mutated protein. The only difference is the copy number.

At this point, we do not have a reason to explain why these seemingly similar mice behave so differently. The locomotor data need to be replicated with new cohorts of mice

preferentially generated at the same time. If the distinct phenotypes reproduced, it will mean that copy number is relevant. Expression of KCC3 by Western blot analysis and immunocytochemistry will need to be performed to assess level of protein expression and whether some mutated transporter successfully traffic to the membrane in the mice. This would be in contrast to what we observed in heterologous expression systems. It is difficult to understand why trafficking would happen in the mouse and not in heterologous expression systems, especially in frog oocytes as they are kept at a lower temperature and many transporter and channel protein mutants have been shown to traffic better at lower temperatures (Denning et al., 1992; Mall et al., 2004). If some of the KCC3 mutant proteins were to successfully traffic, they might function at the plasma membrane and therefore rescue the locomotor phenotype. If on the other hand the mutant transporter does not traffic, but is fully translated and some C-terminal parts interact with other proteins (even in the endoplasmic reticulum), this could explain why expression of KCC3-E289G could rescue the locomotor phenotype. Brain-type creatine kinase (CK-B), for instance, is known to bind to the large C-terminal domain of KCC3 (Salin-Cantegrel et al., 2008). CK-B is an isoform of creatine kinase, an enzyme that generates ATP and transfers a high-energy phosphate group from phosphocreatine to ADP, resulting in the regulation of the cellular ATP (Inoue et al., 2004). Several lines of evidence have shown that several membrane proteins form interaction with creatine kinase and affect its activity. Therefore, because of its location at the plasma membrane CK-B is thought to be producing the ATP that is required for the function of energy-driven transport proteins. A previous study showed that creatine kinase was required for swelling-activated potassium-chloride co-transport in red blood cells (Colclasure et al., 1995); other groups

have also reported a strong link between ATP and KCC activation (Lauf, 1983; Lauf et al., 1992; OrtizCarranza et al., 1996). The detailed mechanism of KCC3 activation by ATP is very complex, but it is already known that the CK-B binding on KCC3 involves the last 18 amino acids of the transporter, a region that is lost in all ACCPN-associated truncation mutations, but remains intact in the KCC3-E289G protein (Ding et al., 2013). Interaction of CK-B with KCC3 could be important either at the endoplasmic reticulum level or if some of the mutant transporter makes it to the membrane.

Among the HSN/ACC mutations, the R207C mutant was reported to be a full length protein, however, expressed at lower levels and also failing to reach the plasma membrane. The arginine at position 207 is located critically within a transmembrane domain and its replacement with a cysteine might completely affect the topology of the transporter. Furthermore, there was a dominant presence noted of KCC3-R207 dimers instead of monomer (Salin-Cantegrel et al., 2011). The possible misfolding, misclocalizaion, and dimerization of R207 mutant could have potentially affected interaction with a binding partner.

Another interesting feature of ACCPN patients is that patients with a truncated KCC3 mutation usually are associated with more severe clinical manifestations, while the patients bearing the missense mutation presents milder phenotype. Further investigation will be needed to further clarify the linkage between genotypes and phenotypes. For instance, beside the motor coordination deficiency, the KCC3 null mice also had phenotypes such as seizure susceptibility, hypertension, and gradual loss of hearing. Thus,

it would be worth investigating whether the loss of chloride function in these genetically modified animals was directly relevant to these phenotypes.

In summary, our studies of the E289G mutation in mice gave ambiguous data with one line of mouse showing a completely normal locomotor function and the other line showing a locomotor deficit. Whether this can be explained by copy number still needs to be resolved. Even though the E289G mutation is not found in nature, its study has shown it to be a useful tool to investigate the mechanisms by which disruption of KCC3 leads to HSN/ACC.

IV. Cellular origin of ACCPN: Tissue-specific knockouts

1. Introduction

Peripheral neuropathy with or without agenesis of the corpus callosum (Andermann syndrome or ACCPN) is an autosomal recessive disorder characterized by a progressive sensorimotor neuropathy, general learning disability, as well as bone deformities (facial abnormalities and fused fingers) (Andermann et al., 1972; Labrisseau et al., 1984). Genetic linkage in fourteen families mapped the autosomal recessive disorder to chromosome 15q (Casaubon et al., 1996) and several mutations in SLC12A6, the human gene which encodes the K-Cl cotransporter-3 (KCC3), were later identified in HMSN/ACC patients (Boettger et al., 2003; Howard et al., 2002; Rudnik-Schöneborn et al., 2009; Uyanik et al., 2006). In a mouse model where the KCC3 gene was disrupted to produce a global knockout, an early onset and severe locomotor deficit similar to the crippling human peripheral neuropathy disorder was observed (Howard et al., 2002). The mice also developed high blood pressure (Boettger et al., 2003), age-related deafness (Adragna et al., 2004; Boettger et al., 2003), and renal dysfunction (Wang et al., 2003). At the ultra-structural level, KCC3-deficient mice exhibited axonal and peri-axonal swelling, suggesting both neuronal and Schwann cell defects (Byun and Delpire, 2007). In a recent study, Shekarabi et al used a synapsin 1 promoter-CRE mouse to drive deletion of KCC3 in neurons, and demonstrated that loss of neuronal KCC3 reproduced the neuropathy phenotype observed in the KCC3 knockout mouse (Shekarabi et al., 2012). However, since synapsin 1 promoter is present in all neurons, it remains to be determined which specific neuronal cell type play underlies the development of the peripheral

neuropathy, and whether KCC3 in Schwann cells are also involved in the ontogeny of the disease.

In the present study, we created several novel mouse models to target deletion of KCC3 in specific cell types by using specific transgenic CRE lines. CRE recombinase is an enzyme derived from the P1 Bacteriophage which catalyzes the specific recombination between two 34 bp DNA recognition sites (*lox*P sites). The artificial *lox*P sites are introduced in the target gene, *Slc12a6* in this case, and a mutant mouse is produced. The recombinase which is under a tissue-specific promoter is expressed from DNA (transgene) inserted in the genome of a separate mouse. The Sc12a6 gene with *lox*P sites flanking an exon of interest and the recombinase transgene are brought together by crossing the two lines of mice. Deletion of KCC3 in small sensory neurons, driven by the Nav1.8 Na^+ channel promoter, resulted in mice that exhibited no motor coordination phenotype. In contrast, deletion of KCC3 in larger type-Ia proprioceptive afferent neurons driven by parvalbumin resulted in a significant loss of locomotion. In these mice, there was also trend towards a hyperactivity phenotype. Surprisingly, deletion of KCC3 driven by enolase-2, which is supposedly expressed in most mature neurons, failed to recapitulate this phenotype. The KCC3 deletion in the Schwann cells driven by desert hedgehog also failed to induce a locomotor phenotype. Histology analysis showed that parvalbumin positive neurons and enolase2 positive neurons in dorsal root ganglion had different expression profiles, consistent with the distinct performances in locomotor tests. Finally, histological analysis revealed a significant pathology associated with cells that were immunoreactive to parvalbumin. Therefore, our study demonstrates that parvalbumin positive neurons played a key role in producing the ACCPN-like locomotor phenotype.

2. Methods

Generation of tissue-specific KCC3 knockout mice. All procedures performed with mice were approved by the Vanderbilt University Institutional Animal Care and Use Committee. We disrupted the mouse *Slc12a6* gene by inserting *lox*P sites around exon 7 (131 bp), followed by a neomycin resistance gene cassette flanked by *Frt* sites. The targeting vector was constructed using recombineering techniques to drop the short 5' end and long 3' end arms of recombination from BAC clone bMQ-302F12 (Geneservice Ltd, Cambridge, UK) into a vector containing 3 *lox*P sites, 2 *Frt* sites, and a PGK-driven neomycin resistance gene cassette. Briefly, a 2526 bp fragment (short arm) was dropped from the BAC clone between unique sites located upstream of the first *lox*P site. A small PCR fragment consisting of exon 7 surrounded by short intronic sequences was then ligated downstream of the first *lox*P site. In a final step, larger 7.5 kb fragment (large arm) was dropped from the BAC clone downstream of the last *lox*P site. The construct, verified by map digest and partial sequencing, was linearized using *Not*I. To target the gene for homologous recombination, TL-1 ES cells were electroporated with the linearized construct and grown on fibroblast feeder cells in Dulbecco's Modified Eagle Medium (D-MEM) medium supplemented with 15% fetal bovine serum, 50 mg/ml gentamicin, 1000U/ml LIF, 90 mM β-mercaptoethanol, and 0.2 mg/ml G418. Three hundred and fifty independent neomycin-resistant colonies were picked and grown in 96-well plates on feeder layer, expanded, and analyzed for the presence of the mutant gene by performing Southern blot analysis using genomic DNA digested with *Sph*I and hybridized with a ^{32}P-labeled probe consisting of 347 bp upstream of the left arm of recombination. Eight positive clones were identified and one clone (5B1) was injected

into C57BL/6J blastocysts. Two chimeric males (> 90% brown fur) were mated with C57BL/6J females and germline transmission was obtained. Since these mice carried one allele containing the neomycin-resistance gene cassette (3 *lox*P), they were mated with FLPeR mice (obtained from Susan Dymicki, Harvard and backcrossed in our laboratory for > 10 generations in C57BL/6J background) to eliminate the neomycin-resistance gene cassette.

Heterozygous KCC3flox mice were first crossed to obtain viable homozygous mice. The mice were genotyped using oligonucleotide primers flanking the *lox*P site located upstream of exon 7: forward primer: 5' TGTGACAGACACTTCCTACAAGCC 3' and reverse primer: 5' TCAGACTTTGGGAAATTGAACGTAAC 3'. The PCR amplification was done using an annealing temperature of 60^{o}C and yielded a 294 bp fragment from the mutant allele and a smaller 254 bp fragment from the wild-type allele. The mice were then crossed with the different transgenic CRE mice to obtain in a first step mice carrying the CRE transgenes with one copy of the KCC3floxed allele and in a second step mice carrying or not the CRE transgenes with two copies of the KCC3floxed allele, i.e. tissue-specific KCC3 knockout mice. Behavioral tests were performed with age of mice ranging from 90 – 130 days.

Accelerated Rotarod. The accelerated rotarod test was performed as previously described (Geng et al., 20010). Briefly, neuromotor coordination task was performed using an accelerating rotating cylinder (model 47600: Ugo Basile, S.R. Biological Research Apparatus, Comerio, Italy). The cylinder was 3 cm in diameter and was covered with scored plastic. Mice were confined to a 4 cm long section of the cylinder by gray Plexiglas dividers. Three to five mice were placed on the cylinder at once. The rotation

rate of the cylinder increased over a 5 min period from 4 to 40 rpm. The latency of each mouse to fall off the rotating cylinder was automatically recorded by the device. Mice that remained on the rotarod during the 300 s trial period were removed and given a score of 300 s. The test was performed for three trials a day for 3 consecutive days.

Open field. This test was also executed as described earlier (Geng et al., 2010). Exploratory and locomotor activities were tested using an open-field activity chamber surrounded by a Plexglas enclosure within sound-attenuating cubicles (ENV-022MD-027; Med Associates, Inc., St. Albans, VT). The mice were placed in the center of the open field and their activity was monitored for 60 min. The test was performed at ambient room temperature (25^{o}C), moderate light (60 lx), and background noise (80 dB). Distance traveled and time spend in the periphery (thigmotaxis) of the chamber were quantified by the number of beam crossings.

Hot-plate assay in Nav1.8-CRE x KCC3$^{f/f}$ mice. The hotplate assay was performed by placing the mice individually on a platform maintained at 52 ℃ to 55 ℃ (Hot-Plate Analgesia Meter; Columbus Instruments, Columbus, OH). A plastic cylinder measuring 15 cm (diameter) and 20 cm (height) confined the mouse to the surface of the hotplate. The time necessary for the mouse to respond to the thermal stimulus (hindpaw fluttering, licking, or withdrawal) was measured using a stopwatch. After the initial response or the maximal cutoff time of 15 seconds, the mouse was removed from the hotplate and returned to its home cage. A minimal recovery period of 1 day was implemented between assays at the two temperatures.

Dorsal root ganglia fixation and immunofluorescence staining. Dorsal root ganglia were dissected from the lower thoracic to mid-lumbar regions of the vertebral column and were placed in a 4% (w/v) solution of PFA (Sigma Aldrich) in 0.1 M PBS (4^{o}C, pH 7.4) overnight. Following fixation, DRG neurons were transferred to a 30% (w/v) sucrose solution in 0.1 M PBS for 24 hours ~48 hours before embedding into O.C.T. compound (Sakura Tissue-Tek, Thermo Fisher Scientific) blocks. The O.C.T. blocks were stored at −20°C before being transferred for cryostat sectioning. Sections were cut 10 μm thick in the cryostat microtome at −20°C and were immediately transferred to a room temperature microscope slide by gentle touching. The slides were stored at −20°C for further histology study. Routine H&E staining was performed for general histology. For immunostaining, the slides were defrosted at room temperature for 10 min., and then permeabilized with 0.1% Triton X-100 for 5 min. After 2 washes in PBS for 5 min. each, the slides were blocked for 30 min with 1% BSA + 1% goat serum in PBS. Primary antibodies (anti-PDI antibody (Abcam, Ab27043 1:200), anti-NSE antibody (Abcam, ab53025, 1:250), anti-parvalbumin antibody (Abcam, MAB1572, 1:500), anti-Cre antibody (Abcam, ab24607, 1:500)) were applied in 1%BSA with PBS at 4 ℃, overnight. On the second day, the slides were washed twice separately with high salt PBS and regular PBS, then blocked with 1% BSA + 4% goat serum in PBS for 30 min. Secondary antibodies (100 ul, Cy3 conjugated anti-rabbit antibody (1:1000, Jackson Immunochemicals) or Alexa Fluor anti-mouse IgG (H+L) (1:400, Invitrogen) were then applied and incubated for 60 min at room temperature. After final washes with high salt PBS and regular PBS, coverslips were mounted on slides using VectaShield (Vector

Laboratories, Burlingame, CA) and sealed with nail polish. Fluorescence signal was visualized using a Carl Zeiss LMS 510 META confocal microscope.

Spinal cord fixation and immunohistochemistry. Mice were euthanized and lumbar vertebra were collected and submerged in 10% neutral buffered formalin for overnight fixation. Following overnight fixation, vertebrae were decalcified in 23% formic acid for 48 hours. The vertebrae were cut in cross sections, placed in tissue cassettes, processed routinely, embedded in paraffin, cut in 4 m sections, mounted on slides and stained with hematoxylin and eosin for identification of dorsal root ganglia. Once the sections containing DRGs were identified, unstained slides were cut for immunohistochemical labeling with anti-mouse parvalbumin (Cat# p3088, Sigma) at a 1:200 dilution on a Bond Max Autostainer (Leica), using EDTA antigen retrieval for 20 minutes, and Ultravision^{TM} Quanto Mouse-on-mouse blocking kit (Thermo Fisher Scientific).

Western blot analysis. After euthanasia, brains from Eno2-CRE x KCC3$^{f/f}$ and KCC3$^{f/f}$ control mice were promptly removed and flash frozen in liquid Nitrogen. Tissue was then homogenized using a dounce/Teflon pestle in 0.32M sucrose buffer (0.32 M sucrose, 5 mM Tris-Cl pH 7.5, 2 mM EDTA, 2.5 mM β-mercaptoethanol and protease inhibitors), spun at 4,000 rpm for 10 min, followed by 9,000 rpm for 20 min, and 100,000 rpm for 1 hour. Pellets (microsomal fractions) were resuspended in sucrose buffer and the protein concentration was measured using standard Bradford Assay. Equal amount of protein (200 ug) was loaded on a 9% SDS-polyacrylamide gel, separated, and electrotransferred onto 0.45 m polyvinylidine fluoride membranes (ThermoFisher Scientific). The membrane was incubated for 2 h at room temperature in blocking solution (5% nonfat milk in TBST, i.e. 150 mM NaCl, 10 mM Tris, 0.5% Tween 20), and incubated with

rabbit polyclonal anti-KCC3 antibody (1:1000) overnight at 4^{o}C. The membrane was the thoroughly washed in TBST, incubated with horseradish peroxidase-conjugated secondary antibody in blocking solution (1:5000) for 1 hour at RT, and washed again for 2 h in TBST. Protein bands were visualized by chemiluminescence (ECL Plus, Amersham Biosciences, Piscataway, NJ).

Statistical analysis. For rotarod experiment, statistical analyses were performed using SAS software (version 9.3, SAS Institute, Inc., Cary, NC). To account for the effects of animal group, days, and trials on rotorod times, a three-way repeated measures ANOVA test was utilized. The error terms of the different animal groups was modeled as independent variables while both the error terms of days and trials were correlated variables. Numerous covariate matrices were used to model both days and trials with the matrix that best fit the data ultimately being used (autoregressive model of order 1). To analyze the trends of rotorod times based on days and trials, Bonferroni-corrected linear and quadratic contrasts were constructed for both of these variables. $P < 0.05$ was considered statistically significant. For other analyses, two-tailed paired t-tests were performed using GraphPad Prism (version 3.0, GraphPad Sotwares, Inc., La Jolla, CA). Data were noted to be significant at $P < 0.05$ and highly significant at $P < 0.001$.

3. Results

In order to determine the cellular origin of HSMN/ACC, we created several conditional KCC3 knockout mouse lines by using Cre mediated recombination under the control of tissue-specific promoters. First we created a mouse in which the KCC3 was flanked by

loxP sites. A construct targeting exon 7 was engineered (Figure 22) and electroporated in mouse embryonic stem cells. After germline transmission and elimination of the neomycin-resistance gene cassette, a 3 kb fragment was PCR amplified to demonstrate recombination in the proper locus. Sequencing of the fragment revealed correct 5' sequence and presence of the exon and of loxP sites at the 3' end, demonstrating recombination in the proper KCC3 locus.

As previous report has shown that KCC3 KO mice display severe motor and locomotor abnormalities (Boettger et al., 2003; Howard et al., 2002), we subjected all our conditional KCC3 knockout mice to a standard protocol of accelerating rotarod: 3 trials a day for 3 days. The test assesses fore- and hindlimb balance coordination as well as a learning component for this motor task (Karl et al., 2003). Locomotor activity was also assessed in an open-field chamber equipped with infrared beams. Each mouse was separately monitored for distance traveled during a specific time period. For our first tissue-specific knockout mouse line, we crossed $KCC3^{flox/flox}$ mice with animals that express the Cre recombinase under the Nav1.8 promoter (Stirling et al., 2005). Nav 1.8 is a voltage-gated sodium channel which is expressed in a subset of sensory neurons, 85% or more of which are nociceptors. Thus, we generated a mouse where KCC3 deletion is targeted in nociceptive neurons. As shown in Figure 23, we observed no difference between wild-type and Nav1.8-driven KCC3 knockout mice ($F_{(1, 15)} = 2.76$; $P = 0.1173$, 8-9 mice per group). When we performed statistical analysis of trials or days, we observed a very significant difference: $F_{(6, 90)} = 4.4$, $P = 0.0006$ for trials and $F_{(2, 30)} = 7.88$, $P = 0.0018$ for days, indicating that the mice are learning the task or performing better with each trial and each day of trials. The relationship between trials was linear: $F_{(2, 90)} =$

5.84, $P = 0.002$, instead of quadratic: $F_{(1,90)} = 0.57$, $P = 0.05778$. There was also no difference in total distance travelled in the open field test, as the two tailed t-test demonstrated a P value of 0.3696 (t = 0.9270, df = 14, n = 8-9 mice per group). As Nav1.8 is expressed in nociceptive neurons, we also tested the mice for a nociception phenotype. There was no statistical differences between the two groups of mice in the response latency (withdrawal times) to heat-evoked nociceptive stimuli at 52^{o}C (t = 0.8307, df = 15, $P = 0.4192$), or 55^{o}C (t = 0.6465, df = 15, $P = 0.5277$).

To explore the possibility that the locomotor deficit is caused by KCC3 deletion in Schwann cells, we utilized a transgenic mouse expressing the CRE recombinase under the desert hedgehog (Dhh) promoter, desert hedgehog being a protein expressed exclusively in Schwann cells (Parmantier et al., 1999) and Sertoli cells in testis (Bitgood et al., 1996). Figure 24 presents the data of the accelerated rotorod and open field tests performed in control (KCC3$^{f/f}$) and Schwann cell knockout (Dhh-CRE x KCC3$^{f/f}$) sibling mice. No differences were observed between genotypes in the rotorod test ($F_{(1, 14)} = 0$; $P = 0.9741$, 8 mice per group). Again, all mice learned the task as the differences between trials and days were highly significant: $F_{(6, 84)} = 4.82$, $P = 0.0003$ and F(2, 28) = 18.99, $P < 0.,0001$), respectively. Similarly, we observed no phenotype in the open field test (t = 0.2828, df = 15, $P = 0.7812$).

To confirm that neurons were involved in the development of the phenotype, we used enolase-2-CRE (Eno2-CRE) mice to drive deletion of KCC3 in neurons. Surprisingly, we observed no locomotor deficit in these mice (Figure 25).There was no difference between genotypes in the latency to fall the accelerating rod: $F_{(1,10)} = 3.37$, $P = 0.0962$ nor in the

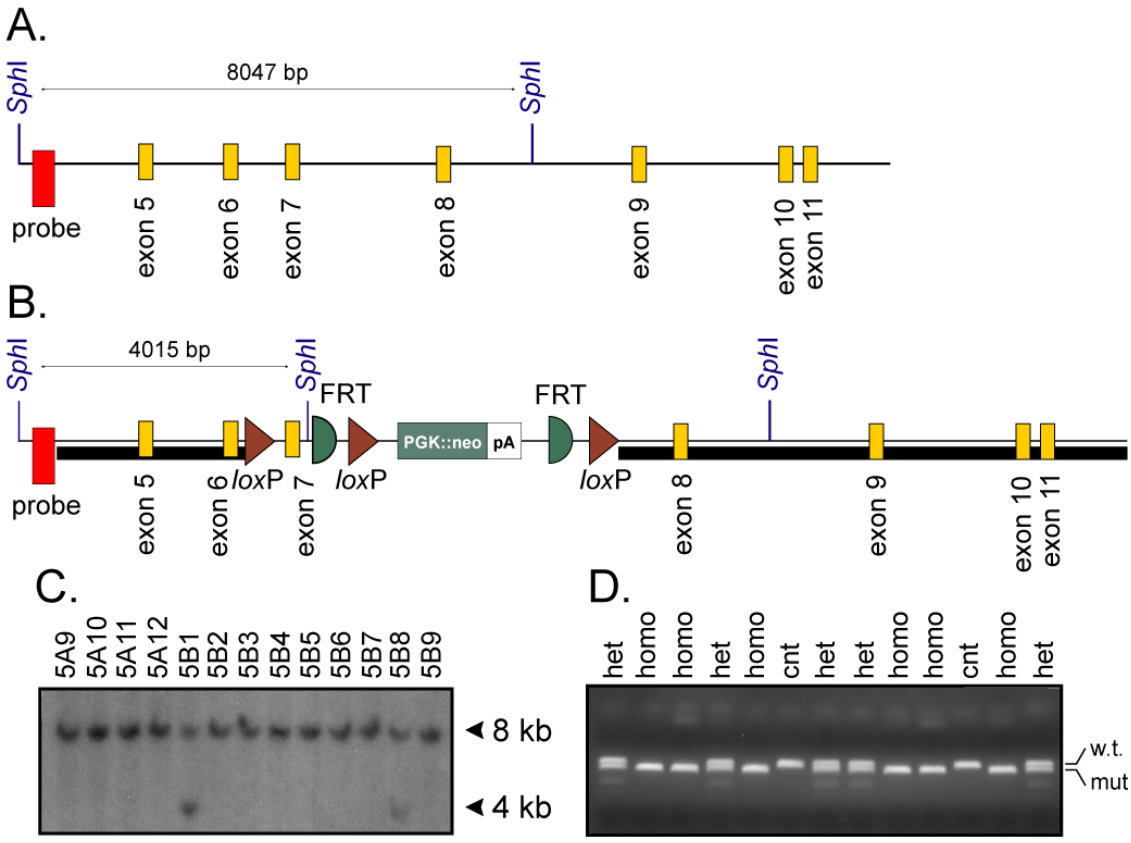

Figure 22. Generation of the KCC3$^{flox/flox}$ mouse.

A. Schematic representation of the *Slc12a6* (KCC3) gene around exon 5-11. Highlighted are two S*ph*I restriction sites separated by 8 kb genomic sequence. Location of a 347 bp PCR fragment/^{32}P-labelled probe (red box) is also indicated. **B**. Construct containing a 2950 bp genomic DNA sequence representing the 5' arm of recombination (short black box), *lox*P sites flanking exon 7, followed by a PGK-driven neomycin resistance gene cassette flanked by FRT sites, and a 7500 bp 3' arm of recombination (long black box). A *Sph*I site was inserted downstream of exon 7, reducing the size of the SphI fragment recognized by the 5' probe from 8 to 4 kb. **C**. Portion of the ES cell screening Southern blot (*Sph*I digest) showing 13 clones with 8 kb genomic fragment (wild-type allele), including 2 clones with an additional 4 kb fragment (mutant allele). **D**. Genotyping of 2 litters of pups from heterozygous breeding showing PCR fragments from wild-type and mutant alleles.

ability to learn the task, as there was highly significant difference between trials ($F_{(6, 60)}$ = 8.44, $P < 0.0001$) or days ($F_{(2, 20)}$ = 8.38, $P = 0.0023$). There was also no difference in the distance traveled in the open-field test (two-tailed t test with t = 0.03740, df = 10, P = 0.9709). To determine the extent of KCC3 deletion in central neurons, we performed a Western blot analysis of KCC3 from brains obtained from control ($KCC3^{f/f}$) and tissue-specific knockout (Eno2-CRE x $KCC3^{f/f}$) mice. As seen in the inset of Figure 25, there was significant decrease in KCC3 expression in the brain of Eno2-CRE x $KCC3^{f/f}$ mice, indicating that this promoter efficiently drove deletion of the cotransporter in neuronal populations in the brain. Expression of the CRE recombinase in sensory DRG neurons was examined by immunofluorescence in a later Figure.

Next, we targeted deletion of KCC3 in proprioceptive neurons (Arber et al., 2000) by using a parvalbumin-CRE (Prvlb-CRE) transgenic mouse (Hippenmeyer et al., 2005). When locomotion and balance coordination was measured in Prvlb-CRE x $KCC3^{f/f}$ mice compared to their control littermate, we observed a phenotype with knockout mice falling significantly faster: < 150 sec versus >250 sec: $F_{(1,17)} = 42$, $P < 0.0001$(Figure 26). The knockout mice, however, were able to improve their performance as the difference between trials was highly significant ($F_{(6,102)} = 10.38$, $P < 0.0001$), as was the difference between days ($F_{(2,34)} = 20.76$, $P < 0.001$). The differences in the average rotorod times between the two animal groups were similar for each of the three days ($F_{(2,34)} = 3.04$, P = 0.0592) and each of the three trials within each day ($F_{(6,102)} = 1.89$, $P = 0.0897$), indicating absence of group day interaction or group trial interaction. When the locomotor activity was assessed through the open field, we observed a trend towards hyperactivity, although it did not reach statistical significance.

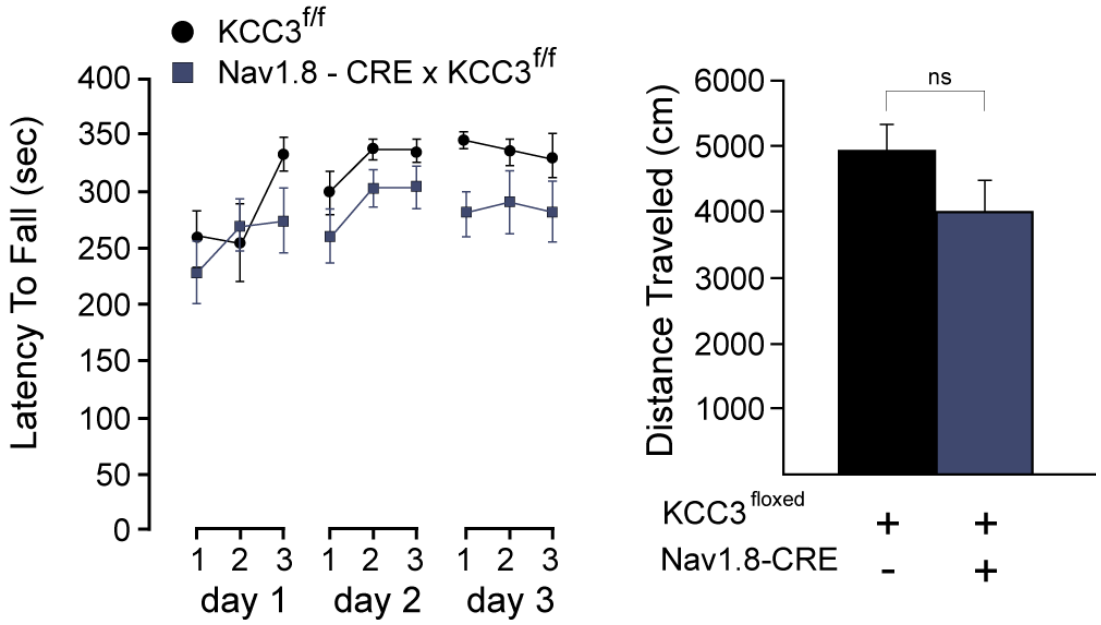

Figure 23. Absence of locomotor phenotype in Nav1.8-driven KCC3 knockout mice.

A. Accelerated rotorod test (4 to 40 rpm, 5 min) performed in control ($KCC3^{f/f}$) and tissue-specific knockout (Nav1.8-CRE x $KCC3^{f/f}$) mice. Test was given three times a day for 3 consecutive days. The latency to fall from the rotating rod to the platform was measured in seconds. B. Locomotor activity as measured by the distance traveled (cm) in the open filed chamber over a period of 60 min. Statistical analyses showed no significant differences between groups (see text). N = 8-9 mice per group.

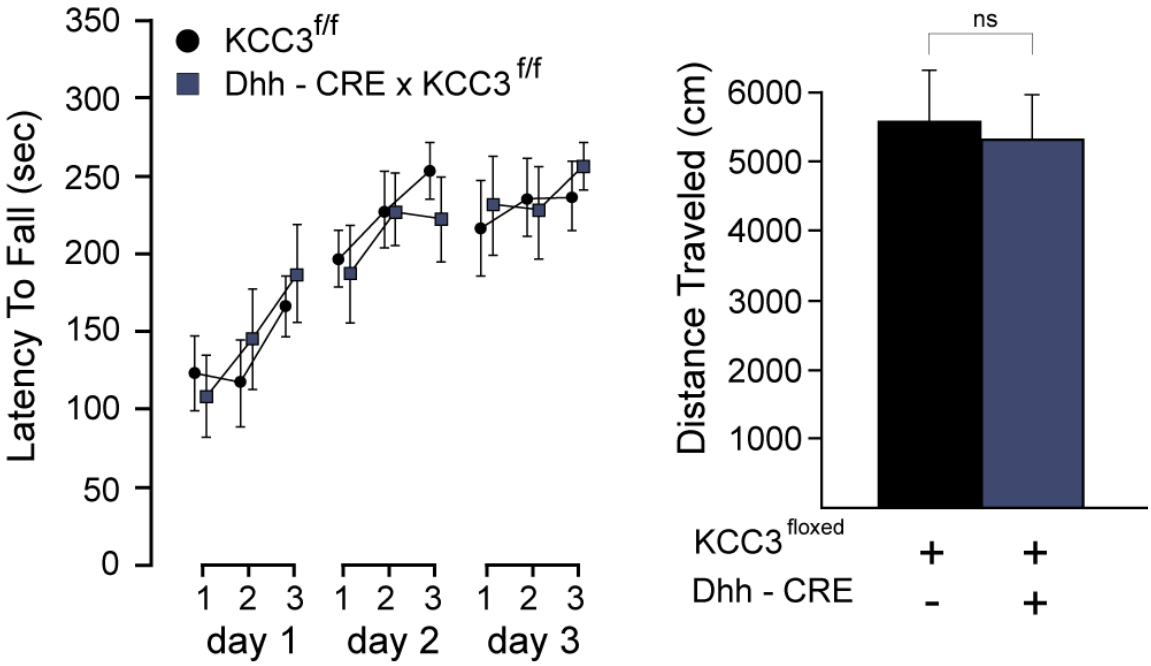

Figure 24. Absence of locomotor phenotype in Dhh-driven KCC3 knockout mice.

A. Accelerated rotorod test (4 to 40 rpm, 5 min) performed in control ($KCC3^{f/f}$) and tissue-specific knockout (Dhh-CRE x $KCC3^{f/f}$) mice. Test was given three times a day for 3 consecutive days. The latency to fall from the rotating rod to the platform was measured in seconds. B. Locomotor activity as measured by the distance traveled (cm) in the open filed chamber over a period of 60 min. Statistical analyses showed no significant differences between groups (see text). N = 10 mice per group.

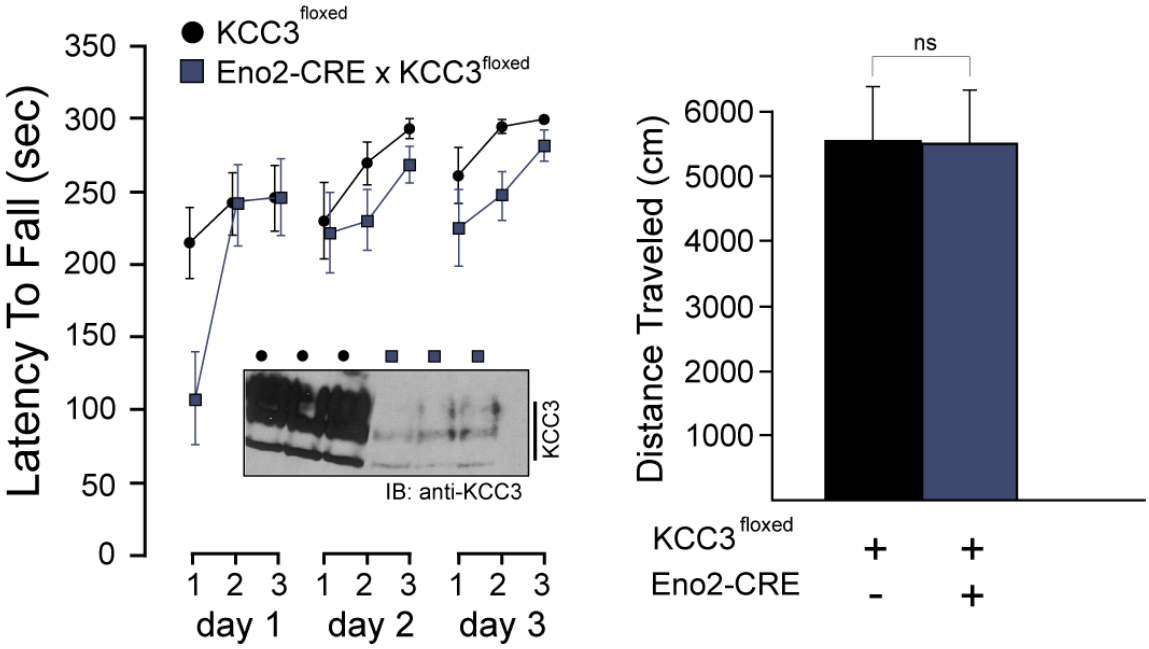

Figure 25. Absence of locomotor phenotype in Eno2-driven KCC3 knockout mice.

A. Accelerated rotorod test (4 to 40 rpm, 5 min) performed in control ($KCC3^{f/f}$) and tissue-specific knockout (Eno2-CRE x $KCC3^{f/f}$) mice. Test was given three times a day for 3 consecutive days. The latency to fall from the rotating rod to the platform was measured in seconds. Inset: Western blot analysis of KCC3 expression in brain of 3 controls and 3 Eno2-CRE driven knockout mice. B. Locomotor activity as measured by the distance traveled (cm) in the open filed chamber over a period of 60 min. Statistical analyses showed no significant differences between groups (see text). N = 6 mice per group.

Using immunofluorescence, we examined the expression of parvalbumin and enolase-2 in isolated dorsal root ganglion from wild-type mice, and expression of CRE in DRGs isolated from Prvlb-CRE x KCC3$^{f/f}$ and Eno2-CRE x KCC3$^{f/f}$ mice. As described in the method section, the ganglia were promptly removed from the spinal cord, fixed, cryoprotected, embedded, and cryosectioned. As seen in Figure 27A, strong parvalbumin staining was observed in a subset of large cells, whereas other cells showed weak or no staining. In contrast, enolase staining was punctated in dorsal root ganglia (Fig. 27B), demonstrating a very different pattern of expression (merge, Fig. 27C). Consistent with this staining pattern in wild-type mice, CRE expression was observed in large neurons in the Prvlb-CRE mouse, while punctated staining was observed in the Eno2-CRE mouse.

Further analyses of dorsal root ganglia were performed by immunocytochemistry. Entire spinal cord sections were H&E stained and when dorsal root ganglia were observed, the next contiguous section was stained with anti-parvalbumin antibody. Large vacuoles, reminiscent of what was observed in brain and spinal cord in the global KCC3 knockout (Boettger et al., 2003), were observed in dorsal roots of Prvlb-CRE x KCC3 knockout mice (Figure 28, arrows). In addition, many structures containing dense material (arrow heads) were also observed in the DRG of these mice. The vacuoles and structures were immuno-reactive with the anti-parvalbumin antibody (Figure 28C, 28D). To better understand the histopathlogy of the dorsal root ganglia in these tissue-specific knockout mice, we isolated spinal cords from wild-type mice and KCC3 global knockout mice. The tissues were subjected to the exact same protocol, from animal perfusion to parvalbumin antibody detection. While no vacuoles or dense materials were observed in DRGs from wild-type mice (Figure 29A, B), pathology similar to that observed in parvalbumin-

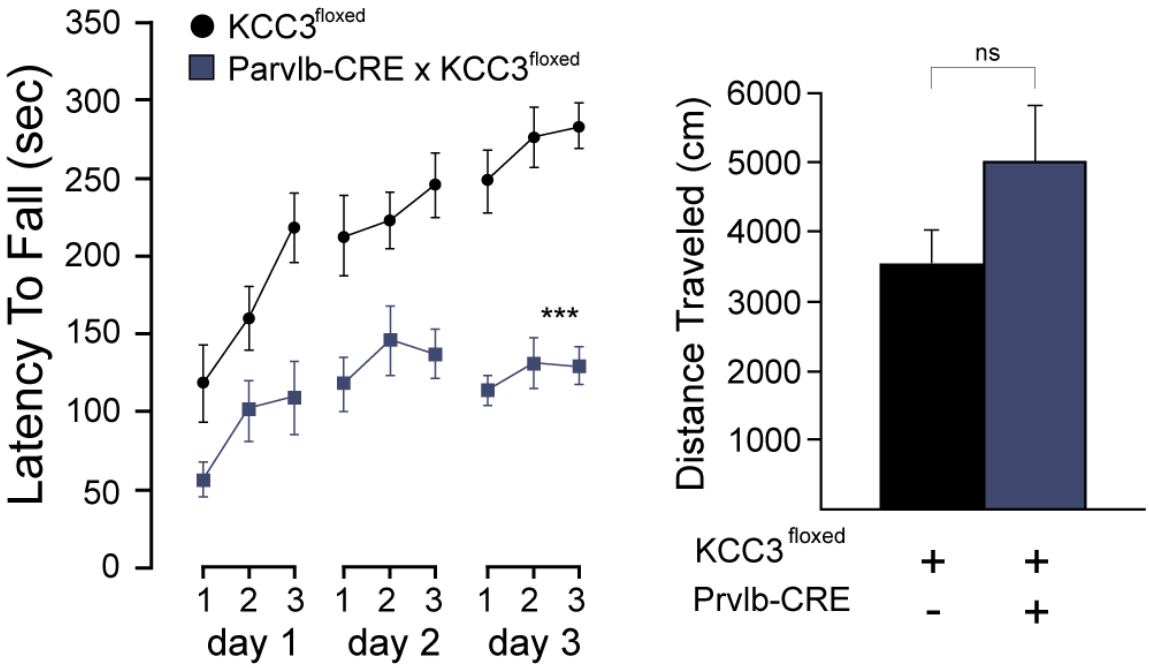

Figure 26. A locomotor phenotype is observed in parvalbumin-driven KCC3 knockout mice.

A. Accelerated rotorod test (4 to 40 rpm, 5 min) performed in control ($KCC3^{f/f}$) and tissue-specific knockout (Eno2-CRE x $KCC3^{f/f}$) mice. Test was given three times a day for 3 consecutive days. The latency to fall from the rotating rod to the platform was measured in seconds. B. Locomotor activity as measured by the distance traveled (cm) in the open filed chamber over a period of 60 min. Statistical analyses showed highly significant difference between groups in the rotorod test (see text), but no difference in the activity/open field test. N = 8-11 mice per group. *** $P < 0.001$, highly significant.

driven KCC3 knockout was also observed in the DRGs of global knockout mice (Figure 29C, D).

4. Discussion

To address the cellular origin of the locomotor deficit associated with the disruption of KCC3 in mice and the development of the early onset peripheral neuropathy disorder observed in HSN/ACC patients (Boettger et al., 2003; Howard et al., 2002), we created several tissue-specific knockout lines. Only when KCC3 was targeted in parvalbumin positive neurons did we detect a locomotor deficit similar to the one observed in the global knockout animals. Parvalbumin is a member of a large family of EF-hand containing calcium-binding proteins, which contains in excess of 200 members in human (Popelár et al., 2013). It is essential for Ca^{2+} homeostasis and the modulation of intracellular Ca^{2+} concentration in specific populations of neurons (Celio, 1990). In the brain, parvalbumin is almost exclusively expressed in subpopulations of inhibitory fast-spiking GABAergic interneurons located in many different brain regions such as cortex, cerebellum, hippocampus and the reticular nucleus of the thalamus (Celio, 1990; Mùnkle et al., 2000; Ohshima et al., 1991). Deficits in parvalbumin expressing interneurons have been linked to cognitive impairments in animal models of Alzheimer disease (Verret et al., 2012). In the peripheral nervous system, parvalbumin is expressed in proprioceptive type Ia fibers (Figure 30). The locomotor deficit observed in the Prvlb-CRE x $KCC3^{f/f}$ mice is unlikely related to a disruption of parvalbumin in these mice. Indeed, the transgenic mouse was created by inserting the CRE recombinase in the parvalbumin gene locus using an internal ribosomal entry site (IRES) at the end of the exons encoding the

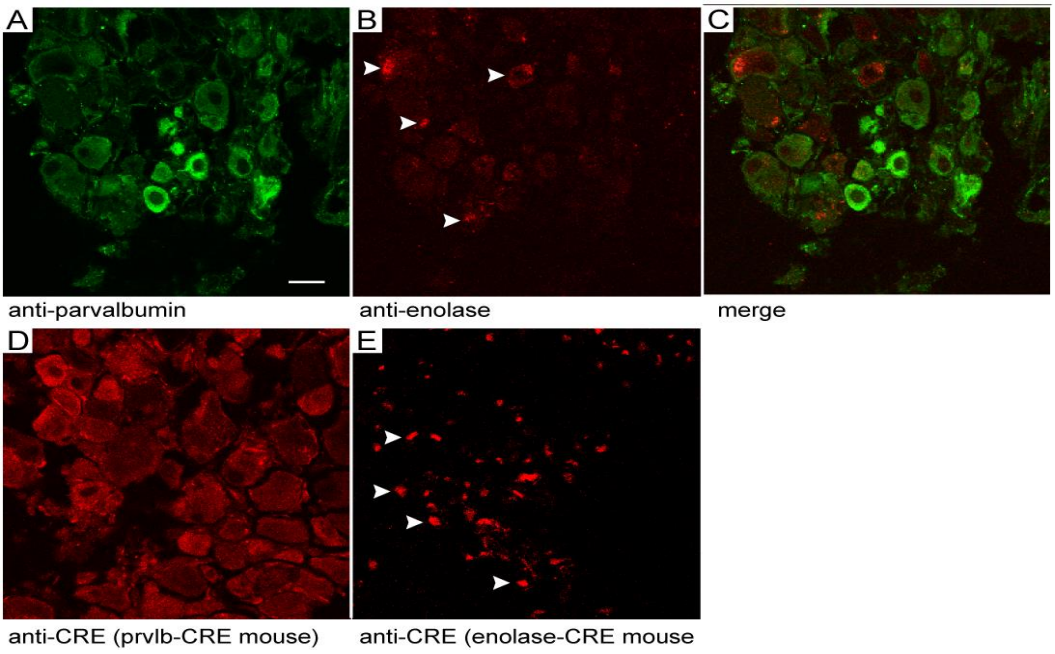

Figure 27. Parvalbumin and enolase 2 were expressed in different structures of DRG neurons.

A-C. Longitudinal sections of DRG neurons from wild-type (n=3) mice were analyzed using immunofluorescence antibody against parvalbumin (A, green) and enolase 2 (B, red). Panel C represents the summation of both signals. **D-E**. Longitudinal sections of DRG neurons from parvalbumin-CRE x KCC3$^{f/f}$ mice and Eno2-CRE x KCC3$^{f/f}$ mice were immunostained with CRE antibody. CRE expression was observed in both mice and mirrored the signal seen with the two protein-specific antibodies.

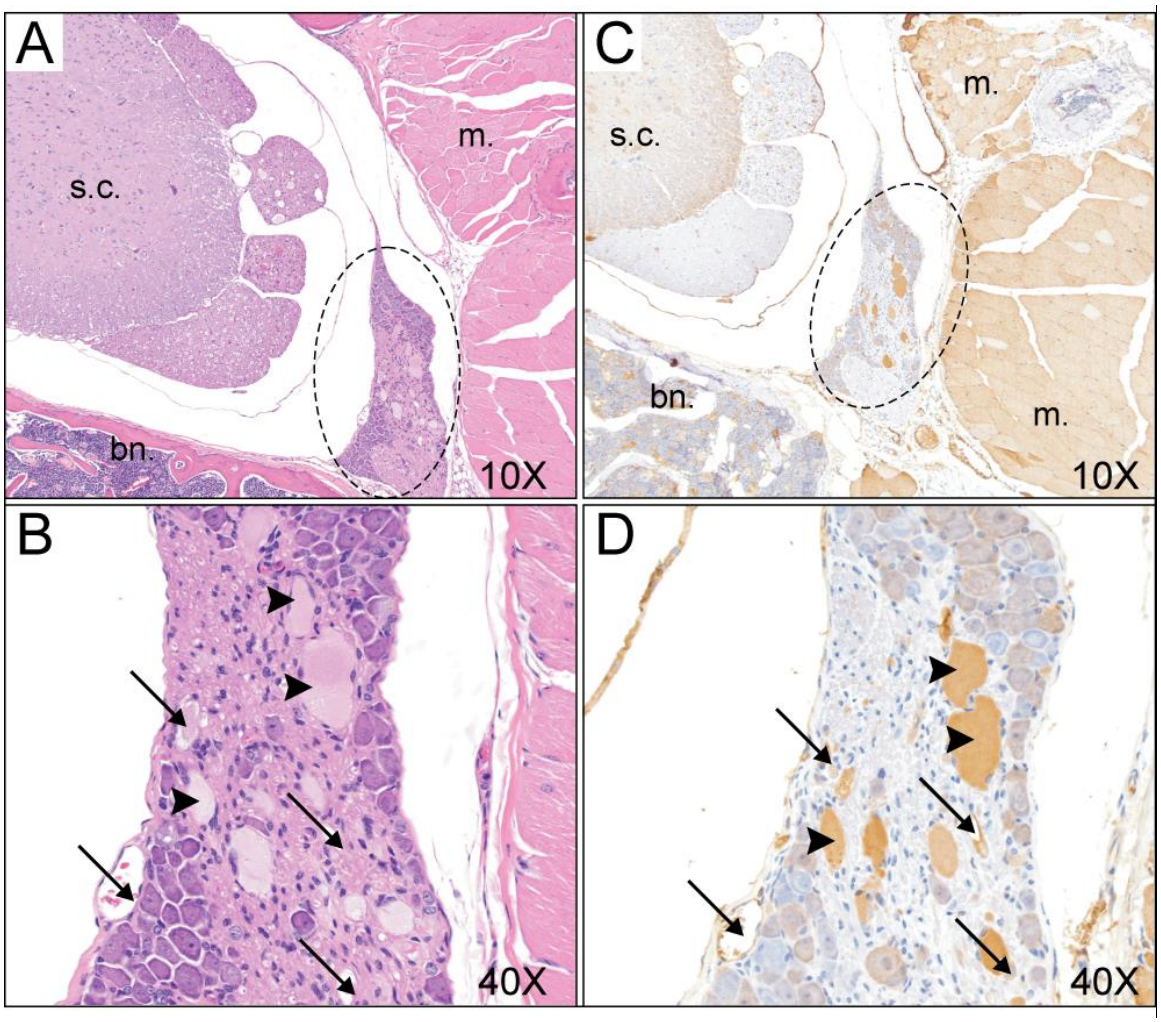

Figure 28. Histological analysis of dorsal root ganglia in Prvlb-CRE x KCC3$^{f/f}$ mice.

A. Partial view of spinal cord with dorsal root with H&E stain at a magnification of 10x. **B**. Higher magnification (40x) of the dorsal root of Panel A. C. Contiguous section showing spinal cord stained with anti-parvalbumin antibody. D. Higher magnification (40x) of the dorsal root showing parvalbumin staining of structures surrounding vacuoles (arrows) as well as some dense material which is parvalbumin immunoreactive. The following structures are labeled: s.c. = spinal cord; m. = muscle; bn. = bone, dashed circle = dorsal root ganglion.

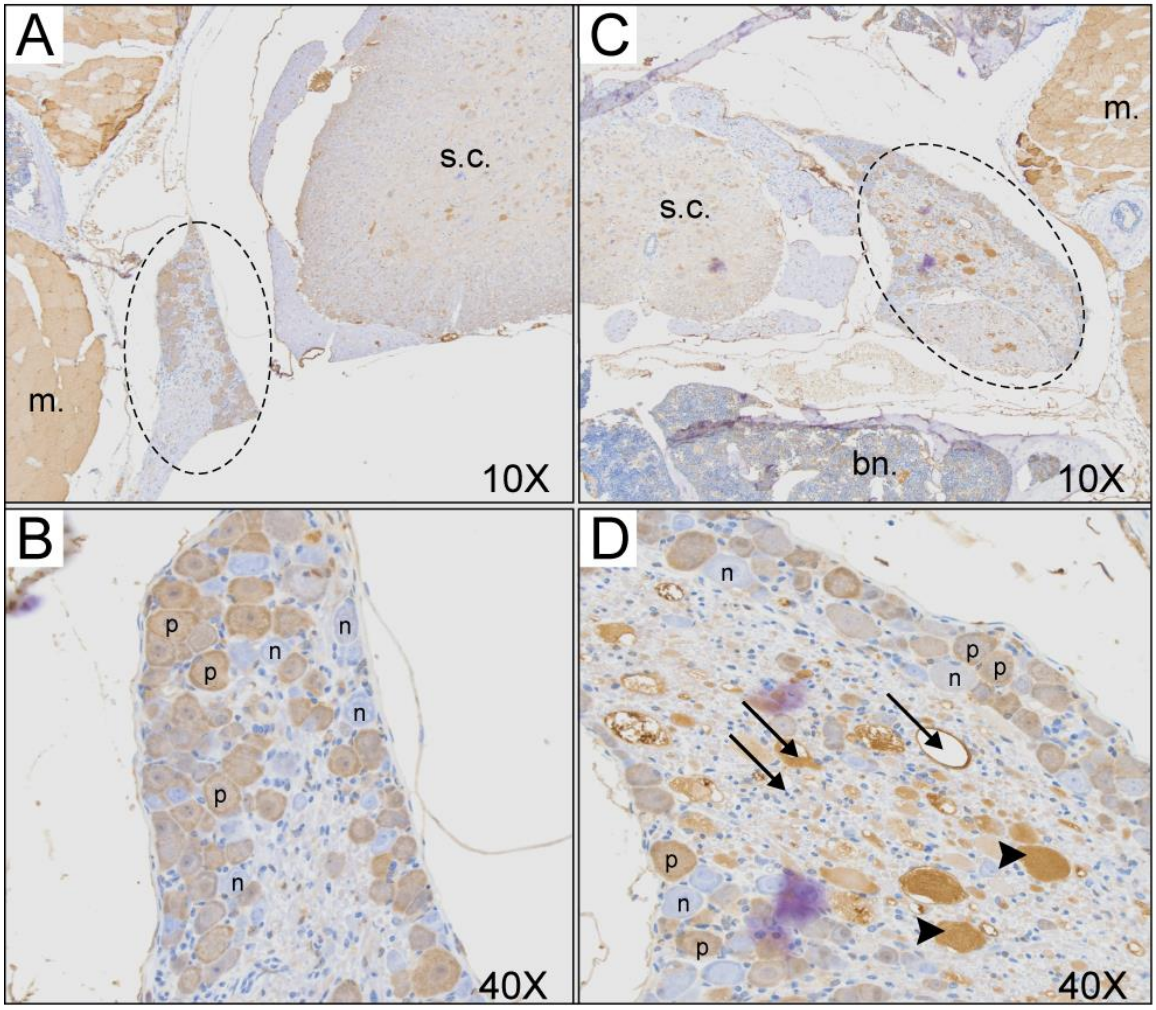

Figure 29. Histological analysis of dorsal root ganglia from wild-type and global KCC3 knockout mice.

A. Partial view of spinal cord with dorsal root and parvalbumin staining in wild-type mouse at a magnification of 10x. **B**. Higher magnification (40x) of the dorsal root of Panel A, showing absence of pathology. **C**. Partial view of spinal cord with dorsal root and parvalbumin staining in global KCC3 knockout mouse at a magnification of 10x. **D**. Higher magnification (40x) of the dorsal root of Panel C, showing pathology similar to that observed in Figure 7. The following structures are labeled: s.c. = spinal cord; m. = muscle; bn. = bone, dashed circle = dorsal root ganglion, p = positive neuron, n = negative neuron.

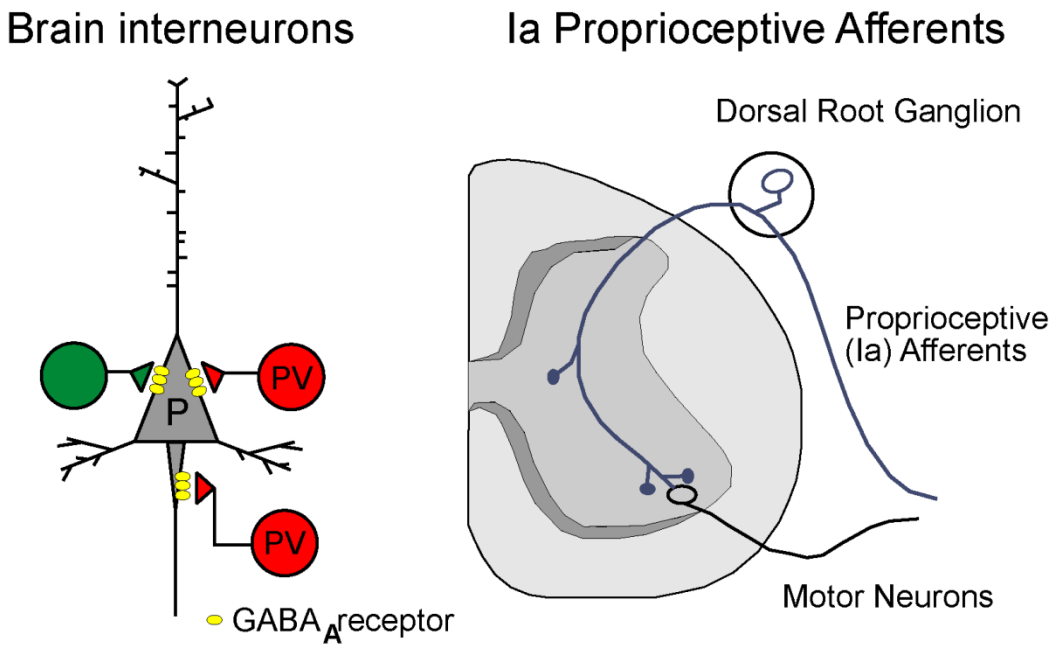

Figure 30. Schematic representation of parvalbumin expression in neurons.

In brain, parvalbumin is expressed in fast-spiking GABAergic interneurons (PV) which provide inhibitory input to pyramidal neurons (P). Another type of interneuron is depicted green. In the periphery, parvalbumin is expressed in type Ia large diameter proprioceptive afferents neurons which project to both middle spinal cord interneurons and to ventral motor neurons.

calcium binding protein. Thus, both parvalbumin and CRE transcripts are expressed under the parvalbumin promoter. Parvalbumin expression was verified by our immunocytochemistry studies of dorsal root ganglia which showed parvalbumin expression in the tissue-specific knockout mice (Figures 28). Furthermore, it was shown that disruption of parvalbumin in mice had no phenotype in the rotarod assay (Farré-Castany et al., 2007). Therefore, the observed phenotype likely originates from disruption of KCC3 in proprioceptive DRG neurons. In fact, we demonstrated that the abnormal structures in the dorsal root ganglia of either tissue-specific or global KCC3 knockout, i.e. vacuoles and dense material, had parvalbumin immunoreactivity (Figures 28 and 29). Thus, the pathology clearly involves parvalbumin fibers. This observation makes the involvement of CNS interneurons (e.g. in cerebellum) in the locomotor phenotype less likely. On the other hand, decreased KCC3 expression in CNS interneurons might explain the hyperactivity observed in the neuronal-specific KCC3 knockout mouse (Shekarabi et al., 2012), and the hyperactivity trend observed in our parvalbumin-driven KCC3 knockout mouse. Decreased activity of parvalbumin-positive interneurons would result in an increased excitatory network drive, leading to hyperactivity. Interestingly, network hyperexcitability and increased susceptibility to epileptic seizures were also demonstrated in parvalbumin null mice (Schwaller et al., 2004). Although not tested in this study, global KCC3 knockout mice also demonstrate a reduced threshold to develop seizures (Boettger et al., 2003).

None of the other 3 tissue specific knockout mice showed the same locomotor deficit as the Parvlb-CRE x KCC3$^{f/f}$ mice. Because global KCC3 knockout mice demonstrated hypomyelination and periaxonal swelling (Byun and Delpire, 2007), we postulated that

Schwann cells might contribute to the phenotype, and more specifically KCC3 as a mechanism which drive salts and water out of the cell might be involved in the process of myelin compaction. We therefore targeted KCC3 in Schwann cells by crossing our floxed mouse with Desert hedgehog (Dhh)-driven CRE mice. These mice have been used to successfully delete Pten in Schwann cells (Keng et al., 2012). Dhh is a member of the Hedgehogs family of intercellular signaling proteins that are best known for controlling tissue patterning during development (Ferent and Traiffort, 2014). Dhh is specifically expressed in Schwann cells of the nervous system and Sertoli cells in the testis in mammals. Mutations in human DHH have been identified resulting in gonade dysgenesis associated with polyneuropathy (Umehara et al., 2000). In addition, Dhh knockout (KO) mice have abnormal perineurial sheath formation, suggesting a key role of controlling the connective tissue sheaths formation around peripheral nerves (Bitgood et al., 1996; Parmantier et al., 1999). Our results showed no locomotor phenotype in these mice, indicating no participation of Schwann cell KCC3 in the development of ACCPN. Note that this observation does not rule out the participation of Schwann cells themselves in ACCPN, as these cells clearly interact with both normal and degenerating neurons in the nerves of KCC3 knockout mice or ACCPN patients. The lack of phenotype also indicates that the Schwann cell deficit observed in the global KCC3 knockout and in patients is likely to be secondary to the neuronal degeneration(Byun and Delpire, 2007; Larbrisseau et al., 1984).

To test whether the locomotor and balance deficit is related to an inability to sense mechanical pressure, we crossed the $KCC3^{f/f}$ line with Nav1.8-driven CRE mice (Stirling et al., 2005). Indeed, Nav1.8 is a voltage-gated sodium channel alpha subunit which is

found within small-diameter sensory DRG neurons and is involved in temperature and mechanical pressure perception as well as nociception (Liu and Wood, 2011). As no locomotor deficit was observed in these mice, we can conclude that the accelerated rotarod phenotype observed in the global KCC3 knockout mice is not related to a role of the cotransporter in these small sensory fibers. As we had the Nav1.8-CRE x KCC3f/f mouse line, we also tested the mice for a heat-evoked nociception phenotype at two noxious temperatures (52^{o}C and 55^{o}C). There was no difference observed between genotypes in the latency to respond to the thermal stimuli. Our data therefore indicate that KCC3 is unlikely to play a key role in the physiology of these neurons.

In our studies, we included a CRE line, Eno2-CRE, that we thought would produce knockout of KCC3 in all neurons. This line was our version of the synapsin 1-CRE line used by Shekarabi and coworkers (Shekarabi et al., 2012). Neuron specific enolase (Eno2, γ-enolase) is a glycolytic enzyme that catalyzes the conversion of phosphoglycerate to phosphoenol pyruvate in neurons (Marangos and Schmechel, 1987). Enolase 2 expression started shortly after synaptogenesis and is shown to be expressed in most mature neurons and neuroendocrine cells, thus making it a useful mature neuron specific marker (Bock and Dissing, 1975; Whitehead et al., 1982). We were surprised by the absence of a locomotor phenotype in Eno2-CRE x KCC3$^{f/f}$ mice (Figure 25). To generate the transgenic Eno2-CRE mice, a 1.8-kb DNA promoter element which is located upstream of the rat NSE gene was inserted upstream of the CRE recombinase (Frugier et al., 2000). As demonstrated by our Western blot analysis of KCC3 expression, recombination was extremely efficient in the brain of Eno2-CRE positive mice. These data suggest that expression of the recombinase is optimal in central but not peripheral neurons. This could

be due to either poor enolase-2 expression or weak promoter activity of the transgene in sensory neurons. Our immunofluorescence data (Figure 27) showed punctated CRE expression signal in DRG, different from the large cell bodies staining we observed in Parvlb-CRE mice.

In conclusion, our study establishes a key role for parvalbumin expressing neurons in the development of the locomotor phenotype associated with HSN/ACC. The precise function of KCC3 in these cells is still unknown. Our study also indicates that the lack of function of KCC3 in Schwann cells nor in neurons sensing mechanical signals does not contribute to the locomotor phenotype observed in the HSN/ACC disorder.

V. Conclusions and future directions

1. Summary of work

The goal of my work was to understand the underlying pathogenic mechanism of HSN/ACC or ACCPN. ACCPN is a devastating disease with progressive neuropathy and partial or complete agenesis of corpus callosum. Scientists have spent decades trying to uncover the origin of this disease, and have made important steps towards a better understanding of this disorder. Today we know that ACCPN is caused by genetic mutations in the *SLC12A6* gene KCC3, and through a neuron-specific tissue specific KCC3 knockout, it has been established that the ACCPN disease is mostly driven by neural tissues. However, the current progress or understanding is still far away from allowing for the development of therapies for this disease.

In my study, I first characterized in heterologous expression systems the properties of a KCC3 mutation that was found during the cloning of the cDNA encoding the mouse KCC3. Compared with other known KCC3 mutations, KCC3-E289G was able to be produced as a full-length protein, therefore conserving the C-terminal which was lost in most other mutations. Through uptake experiments performed in frog oocytes, we demonstrated that KCC3 is functionally silent. Through cell surface expression studies in oocytes and immunofluorescence studies in HEK293 cells, we demonstrated that the KCC3-E289G mutant protein was not properly trafficked to the plasma membrane. The mutant protein was glycosylation-deficient and arrested in the endoplasmic reticulum or the early Golgi. Through co-immunoprecipitation experiments, we showed that hetero-dimers formed between wild-type and mutant KCC3 proteins, and this dimerization was

specific for the K-Cl cotransporters, as it was not observed for NKCC1. We demonstrated that glutamic acid residue (E289) was essential for proper trafficking and function of the K-Cl cotransporters and had potential dominant-negative effects on other K-Cl cotransporters in heterologous expressions systems.

Concurrently, I created a KCC3 knock-in transgenic mouse with this E289G mutation. The first line of KCC3E289G mice was embryonic lethal due to unknown reasons, but unrelated to the mutant exon. Through the injection of an independent ES cell clone, I was able to generate a new line of KCC3E289G knock-in mice, which was fully viable. I performed locomotor behavior tests on these mice and was able to observe a significant motor deficit reminiscent of the ACCPN phenotype. I went ahead and performed immunohistochemistry studies on isolated DRG neurons from these mice. The fact that the KCC3 $^{E289G/-}$ double mutation mice did not shown any locomotor deficit was quite puzzling, given that the only KCC3 present in this mouse line was the non-functional KCC3E289G. More work needs to be done to analyze whether the copy number is a potential reason for the distinct phenotypes of KCC3 $^{E289G/-}$ and KCC3 $^{E289G/E289G}$.

In a separate study, I addressed the origin of the cells responsible for the development of ACCPN. I created four lines of tissue-specific KCC3 knockout mice by taking advantage of the Cre-Lox technology. In these conditional lines, KCC3 was deleted by expressing Cre in different cell populations through the use of gene specific promoters: Nav1.8, parvalbumin, enolase-2, and desert hedgehog. Among the 4 lines of mice, only the parvalbumin-driven line showed a significant locomotor deficit, although not as severe as the one observed in the global knockout (Figure 32). The fact that enolase-2 driven transgenic mouse did not show a phenotype was quite surprising, as it was widely

believed that the enolase-2 Cre mice was able to drive the recombination in most mature neurons of mice. Through immunostaining in isolated DRG neurons, I was able to confirm that enolase-2 was not present in all DRG neuron populations and it had a distinct expression profile than parvalbumin. Furthermore, H&E staining and parvalbumin antibody staining were performed on sections of spinal cords isolated from parvalbumin-driven KCC3 mice. Vacuolization and cell degeneration similar to the ones observed in global KCC3 knockout were observed in DRG of parvalbumin-driven KCC3 knockout mice, indicating that these specific proprioceptive neurons are responsible for HSN/ACC.

In the meantime, I noticed that the locomotor deficit in the parvalbumin-driven KCC3 was milder than the KCC3 global knock out, suggesting there might be other key factors contributing to the overall pathology of ACCPN. In fact, when we examine the detailed pathological analysis of ACCPN disease in patients, a number of tissues and organs are affected. Even though the agenesis of corpus callosum phenotype varies in different patients, the sporadic oval vacuoles in the white matter are present in brains of all patients, revealing neuron degeneration process in the central nervous systems. This phenotype was observed in both the global KO and tissue specific KO mouse models.

Similar to the nerve degeneration and demyelination in peripheral nerves of mouse models, severe nerve pathology in the ACCPN patients is also observed. One of the most striking phenotype is the presence of massive enlarged axons and significant decrease of myelinated fibers in the dorsal root neurons. A moderate axonal loss is also observed, suggesting the abnormal neuron degeneration. In 2 patients from Austria, sensory action

potential was absent (Hauser et al., 1993). Since the parvalbumin positive neurons are mostly expressed in large diameter myelinated primary afferents, these pathological observations from human and mouse models fit rather quite well, confirming a key role for the large myelinated primary afferents during the development of ACCPN disease.

However, autopsy examination on ACCPN patients suggested that motor neurons could also be a contributing factor to the disease. The presence of onion bulbs, formed by the concentric lamellae of Schwann cells, was very common in nerve roots. Thin myelin sheaths were also observed in a large part of neurons. The nerve conduction velocity was reduced in motor neuron of 2 patients, consistent with a similar report in mouse models (Byun and Delpire, 2007; Hauser et al., 1993). Most of the patients showed severe delayed development of motor function by starting to walk very late or being not able to walk without help. Detailed examination on patient showed severe muscular hypotonia, significant reduction of spontaneous motility and absence of tendon flexes. Profound muscular hypertrophy was observed in some patients and the normal muscle structures such as sarcomeric architecture and banding were disrupted in many fibers as well.

These complicated pathological observations from ACCPN patients revealed the complexity of the origin and development of this disease, the discovery of the key roles of parvalbumin positive neurons is an important step towards a full understand of this syndrome has provided some important clinical insights on potential therapeutic methods of ACCPN. One of the first studies following this is to evaluate the possibility whether the locomotor phenotype caused by parvalbumin specific KCC3 deletion could be rescued, either through genetic method or through small molecular activating KCC3. As

discussed in the future direction segment, an inducible parvalbumin specific KCC3 knockout mouse models would be very helpful to explore this further. However, due to the significant differences between human being and mouse nervous systems, the application of potential effective ACCPN treatment on mouse should be evaluated cautiously.

2. Future directions

Further studies are clearly needed to understand the connection between KCC3 and the physiology of parvalbumin-positive nociceptive neurons. A more detailed phenotyping of the mice is needed to assess whether other neurological phenotypes are also related to parvalbumin positive neurons. Indeed, parvalbumin is also expressed in central interneurons which provide inhibitory input to large pyramidal neurons. Thus, the increased activity which was demonstrated in a synapsin-1-driven KCC3 knockout (Shekarabi et al., 2012), and suggested in our parvalbumin-driven knockout mouse, might be related to the function of KCC3 in interneurons. Note that loss of interneurons expressing calbindin or parvalbumin results in increased locomotor phenotype (Farre-Castany et al., 2007; Shekarabi et al., 2012). Similarly, our parvalbumin-driven KCC3 mice could be tested for prepulse inhibition and susceptibility to develop epileptic seizures (Boettger et al., 2003; Howard et al., 2002; Popelar et al., 2013; Schwaller et al., 2004). It is interesting that that increased activity was not observed in the global KCC3 knockout mouse (Figure 31B). This might be due to the severity of the locomotor phenotype that affects the overall activity of the mice.

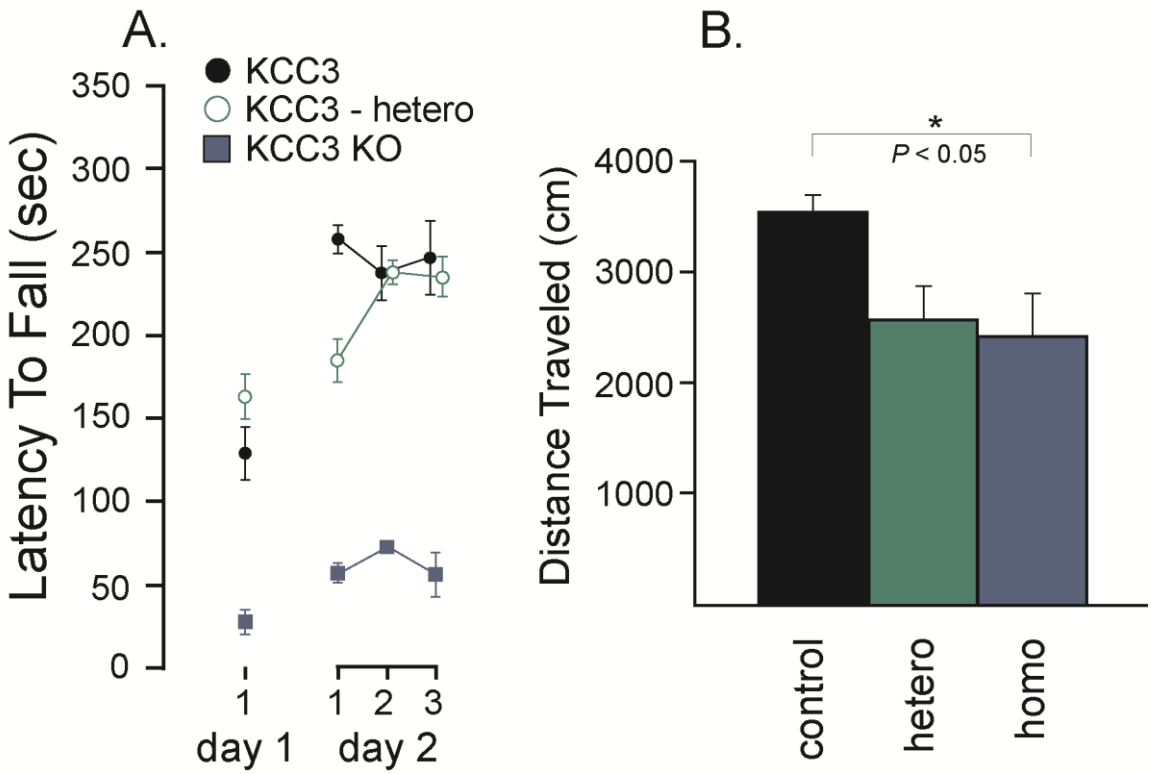

Figure 31. Locomotor phenotype in KCC3 global knockout mice.

A. Accelerated rotorod test (4 to 40 rpm, 5 min) performed on two days in wild-type (KCC3), heterozygous (KCC3 – hetero), and homozygous (KCC3 – homo) mice. The test was given three times on the second day. B. Locomotor activity measured as the distance traveled (cm) in an open filed chamber over a 20 min period. Statistical analysis was performed using ANOVA and showed significant $P < 0.05$ difference between homozygous and wild-type mice. N = 12-14 mice per group.

The fact that a subpopulation of neurons is responsible for the phenotype should also help us address the role of KCC3 in these cells. Indeed, parvalbumin-CRE tdTomato mice could be used to 1) determine if tdTomato is expressed in a subpopulation of DRG neurons and 2) isolate and purify that specific population of cells for cell culture and *in vitro* studies.

The cells could be enriched by Fluorescence Activated Cell Sorting (FCTS) and placed in culture. The role of KCC3 modulating the Cl^- reversal potential could be measured as previously done with NKCC1 in the laboratory (Sung et al., 2000). Imaging and cell volume reconstruction could also be measured to assess the cell volume regulation role of KCC3 in these cells. Then, parvalbumin-positive cells could be isolated from the KCC3 knockout mice, hopefully as soon as parvalbumin positive cells are visible in the mouse and before the cells start to degenerate. Cell survival could be measured by plating identical number of cells in culture and counting them as a function of time (days) in culture.

The studies we presented with our current KCC3 antibodies were not optimal as cotransporter expression could not be easily detected in the plasma membrane. Future studies should work at optimizing the conditions for the antibody or at creating additional antibodies to detect cell surface expression of KCC3. One possibility would be to generate an antibody directed against an external epitope (extracellular loop), which could be used to visualize the cotransporter and quantitate cell surface expression, without permeabilizing the cells.

The appearance and development of HSN/ACC occurs in early childhood and the locomotor phenotype is also noticeable in very young mice. Thus, there is likely a developmental component to the disease, even if there is a degenerative component. Whether the phenotype can be rescued at any point in time by re-expressing KCC3 can be tested in mice. The laboratory has created a new genetically modified KCC3 mouse model in which exon 7 (including 100-150 bp upstream and downstream sequence) is duplicated with a stop codon introduced in the duplicated exon (Figure 32). The duplicated exon is also flanked by *lox*P sites. This mouse will be used in combination with an existing parvalbumin-tTA mouse (available at the Jackson laboratories) and a phCMV-teto-CRE mouse available in the laboratory to create an inducible 'rescue' mouse. Before recombination, the mutated exon 7 will produce a transcript that contains a premature stop codon. The mouse will therefore be diseased as KCC3 will not be expressed. Upon recombination (induced with doxyxcycline or doxycycline withdrawal from food), the exon will be excised and full-length KCC3 will be initiated. There is hope that by playing with time of induction, one should be able to determine up to what point (if any) the rescue of the phenotype is possible.

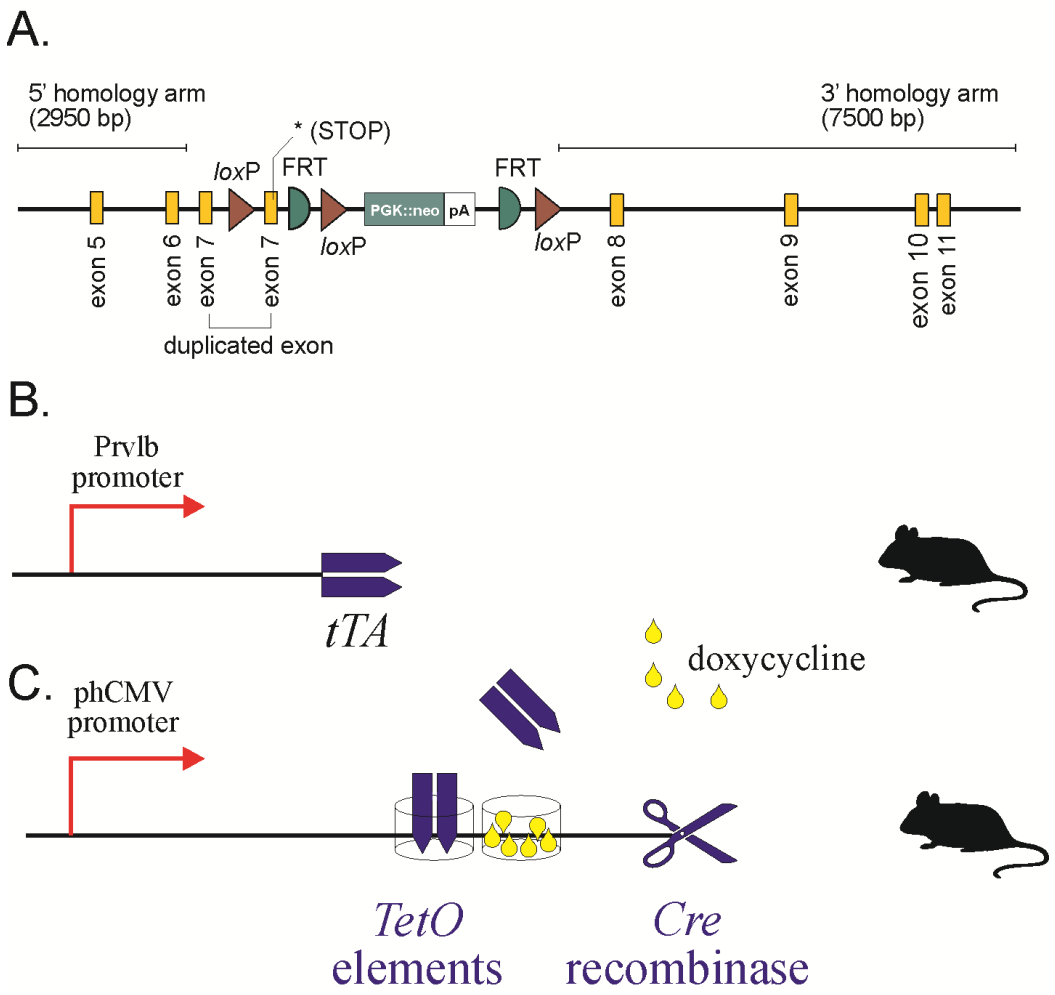

Figure 32. Design of a KCC3 rescue mouse.

Construct of a KCC3 rescue mouse with exon 7 duplicated. Although insertion of the exon places the remainder out of frame, the duplicated exon also includes stop codons. The mouse would be crossed to two transgenic lines: one carrying tetracycline transactivator gene product under the parvalbumin promoter (B), the other carrying the CRE recombinase with a global promoter (phCMV) and tetO elements. Doxycycline (provided in the diet) prevents binding of tTA to the TetO elements. Upon doxycycline withdrawal, tTA expressed in parvalbumin-positive cells can now bind to TetO elements and initiate expression of the recombinase. Upon recombinase expression, the mutant exon 7 is excised and a full-length (wild-type) KCC3 protein can be expressed.

LITERATURE CITED

Adragna NC, Chen Y, Delpire E, Lauf PK, Morris M (2004) Hypertension in K-Cl cotransporter-3 knockout mice. Adv Exp Med Biol 559: 379-385.

Adragna NC, White RE, Orlov SN, Lauf PK (2000) K-Cl cotransport in vascular smooth muscle and erythrocytes: possible implication in vasodilation. Am J Physiol Cell Physiol 278: C381-390.

Amlal H, Paillard M, Bichara M (1994) Cl(-)-dependent NH4+ transport mechanisms in medullary thick ascending limb cells. Am J Physiol 267: C1607-1615.

Anagnostopoulos AV, Mobraaten LE, Sharp JJ, Davisson MT (2001) Transgenic and knockout databases: behavioral profiles of mouse mutants. Physiol Behav 73: 675-689.

Andermann E, Andermann F, Joubert M, Melancon D, Karpati G, Carpenter S (1975) Three familial midline malformtion syndromes of the central nervous system: agenesis of the corpus callosum and anterior horn-cell disease; agenesis of cerebellar vermis; and atrophy of the cerebellar vermis. Birth Defects Orig Artic Ser 11: 269-293.

Andermann F, Andermann E, Joubert M, Karpati G, Carpenter S, Melancon D (1972) Familial agenesis of the corpus callosum with anterior horn cell disease. A syndrome of mental retardation, areflexia, and paraplegia. Transactions of the American Neurological Association 97: 242-244.

Andermann F, Andermann E, Joubert M, Karpati G, Carpenter S, Melancon D (1972) Familial agenesis of the corpus callosum with anterior horn cell disease: a syndrome of mental retardation, areflexia and paraparesis. Trans Amer Neurol Ass 97: 242-244.

Arber S, Ladle DR, Lin JH, Jessell FE (2000) ETS gene Er81 controls the formation of functional connections between group Ia sensory afferents and motor neurons. Cell 101.

Belenky MA, Sollars PJ, Mount DB, Alper SL, Yarom Y, Pickard GE (2010) Cell-type specific distribution of chloride transporters in the rat suprachiasmatic nucleus. Neuroscience 165: 1519-1537.

Ben-Ari Y, Khalilov I, Kahle KT, Cherubini E (2012) The GABA excitatory/inhibitory shift in brain maturation and neurological disorders. Neuroscientist 18: 467-486.

Bitgood MJ, Shen L, McMahon AP (1996) Sertoli cell signaling by Desert hedgehog regulates the male germline. Curr Biol 6: 298-304.

Blaesse P, Airaksinen MS, Rivera C, Kaila K (2009) Cation-chloride cotransporters and neuronal function. Neuron 61: 820-838.

Bock E, Dissing J (1975) Demonstration of Enolase Activity Connected to Brain-Specific Protein 14.3.2. Scandinavian Journal of Immunology: 31-36.

Boettger T, Rust MB, Maier H, Seidenbecher T, Schweizer M, Keating DJ, Faulhaber J, Ehmke H, Pfeffer C, Scheel O, Lemcke B, Horst J, Leuwer R, Pape HC, Volkl H, Hubner CA, Jentsch TJ (2003) Loss of K-Cl co-transporter KCC3 causes deafness, neurodegeneration and reduced seizure threshold. EMBO J 22: 5422-5434.

Boettger T, Rust MB, Maier H, Seidenbecher T, Schweizer M, Keating DJ, Faulhaber J, Ehmke H, Pfeffer C, Scheel O, Lemcke B, Horst J, Leuwer R, Pape HC, Volkl H, Hubner CA, Jentsch TJ (2003) Loss of K-Cl co-transporter KCC3 causes deafness, neurodegeneration and reduced seizure threshold. EMBO J 22: 5422-5434.

Byun N, Delpire E (2007) Axonal and periaxonal swelling precede peripheral neurodegeneration in KCC3 knockout mice. Neurobiol Dis 28: 39-51.

Byun N, Delpire E (2007) Axonal and periaxonal swelling precede peripheral neurodegeneration in KCC3 knockout mice. Neurobiol Dis 28: 39-51.

Casaubon LK, Melanson M, Lopes-Cendes I, Marineau C, Andermann E, Andermann F, Weissenbach J, Prevost C, Bouchard JP, Mathieu J, Rouleau GA (1996) The gene responsible for a severe form of peripheral neuropathy and agenesis of the corpus callosum maps to chromosome 15q. Am J Hum Genet 58: 28-34.

Casaubon LK, Melanson M, Lopes-Cendes I, Marineau C, Andermann E, Andermann F, Weissenbach J, Prevost C, Bouchard JP, Mathieu J, Rouleau GA (1996) The gene responsible for a severe form of peripheral neuropathy and agenesis of the corpus callosum maps to chromosome 15q. Am J Hum Genet 58: 28-34.

Casula S, Shmukler BE, Wilhelm S, Stuart-Tilley AK, Su W, Chernova MN, Brugnara C, Alper SL (2001) A dominant negative mutant of the KCC1 K-Cl cotransporter: both N- and C-terminal cytoplasmic domains are required for K-Cl cotransport activity. J Biol Chem 276: 41870-41878.

Celio MR (1990) Calbindin D-28k and parvalbumin in the rat nervous system. Neuroscience 35: 375-475.

Chen YF, Chou CY, Ellory JC, Shen MR (2010) The emerging role of KCl cotransport in tumor biology. Am J Transl Res 2: 345-355.

Colclasure GC, Parker JC, Dunham PB (1995) Creatine-Kinase Is Required for Swelling-Activated K-Cl Cotransport in Dog Red-Blood-Cells. American Journal of Physiology-Cell Physiology 268: C660-C668.

Crable SC, Hammond SM, Papes R, Rettig RK, Zhou GP, Gallagher PG, Joiner CH, Anderson KP (2005) Multiple isoforms of the KC1 cotransporter are expressed in sickle and normal erythroid cells. Exp Hematol 33: 624-631.

De Braekeleer M, Dallaire A, Mathieu J (1993) Genetic epidemiology of sensorimotor polyneuropathy with or without agenesis of the corpus callosum in northeastern Quebec. Hum Genet 91: 223-227.

de Los Heros P, Kahle KT, Rinehart J, Bobadilla NA, Vazquez N, San Cristobal P, Mount DB, Lifton RP, Hebert SC, Gamba G (2006) WNK3 bypasses the tonicity requirement for K-Cl cotransporter activation via a phosphatase-dependent pathway. Proc Natl Acad Sci U S A 103: 1976-1981.

Delpire E (2000) Cation-Chloride Cotransporters in Neuronal Communication. News Physiol Sci 15: 309-312.

Delpire E, Gagnon KB, Ledford J, Wallace J (2011) Housing and husbandry of *Xenopus laevis* impact the quality of oocytes for heterologous expression studies. J Am Assoc Lab Anim Sci 50: 46-53.

Delpire E, Lu J, England R, Dull C, Thorne T (1999) Deafness and imbalance associated with inactivation of the secretory Na-K-2Cl co-transporter. Nat Genet 22: 192-195.

Denning GM, Anderson MP, Amara JF, Marshall J, Smith AE, Welsh MJ (1992) Processing of Mutant Cystic-Fibrosis Transmembrane Conductance Regulator Is Temperature-Sensitive. Nature 358: 761-764.

Di Fulvio M, Lincoln TM, Lauf PK, Adragna NC (2001) Protein kinase G regulates potassium chloride cotransporter-4 [corrected] expression in primary cultures of rat vascular smooth muscle cells. J Biol Chem 276: 21046-21052.

Ding J, Ponce-Coria J, Delpire E (2013) A trafficking-deficient mutant of KCC3 reveals dominant-negative effects on K-Cl cotransport function. PLoS One 8: e61112.

Dixon MJ, Gazzard J, Chaudhry SS, Sampson N, Schulte BA, Steel KP (1999) Mutation of the Na-K-Cl co-transporter gene Slc12a2 results in deafness in mice. Hum Mol Genet 8: 1579-1584.

Dunham PB, Ellory JC (1981) Passive potassium transport in low potassium sheep red cells: dependence upon cell volume and chloride. J Physiol 318: 511-530.

Dupre N, Howard HC, Mathieu J, Karpati G, Vanasse M, Bouchard JP, Carpenter S, Rouleau GA (2003) Hereditary motor and sensory neuropathy with agenesis of the corpus callosum. Ann Neurol 54: 9-18.

England JD, Asbury AK (2004) Peripheral neuropathy. Lancet 363: 2151-2161.

Farré-Castany M, A., Schwaller B, Gregory P, Barski J, Mariethoz C, Eriksson JL, Tetko IV, Wolfer D, Celio MR, Schmutz I, Albrecht U, Villa AE (2007) Differences in locomotor behavior revealed in mice deficient for the calcium-binding proteins parvalbumin, calbindin D-28k or both. Behav Brain Res 178: 250-261.

Farre-Castany MA, Schwaller B, Gregory P, Barski J, Mariethoz C, Eriksson JL, Tetko IV, Wolfer D, Celio MR, Schmutz I, Albrecht U, Villa AE (2007) Differences in locomotor behavior revealed in mice deficient for the calcium-binding proteins parvalbumin, calbindin D-28k or both. Behav Brain Res 178: 250-261.

Ferent J, Traiffort E (2014) Hedgehog: Multiple Paths for Multiple Roles in Shaping the Brain and Spinal Cord. Neuroscientist.

Fields S, Johnston M (2005) Cell biology. Whither model organism research? Science 307: 1885-1886.

Filteau MJ, Pourcher E, Bouchard RH, Baruch P, Mathieu J, Bedard F, Simard N, Vincent P (1991) Corpus callosum agenesis and psychosis in Andermann syndrome. Arch Neurol 48: 1275-1280.

Flagella M, Clarke LL, Miller ML, Erway LC, Giannella RA, Andringa A, Gawenis LR, Kramer J, Duffy JJ, Doetschman T, Lorenz JN, Yamoah EN, Cardell EL, Shull GE (1999) Mice lacking the basolateral Na-K-2Cl cotransporter have impaired epithelial chloride secretion and are profoundly deaf. J Biol Chem 274: 26946-26955.

Friedel RH, Wurst W, Wefers B, Kuhn R (2011) Generating conditional knockout mice. Methods Mol Biol 693: 205-231.

Frugier T, Tiziano FD, Cifuentes-Diaz C, Miniou P, Roblot N, Dierich A, Le Meur M, Melki J (2000) Nuclear targeting defect of SMN lacking the C-terminus in a mouse model of spinal muscular atrophy. Hum Mol Genet 9: 849-858.

Gagnon KB, Adragna NC, Fyffe RE, Lauf PK (2007) Characterization of glial cell K-Cl cotransport. Cell Physiol Biochem 20: 121-130.

Gagnon KB, Delpire E (2010) Molecular determinants of hyperosmotically activated NKCC1-mediated K^+/K^+ exchange. J Physiol (Lond) 588: 3385-3396.

Gagnon KB, Delpire E (2012) Molecular Physiology of SPAK and OSR1: Two Ste20-Related Protein Kinases Regulating Ion Transport. Physiol Rev 92: 1577-1617.

Gagnon KB, Delpire E (2012) Molecular physiology of SPAK and OSR1: two Ste20-related protein kinases regulating ion transport. Physiol Rev 92: 1577-1617.

Gagnon KB, Delpire E (2013) Physiology of SLC12 transporters: lessons from inherited human genetic mutations and genetically engineered mouse knockouts. Am J Physiol Cell Physiol 304: C693-714.

Gagnon KB, Rios K, Delpire E (2011) Functional insights into the activation mechanism of Ste20-related kinases. Cell Physiol Biochem 28: 1219-1230.

Gamba G (2005) Molecular physiology and pathophysiology of electroneutral cation-chloride cotransporters. Physiol Rev 85: 423-493.

Garcia-Otin AL, Guillou F (2006) Mammalian genome targeting using site-specific recombinases. Front Biosci 11: 1108-1136.

Garzon-Muvdi T, Pacheco-Alvarez D, Gagnon KB, Vazquez N, Ponce-Coria J, Moreno E, Delpire E, Gamba G (2007) WNK4 kinase is a negative regulator of K+-Cl- cotransporters. Am J Physiol Renal Physiol 292: F1197-1207.

Gillen CM, Brill S, Payne JA, Forbush B, 3rd (1996) Molecular cloning and functional expression of the K-Cl cotransporter from rabbit, rat, and human. A new member of the cation-chloride cotransporter family. J Biol Chem 271: 16237-16244.

Greger R, Schlatter E (1983) Properties of the basolateral membrane of the cortical thick ascending limb of Henle's loop of rabbit kidney. A model for secondary active chloride transport. Pflugers Arch 396: 325-334.

Hauser E, Bittner R, Liegl C, Bernert G, Zeitlhofer J (1993) Occurrence of Andermann syndrome out of French Canada--agenesis of the corpus callosum with neuronopathy. Neuropediatrics 24: 107-110.

Hebert SC, Mount DB, Gamba G (2004) Molecular physiology of cation-coupled Cl(-) cotransport: the SLC12 family. Pflugers Arch 447: 580-593.

Hiki K, D'Andrea RJ, Furze J, Crawford J, Woollatt E, Sutherland GR, Vadas MA, Gamble JR (1999) Cloning, characterization, and chromosomal location of a novel human K+-Cl- cotransporter. J Biol Chem 274: 10661-10667.

Hippenmeyer S, Vrieseling E, Sigrist M, Portmann T, Laengle C, Ladle DR, Arber S (2005) A developmental switch in the response of DRG neurons to ETS transcription factor signaling. PLoS Biol 3: e159.

Hoffmann EK, Lambert IH, Pedersen SF (2009) Physiology of cell volume regulation in vertebrates. Physiol Rev 89: 193-277.

Holden P, Horton WA (2009) Crude subcellular fractionation of cultured mammalian cell lines. BMC Res Notes 2: 243.

Horvitz HR (2003) Worms, life, and death (Nobel lecture). Chembiochem 4: 697-711.

Howard HC, Mount DB, Rochefort D, Byun N, Dupré N, Lu J, Fan X, Song L, Rivière J-B, Prévost C, Welch R, England R, Zhan FQ, Mercado A, Siesser WB, George AL, Horst J, Simonati A, McDonald MP, Bouchard J-P, Mathieu J, Delpire E, Rouleau GA (2002) Mutations in the K-Cl cotransporter KCC3 cause a severe peripheral neuropathy associated with agenesis of the corpus callosum. Nat Genet 32: 384-392.

Howard HC, Mount DB, Rochefort D, Byun N, Dupre N, Lu J, Fan X, Song L, Riviere JB, Prevost C, Horst J, Simonati A, Lemcke B, Welch R, England R, Zhan FQ, Mercado A, Siesser WB, George AL, Jr., McDonald MP, Bouchard JP, Mathieu J, Delpire E, Rouleau GA (2002) The K-Cl cotransporter KCC3 is mutant in a severe peripheral neuropathy associated with agenesis of the corpus callosum. Nat Genet 32: 384-392.

Huan MC (2010) Laboratory evaluation of peripheral neuropathy. Semin Neurol 30: 337-349.

Hubner CA, Stein V, Hermans-Borgmeyer I, Meyer T, Ballanyi K, Jentsch TJ (2001) Disruption of KCC2 reveals an essential role of K-Cl cotransport already in early synaptic inhibition. Neuron 30: 515-524.

Hughes RA (1995) Epidemiology of peripheral neuropathy. Curr Opin Neurol 8: 335-338.

Hughes RA (2002) Peripheral neuropathy. BMJ 324: 466-469.

Inoue K, Ueno S, Fukuda A (2004) Interaction of neuron-specific K+-Cl- cotransporter, KCC2, with brain-type creatine kinase. FEBS Lett 564: 131-135.

Jennings ML, Schulz RK (1991) Okadaic acid inhibition of KCl cotransport. Evidence that protein dephosphorylation is necessary for activation of transport by either cell swelling or N-ethylmaleimide. J Gen Physiol 97: 799-817.

Kahle KT, Rinehart J, de Los Heros P, Louvi A, Meade P, Vazquez N, Hebert SC, Gamba G, Gimenez I, Lifton RP (2005) WNK3 modulates transport of Cl- in and out of cells: implications for control of cell volume and neuronal excitability. Proc Natl Acad Sci U S A 102: 16783-16788.

Kahle KT, Rinehart J, Lifton RP (2010) Phosphoregulation of the Na-K-2Cl and K-Cl cotransporters by the WNK kinases. Biochim Biophys Acta 1802: 1150-1158.

Kahle KT, Rinehart J, Ring A, Gimenez I, Gamba G, Hebert SC, Lifton RP (2006) WNK protein kinases modulate cellular Cl- flux by altering the phosphorylation state of the Na-K-Cl and K-Cl cotransporters. Physiology (Bethesda) 21: 326-335.

Kahle KT, Staley KJ, Nahed BV, Gamba G, Hebert SC, Lifton RP, Mount DB (2008) Roles of the cation-chloride cotransporters in neurological disease. Nat Clin Pract Neurol 4: 490-503.

Karl T, Pabst R, von Horsten S (2003) Behavioral phenotyping of mice in pharmacological and toxicological research. Exp Toxicol Pathol 55: 69-83.

Kemter E, Rathkolb B, Bankir L, Schrewe A, Hans W, Landbrecht C, Klaften M, Ivandic B, Fuchs H, Gailus-Durner V, Hrabe de Angelis M, Wolf E, Wanke R, Aigner B (2010) Mutation of the Na(+)-K(+)-2Cl(-) cotransporter NKCC2 in mice is associated with severe polyuria and a urea-selective concentrating defect without hyperreninemia. Am J Physiol Renal Physiol 298: F1405-1415.

Keng VW, Watson AL, Rahrmann EP, Li H, Tschida BR, Moriarity BS, Choi K, Rizvi TA, Collins MH, Wallace MR, Ratner N, Largaespada DA (2012) Conditional Inactivation of Pten with EGFR Overexpression in Schwann Cells Models Sporadic MPNST. Sarcoma 2012: 620834.

Labrisseau A, Vanasse M, Brochu P, Jasmin G (1984) The andermann syndrome: agenesis of the corpus callosum associated with mental retardation and progressive sesorimotor neuronopathy. Can J Neurol Sci 11: 257-261.

Larbrisseau A, Vanasse M, Brochu P, Jasmin G (1984) The Andermann syndrome: agenesis of the corpus callosum associated with mental retardation and progressive sensorimotor neuronopathy. Can J Neurol Sci 11: 257-261.

Lauf PK (1983) Thiol-dependent passive K+-Cl- transport in sheep red blood cells. V. Dependence on metabolism. Am J Physiol 245: C445-448.

Lauf PK, Bauer J, Adragna NC, Fujise H, Zade-Oppen AM, Ryu KH, Delpire E (1992) Erythrocyte K-Cl cotransport: properties and regulation. Am J Physiol 263: C917-932.

Lauf PK, Theg BE (1980) A chloride dependent K+ flux induced by N-ethylmaleimide in genetically low K+ sheep and goat erythrocytes. Biochem Biophys Res Commun 92: 1422-1428.

Lauf PK, Warwar R, Brown TL, Adragna NC (2006) Regulation of potassium transport in human lens epithelial cells. Exp Eye Res 82: 55-64.

Le Rouzic P, Ivanov TR, Stanley PJ, Baudoin FM, Chan F, Pinteaux E, Brown PD, Luckman S, M. (2006) KCC3 and KCC4 expression in rat adult forebrain. Brain Res 1110: 39-45.

Leduc-Nadeau A, Lahjouji K, Bissonnette P, Lapointe J-Y, Bichet DG (2007) Elaboration of a novel technique for purification of plasma membranes from *Xenopus laevis* oocytes. Am J Physiol Cell Physiol 292: C1132-C1136.

Liu M, Wood JN (2011) The roles of sodium channels in nociception: implications for mechanisms of neuropathic pain. Pain Med 12: S93-S99.

Lu J, Karadsheh M, Delpire E (1999) Developmental regulation of the neuronal-specific isoform of K-Cl cotransporter KCC2 in postnatal rat brains. J Neurobiol 39: 558-568.

Mall M, Kreda SM, Mengos A, Jensen TJ, Hirtz S, Seydewitz HH, Yankaskas J, Kunzelmann K, Riordan JR, Boucher RC (2004) The DeltaF508 mutation results in loss of CFTR function and mature protein in native human colon. Gastroenterology 126: 32-41.

Marangos PJ, Schmechel DE (1987) Neuron specific enolase, a clinically useful marker for neurons and neuroendocrine cells. Annu Rev Neurosci 10: 269-295.

Martyn CN, Hughes RA (1997) Epidemiology of peripheral neuropathy. J Neurol Neurosurg Psychiatry 62: 310-318.

Mercado A, Vazquez N, Song L, Cortes R, Enck AH, Welch R, Delpire E, Gamba G, Mount DB (2005) NH2-terminal heterogeneity in the KCC3 K+-Cl- cotransporter. Am J Physiol Renal Physiol 289: F1246-1261.

Mount DB, Mercado A, Song L, Xu J, George AL, Jr., Delpire E, Gamba G (1999) Cloning and characterization of KCC3 and KCC4, new members of the cation-chloride cotransporter gene family. J Biol Chem 274: 16355-16362.

Münkle MC, Waldvogel HJ, Faull RL (2000) The distribution of calbindin, calretinin and parvalbumin immunoreactivity in the human thalamus. J Chem Neuroanat 19: 155-173.

Ng HY, Lin SH, Hsu CY, Tsai YZ, Chen HC, Lee CT (2006) Hypokalemic paralysis due to Gitelman syndrome: a family study. Neurology 67: 1080-1082.

Ohshima T, Endo T, Onaya T (1991) Distribution of parvalbumin immunoreactivity in the human brain. J Neurol 238: 320-322.

OrtizCarranza O, Adragna NC, Lauf PK (1996) Modulation of K-Cl cotransport in volume-clamped low-K sheep erythrocytes by pH, magnesium, and ATP. American Journal of Physiology-Cell Physiology 271: C1049-C1058.

Parmantier E, Lynn B, Lawson D, Turmaine M, Namini SS, Chakrabarti L, McMahon AP, Jessen KR, Mirsky R (1999) Schwann cell-derived Desert hedgehog controls the development of peripheral nerve sheaths. Neuron 23: 713-724.

Payne JA (2009) The Potassium-Chloride Cotransporters: from Cloning to Structure and Function. In: Alvarez-Leefmans FJ, Delpire E, editors. Physiology and Pathology of Chloride Transporters and Channels in the nervous System: From molecules to diseases. London: Academic Press. pp. 333-356.

Payne JA, Stevenson TJ, Donaldson LF (1996) Molecular characterization of a putative K-Cl cotransporter in rat brain. A neuronal-specific isoform. J Biol Chem 271: 16245-16252.

Pearson M, Lu J, Mount DB, Delpire E (2001) Localization of the K-Cl cotransporter, KCC3, in the central and peripheral nervous systems: expression in choroid plexus, large neurons, and white matter tracts. Neuroscience 103: 483-493.

Pearson MM, Lu J, Mount DB, Delpire E (2001) Localization of the K(+)-Cl(-) cotransporter, KCC3, in the central and peripheral nervous systems: expression in the choroid plexus, large neurons and white matter tracts. Neuroscience 103: 481-491.

Perry PB, O'Neill WC (1993) Swelling-activated K fluxes in vascular endothelial cells: volume regulation via K-Cl cotransport and K channels. Am J Physiol 265: C763-769.

Peters LL, Robledo RF, Bult CJ, Churchill GA, Paigen BJ, Svenson KL (2007) The mouse as a model for human biology: a resource guide for complex trait analysis. Nat Rev Genet 8: 58-69.

Piechotta K, Lu J, Delpire E (2002) Cation chloride cotransporters interact with the stress-related kinases Ste20-related proline-alanine-rich kinase (SPAK) and oxidative stress response 1 (OSR1). J Biol Chem 277: 50812-50819.

Plotkin MD, Snyder EY, Hebert SC, Delpire E (1997) Expression of the Na-K-2Cl cotransporter is developmentally regulated in postnatal rat brains: a possible mechanism underlying GABA's excitatory role in immature brain. J Neurobiol 33: 781-795.

Popelar J, Rybalko N, Burianova J, Schwaller B, Syka J (2013) The effect of parvalbumin deficiency on the acoustic startle response and prepulse inhibition in mice. Neurosci Lett 553: 216-220.

Popelár J, Rybalko N, Burianová J, Schwaller B, Syka J (2013) The effect of parvalbumin deficiency on the acoustic startle response and prepulse inhibition in mice. Neurosci Lett 553: 216-220.

Price TJ, Cervero F, Gold MS, Hammond DL, Prescott SA (2009) Chloride regulation in the pain pathway. Brain Res Rev 60: 149-170.

Race JE, Makhlouf FN, Logue PJ, Wilson FH, Dunham PB, Holtzman EJ (1999) Molecular cloning and functional characterization of KCC3, a new K-Cl cotransporter. Am J Physiol 277: C1210-1219.

Rathmayer W, Djokaj S (2000) Presynaptic inhibition and the participation of GABA(B) receptors at neuromuscular junctions of the crab Eriphia spinifrons. J Comp Physiol A 186: 287-298.

Rivera C, Voipio J, Payne JA, Ruusuvuori E, Lahtinen H, Lamsa K, Pirvola U, Saarma M, Kaila K (1999) The K+/Cl- co-transporter KCC2 renders GABA hyperpolarizing during neuronal maturation. Nature 397: 251-255.

Roser M, Eibl N, Eisenhaber B, Seringer J, Nagel M, Nagorka S, Luft FC, Frei U, Gollasch M (2009) Gitelman syndrome. Hypertension 53: 893-897.

Rubenstein RC, Egan ME, Zeitlin PL (1997) In vitro pharmacologic restoration of CFTR-mediated chloride transport with sodium 4-phenylbutyrate in cystic fibrosis epithelial cells containing delta F508-CFTR. J Clin Invest 100: 2457-2465.

Rudnik-Schöneborn S, Hehr U, von Kalle T, Bornemann A, Winkler J, Zerres K (2009) Andermann syndrome can be a phenocopy of hereditary motor and sensory neuropathy--report of a discordant sibship with a compound heterozygous mutation of the KCC3 gene. Neuropediatrics 40: 129-133.

Rudomin P, Schmidt RF (1999) Presynaptic inhibition in the vertebrate spinal cord revisited. Exp Brain Res 129: 1-37.

Rust MB, Alper SL, Rudhard Y, Shmukler BE, Vicente R, Brugnara C, Trudel M, Jentsch TJ, Hubner CA (2007) Disruption of erythroid K-Cl cotransporters alters erythrocyte volume and partially rescues erythrocyte dehydration in SAD mice. J Clin Invest 117: 1708-1717.

Rust MB, Faulhaber J, Budack MK, Pfeffer C, Maritzen T, Didie M, Beck FX, Boettger T, Schubert R, Ehmke H, Jentsch TJ, Hubner CA (2006) Neurogenic mechanisms contribute to hypertension in mice with disruption of the K-Cl cotransporter KCC3. Circ Res 98: 549-556.

Salin-Cantegrel A, Riviere JB, Shekarabi M, Rasheed S, Dacal S, Laganiere J, Gaudet R, Rochefort D, Lesca G, Gaspar C, Dion PA, Lapointe JY, Rouleau GA (2011) Transit defect of potassium-chloride Co-transporter 3 is a major pathogenic mechanism in hereditary motor and sensory neuropathy with agenesis of the corpus callosum. J Biol Chem 286: 28456-28465.

Salin-Cantegrel A, Shekarabi M, Holbert S, Dion P, Rochefort D, Laganiere J, Dacal S, Hince P, Karemera L, Gaspar C, Lapointe JY, Rouleau GA (2008) HMSN/ACC truncation mutations disrupt brain-type creatine kinase-dependant activation of K+/Cl- co-transporter 3. Hum Mol Genet 17: 2703-2711.

Schultheis PJ, Lorenz JN, Meneton P, Nieman ML, Riddle TM, Flagella M, Duffy JJ, Doetschman T, Miller ML, Shull GE (1998) Phenotype resembling Gitelman's syndrome in mice lacking the apical Na+-Cl- cotransporter of the distal convoluted tubule. J Biol Chem 273: 29150-29155.

Schwaller B, Tetko IV, Tandon P, Silveira DC, Vreugdenhil M, Henzi T, Potier MC, Celio MR, Villa AE (2004) Parvalbumin deficiency affects network properties resulting in increased susceptibility to epileptic seizures. Mol Cell Neurosci 25: 650-663.

Schwaller B, Tetko IV, Tandon P, Silveira DC, Vreugdenhil M, Henzi T, Potier MC, Celio MR, Villa AE (2004) Parvalbumin deficiency affects network properties resulting in increased susceptibility to epileptic seizures. Mol Cell Neurosci 25: 650-653.

Shekarabi M, Moldrich RX, Rasheed S, Salin-Cantegrel A, Laganiere J, Rochefort D, Hince P, Huot K, Gaudet R, Kurniawan N, Sotocinal SG, Ritchie J, Dion PA, Mogil JS, Richards LJ, Rouleau GA (2012) Loss of neuronal potassium/chloride cotransporter 3 (KCC3) is responsible for the degenerative phenotype in a conditional mouse model of hereditary motor and sensory neuropathy associated with agenesis of the corpus callosum. J Neurosci 32: 3865-3876.

Shekarabi M, Moldrich RX, Rasheed S, Salin-Cantegrel A, Laganière J, Rochefort D, Hince P, Huot K, Gaudet R, Kurniawan N, Sotocinal SG, Ritchie J, Dion PA, Mogil JS, Richards LJ, Rouleau GA (2012) Loss of Neuronal Potassium/Chloride Cotransporter 3 (KCC3) Is Responsible for the Degenerative Phenotype in a Conditional Mouse Model of Hereditary Motor and Sensory Neuropathy Associated with Agenesis of the Corpus Callosum. J Neurosci 32: 3865-3876.

Shekarabi M, Salin-Cantegrel A, Laganiere J, Gaudet R, Dion P, Rouleau GA (2011) Cellular Expression of the K(+)-Cl(-) Cotransporter KCC3 in the Central Nervous System of Mouse. Brain Res 1374: 15-26.

Shekarabi M, Salin-Cantegrel A, Laganiere J, Gaudet R, Dion P, Rouleau GA (2011) Cellular expression of the K+-Cl- cotransporter KCC3 in the central nervous system of mouse. Brain Res 1374: 15-26.

Simard CF, Bergeron MJ, Frenette-Cotton R, Carpentier GA, Pelchat ME, Caron L, Isenring P (2007) Homooligomeric and heterooligomeric associations between K^+-Cl^- cotransporter isoforms and between K^+-Cl^- and Na^+-K^+-Cl^- cotransporters. J Biol Chem 282: 18083-18093.

Simon DB, Karet FE, Rodriguez-Soriano J, Hamdan JH, DiPietro A, Trachtman H, Sanjad SA, Lifton RP (1996) Genetic heterogeneity of Bartter's syndrome revealed by mutations in the K+ channel, ROMK. Nat Genet 14: 152-156.

Simon DB, Lifton RP (1996) The molecular basis of inherited hypokalemic alkalosis: Bartter's and Gitelman's syndromes. Am J Physiol 271: F961-966.

Stirling LC, Forlani G, Baker MD, Wood JN, Matthews EA, Dickenson AH, Nassar MA (2005) Nociceptor-specific gene deletion using heterozygous NaV1.8-Cre recombinase mice. Pain 113: 27-36.

Sung KW, Kirby M, McDonald MP, Lovinger DM, Delpire E (2000) Abnormal GABAA receptor-mediated currents in dorsal root ganglion neurons isolated from Na-K-2Cl cotransporter null mice. J Neurosci 20: 7531-7538.

Takahashi N, Chernavvsky DR, Gomez RA, Igarashi P, Gitelman HJ, Smithies O (2000) Uncompensated polyuria in a mouse model of Bartter's syndrome. Proc Natl Acad Sci U S A 97: 5434-5439.

Torpy JM, Kincaid JL, Glass RM (2010) JAMA patient page. Peripheral neuropathy. JAMA 303: 1556.

Umehara F, Tate G, Itoh K, Yamaguchi N, Douchi T, Mitsuya T, Osame M (2000) A novel mutation of desert hedgehog in a patient with 46,XY partial gonadal dysgenesis accompanied by minifascicular neuropathy. Am J Hum Genet 67: 1302-1305.

Uyanik G, Elcioglu N, Penzien J, Gross C, Yilmaz Y, Olmez A, Demir E, Wahl D, Scheglmann K, Winner B, Bogdahn U, Topaloglu H, Hehr U, Winkler J (2006) Novel truncating and missense mutations of the KCC3 gene associated with Andermann syndrome. Neurology 66: 1044-1048.

Van Acker K, Bouhassira D, De Bacquer D, Weiss S, Matthys K, Raemen H, Mathieu C, Colin IM (2009) Prevalence and impact on quality of life of peripheral neuropathy with or without neuropathic pain in type 1 and type 2 diabetic patients attending hospital outpatients clinics. Diabetes & Metabolism 35: 206-213.

Verret L, Mann EO, Hang GB, Barth AM, Cobos I, Ho K, Devidze N, Masliah E, Kreitzer AC, Mody I, Mucke L, Palop JJ (2012) Inhibitory interneuron deficit links altered network activity and cognitive dysfunction in Alzheimer model. Cell 149: 708-721.

Waldegger S, Steuer S, Risler T, Heidland A, Capasso G, Massry S, Lang F (1998) Mechanisms and clinical significance of cell volume regulation. Nephrol Dial Transplant 13: 867-874.

Wang T, Delpire E, Giebisch G, Hebert SC, Mount DB (2003) Impaired fluid and bicarbonate absorption in proximal tubules (PT) of KCC3 knockout mice. FASEB J 17: A464.

Weil-Maslansky E, Gutman Y, Sasson S (1994) Insulin activates furosemide-sensitive K+ and Cl- uptake system in BC3H1 cells. Am J Physiol 267: C932-939.

Whitehead MC, Marangos PJ, Connolly SM, Morest DK (1982) Synapse Formation Is Related to the Onset of Neuron-Specific Enolase Immunoreactivity in the Avian Auditory and Vestibular Systems. Developmental Neuroscience 5: 298-307.

Yan GX, Chen J, Yamada KA, Kleber AG, Corr PB (1996) Contribution of shrinkage of extracellular space to extracellular K+ accumulation in myocardial ischaemia of the rabbit. J Physiol 490 (Pt 1): 215-228.

Zeitlin PL, Diener-West M, Rubenstein RC, Boyle MP, Lee CK, Brass-Ernst L (2002) Evidence of CFTR function in cystic fibrosis after systemic administration of 4-phenylbutyrate. Mol Ther 6: 119-126.